
**Addis Ababa University**

**Addis Ababa Institute of Technology**

**School Of Graduate Studies**

**M.Sc. Thesis**

**On**

# Impact of Climate Change on Hydrological Responses of Gumara Catchment, in the Lake Tana Basin - Upper Blue Nile Basin of Ethiopia

**By**

**Andargachew Melke**

**Advisor**

**Fantahun Abegaz (PhD)**

**January, 2015**

**Addis Ababa, Ethiopia**


Addis Ababa University

School of Graduate Studies

MSc Thesis

On

# Hydrological Response to Climate Change for Gumara River, in the Lake Tana Basin - Upper Blue Nile Basin of Ethiopia

By

Andargachew Melke

Advisor

Fantahun Abegaz (PhD)

Thesis Submitted to the School of Graduate Studies in Partial Fulfillment of the Requirements for the Degree of Master of Science in Civil Engineering (Hydraulic engineering)

January, 2015

Addis Ababa, Ethiopia

**SCHOOLOF GRADUATE STUDIES**

**ADDIS ABABA INTITUTE OF TECHNOLOGY**

As thesis research advisor, I hereby certify that I have read and evaluated this thesis prepared, under my guidance, by Andargachew Melke, entitled**: Impact of Climate Change on Hydrological Responses of Gumara Catchment, in the Lake Tana Basin Upper Blue Nile Basin of Ethiopia.** I recommended that it be accepted as fulfilling the thesis requirement.

Fentaw Abegaz (PhD) _____ _____.

Advisor Signature Date

As a member of the Board of Examiners of the MSc, Thesis Open Defense Examination, we certify that we have read, evaluated the thesis prepared by Andargachew Melke and examined the candidate. We recommended that the thesis be accepted as fulfilling the thesis requirement for the degree of Master of Science in Civil Engineering (Hydraulic Engineering).

_____ _____ _____.

Chairman Signature Date

_____ _____ _____.

External Examiner Signature Date

_____ _____ _____.

Internal Examiner Signature Date

.

## DECLARATION

Herewith I declare that this thesis is my work and is done only using by sources and materials that are duly acknowledged and clearly indicated. This thesis has never been submitted in an equal or similar version to any other examining board for award of any degree or diploma to the best of my knowledge and belief.

Name: Andargachew Melke

Signature: _____.

Date: _____.

## ABSTRACT

*Predictions of the impacts of climate change on the intensity, amount, and spatial and temporal variability of rainfall and temperature are required. The aim of this study was to assess the status of climate change and hydrological response to climate change for Gumara River sub-basin. The HadCM3A2a and HadCM3B2a (Hadley centre Climate model 3), output of Global Circulation Model (GCM), scenarios of climate change were used for predicting the future climates of the study area. Statistical Downscaling Model (SDSM 4.2) was used to downscale large scale predictors into finer scale resolution. To estimate the level of impact of climate change, climate change scenarios of precipitation and temperature were divided into four time windows of 25 years each from 2001- 2099. The Soil and Water Assessment Tool (SWAT) was used to simulate the hydrological response. SWAT was first calibrated and validated using observed data and the SDSM downscaled climate outputs were used as an input into the SWAT model to assess the hydrological responses of Gumara River due to climate change. The period from 1986-2000 were taken as a base period against which a comparison was made. The results showed that the SWAT calibration and validation reveals a good agreement with $R^2$=0.9 during calibration and $R^2$=0.89 during validation whereas NSE= 0.89 during calibration and 0.86 during validation. The monthly and seasonal downscaled precipitation, maximum and minimum temperature in the future time horizons did not show systematic increase and decrease i.e. increases in some months and season and decreases in some other months and seasons. Annually, both precipitation and temperature showed increasing trends in all future time horizons (Precipitation increases up to 13.7% while temperature increases up to a maximum of 1.01$^o$c). Based on monthly, seasonal and annual changes of precipitation, maximum and minimum temperature, the SWAT model was rerun for each time horizons and the results reveal, as that of precipitation and temperature, the monthly flow volume did not show systematic trends i.e. increases from month of April-September up to a maximum of 134.54% for A2a and 127.52% for B2a and decreases in the remaining months by 47.44% (A2a) and 46.62% (B2a). Seasonal and annual flow volume increases in all future time horizons as compared to the base period. Seasonally, the maximum increment was shown in the major parts of the rainy season (Kiremit) and small rainy season (Belg) in which the flow volume increases by 144.65% for A2a scenario and 101.58% for B2a scenario. Moreover, the annual increment showed systematic trends and the increment reaches up to 17.65% for both scenarios at the end of 21$^{st}$ century. Thus, the hydrology of Gumara River is highly vulnerable to climate change especially in the rainy seasons which causes high floods and therefore, considering climate change impacts is advantageous in any water related issues on Gumara sub-basin.*

**Key words:** Blue Nile, Gumara River, Climate Change, SDSM, Hydrological Modeling, SWAT Model Lake Tana Basin, Ethiopia

**ACKNOWLEDGMENT**

Above all I thank the almighty of GOD for his mercy and grace upon me during all my works and in all my life.

I would like to express my thanks and gratitude to Addis Ababa University for granting me this opportunity to study Master of Science degree. I am also grateful to my employer, Madawalabu University, for providing me different expenses without obligating me to do extra works till I have finished this work.

I would like to express my sincere appreciation to Dr. Fantahun Abegaz, my major advisor, for his advice and valuable suggestions, encouragement and guidance from the inception to the completion the research work. Moreover, he devoted his precious time to advise me during the data analysis and suggested valuable comments. His critical comment and advice helped me to accomplish and realized this research work.

I wish to express my heartfelt thanks to Mr. Tegegn Mola for his support by giving me a basic GIS training.

A very sincere word of thanks goes to my parents. I thank my father, Mr. Melke Alemu, for his love, continual encouragement and support in every respect from my childhood. I know that words can't express my feeling for you. Thank you so much for all you have gone through to see me reach at this stage even though today you are not here with me. May God bless you!!!

I would like to thank also National Metrological Agency, Ministry of Water Resource and Water Works Design and Supervision Enterprise, Bahir Dar University.

Last but not least, I would like to thank all my friends who gave me the strength to finalize this research work. Thanks for your encouragement and true friendship!

Andargachew Melke

January, 2015

**DEDICATED**

*To*

*My Father, Melke Alemu*

*You meant a great deal to me!*

**LIST OF ACRONYMS**

CN---------Curve Number

DDC-------Data Distribution Centre

DEM-------Digital Elevation Model

ESCO ------Soil Evaporation Compensation Factor

FAO--------Food and Agricultural Organization

GIS---------Geographic Information System

CCSR----------Center for Climate System Research

CGCM2 -------Canadian Global Coupled Model2

CSIRO ---------Commonwealth Scientific and Industrial Research Organization

ECHAM4 ------European Centre Hamburg Model 4

GCM---------- General Circulation Models

GFDL-R30-----Geophysical Fluid Dynamics Laboratory's Rhomboidal 30 truncation

HadCM3-------Hadley centre Climate Model 3

HRU ----------Hydrologic Response Unit

IPCC----------Inter Governmental Panel on Climate Change

LAM-------- Limited Area Models

MOS-------- Model Output Statistics

MoWR ------Ministry of Water Resources, Ethiopia

MRS----------Mean Relative Sensitivity

NIES---------- National Institute for Environmental Studies

NMSA---------National Meteorological Services Agency

RCM-------- Regional Climate Models

PET---------Potential Evapotranspiration

SCS---------Soil Conservation Service

SDSM-------Statistical Down Scaling Model

SRES-------- Special Report on Emissions Scenarios

STAR---------Statistical Regional Model

SWAT------Soil Water Assessment Tool

TGCIA ----Task Group on Scenarios for Climate and Impact Assessment

TAR-------Third Assessment Report

USDA -------United States Department of Agriculture

SWIM --------Soil and Water Integrated Mode

WWDSE-----Water Work Design and Supervision Enterprise

**TABLE OF CONTENT**

**LIST OF FIGURES**

**LIST OF TABLES**

# 1. INTRODUCTION

## 1.1 Background

According to the Intergovernmental Panel on Climate Change (IPCC) Scientific Assessment Report, global average temperature would rise between 1.4 and 5.8°C by 2100 with the doubling of the $CO_2$ concentration in the atmosphere. Sea level rise, change in precipitation pattern (up to ±20%), and change in other local climate conditions are expected to occur as a consequence of rising global temperature (Cubasch *et al*., 2001).

Developing countries, particularly those in Africa are likely to be especially vulnerable to climate change as recurrent floods and droughts continue to bring misery to millions in Africa (Rizwan et. al, 2010). Climate change will increase the number of people living in water stressed regions globally. The impact will be worse for the contemporary African population where about 25% already experience water stress. Considering population increase and water use, it has been estimated that the portion of the African population at risk for water stress and scarcity will increase to 65% in 2025. Climate change is, however, expected to exacerbate the current stress on water resources availability in Africa (Dile et al, 2013).

From the point of view of the design and management of water resource systems, hydrologists are required to make accurate predictions of the impacts of climate change on the intensity, amount, and spatial and temporal variability of rainfall. Furthermore, and perhaps most important, they also must examine how the stream flow regime (e.g., stream flow hydrographs, peak flow ,etc.) at different spatial and temporal scales is affected by rainfall variability and by the expected changes in that variability as a result of climate change (Boosik *etal*, 2007). One of the most important impacts on society of future climatic changes will be (Chong-Yu Xu, 1999) changes in regional water availability. Such hydrologic changes will affect nearly every aspect of human well-being, from agricultural productivity and energy use to flood control, municipal and industrial water supply, and fish and wildlife management. The tremendous importance of water in both society and nature underscores the necessity of understanding how a change in global climate could affect regional water supplies.

There is increasing interest in understanding how the rising concentration of greenhouse gases might affect climate (the mean and variability of temperature, precipitation, humidity, wind and other climate variables over several decades) at local and regional scales in the Nile basin.

### 1.2 Statement of the Problem

Previous research has shown that the water resources of Ethiopia are highly sensitive to climate change and variability. Appropriate adaptation strategies are important policy options to limit the unprecedented impact of climate change for the livelihoods of the rural Ethiopian poor. While the focus on considering global impact of climate change is primarily on societal responses to the local and regional consequences of large-scale changes. Most climate change studies in Ethiopia have been done either at country or River basin scale. Therefore, results from these studies are highly aggregated and have little importance in informing the impact of climate change at smaller catchment scale and this may cause significant problems for any water resources development activities that will be planted in that particular River sub basins.

Maria (2012) did a study on Gumara River basin based on the Statistical Regional Model (STAR) using three scenarios ($0^{o}$c, $0.7^{o}$c and $1^{o}$c increment at the end of 2050) by taking temperature as the forcing variables. The results showed that the precipitation decreases by 9.5%, 24%, 28.6% for 0.0ºC, 0.7ºC and 1.0ºC scenarios respectively. Moreover, the study was only based on an arbitrary increment of only temperature, and didn't take into consideration the downscaled results of Global Circulation Model (GCMs) outputs. Hence, studies that can narrow this gap are very important.

Thus this research assessed the impact of climate change for Gumara River, one of the major tributaries of the Lake Tana based on statistical downscaling model (SDSM). The study was extending the understanding of the implications of climate change at the Gumara River by applying a process-based hydrological model with finer temporal and spatial resolution and potentially provide valuable insight to decision makers on the local vulnerability of the Gumara and the Lake Tana regarding future change in rainfall and temperature because of climate change.

### 1.3 Research Questions

- How much percentage change in monthly, seasonal, and annual precipitation and absolute changes in temperature for the future period occurs as compared to the baseline period and what looks like the general trend of precipitation and temperature for the future period?
- How will the changes in monthly, seasonal, and annual precipitation and temperature for the future period affect the hydrology of Gumara Catchment?

## 1.4 Objective of the Study

### 1.4.1 General Objective

The general objective of the study encompasses to assess the status of climate change and hydrological response to climate change for Gumara River sub-basin by applying a process-based hydrological model so as to provide valuable insight to decision makers on the local vulnerability of Gumara catchment and Lake Tana regarding future changes of rainfall and temperature due to climate changes.

### 1.4.2 Specific Objective

The specific objectives of the study are:

- To assess the change in precipitation and temperature for the future period as compared to the baseline period based on the General circulation model outputs and Statistical Downscaling Model for Gumara catchment.
- To assess the possible impact of climate change on the hydrology of Gumara Catchment for the future period as compared to the baseline period based on the downscaled climate scenario data using SWAT model.

# 2 LITERATURE REVIEW

## 2.1 Previous Studies in the Upper Blue Nile Basin and Gumara Catchment

Many Water resource development researches have been studied at different stages by different researchers and consultants. The most relevant studies carried out are presented as follows:

Climate and Land Use Change Impact in Gumara catchment has been conducted (Maria, 2012) to assess the hydrological impact at the local watershed scale through the Eco hydrological modeling with the Soil and Water Integrated Model SWIM. The SWIM model was applied to analyze the impact of land use change with four main scenarios and employed for two different purposes: the conversion of land used for grass into crop, and the afforestation of the catchment. The model SWIM was also used to simulate the impacts of climate change on Gumara basin using three scenarios developed based on the Statistical Regional Model (STAR) and by taking temperature as the forcing variables. The results of the study reveal that the precipitation decreases by 9.5%, 24%, 28.6% for increment of 0.0ºC, 0.7ºC and 1.0ºC respectively and the channel flow reduces by 5.61%, 22.77% and 30.55% from the base period (1960-2000).

Taye (2010) studied the hydrological modeling of climate change impact on selected catchment of Nile River basin. Tana basin was one of the selected basins in this research. The study focused on using as many General Circulation Models (GCMs) outputs and two emission scenarios A1B and B1 were selected representing high and low case future climate change scenarios for the 2050s respectively. Furthermore, the hydrological modeling was performed using two lumped conceptual hydrological models, namely NAM and VHM. As the author stated “the results of the study proved that Lake Tana catchment shows unclear trends, neither increasing nor decreasing trend, as half of the GCMs project increases and the other half project decreases. This is mainly the result of downscaled precipitation that reveals both increasing and decreasing projections by different GCMs. However, the ensemble mean of the GCMs used in Lake Tana catchment reveals slight increase in the outflow. This suggests that the catchment may not be adversely affected by climate change.”

Kim *et al* (2008) also conducted researches on Climate Change Impacts on Hydrology and Water Resources of the Upper Blue Nile River Basin. The study used six General Circulation Models (GCMs) outputs namely CCSR/NIES (Center for Climate System Research and National

Institute for Environmental Studies), Canadian Global Coupled Model2 (CGCM2), Common Wealth Scientific and Industrial Research Organization (CSIRO), European Centre Hamburg Model 4 (ECHAM4), Geophysical Fluid Dynamics Laboratory's Rhomboidal 30 Truncation (GFDL-R30), and Hadley Centre Climate Model 3 (HadCM3) and A2 (High Emission Scenario) for 2050s. Moreover, the hydrological simulation has been done using simplified water balance model. Based on results the authors concluded that a general increasing trend was observed in both precipitation and runoff in the northern part of the study area, Amhara, under the weighted scenario (combination of GCM outputs) for the 2050s. In general, the results suggest that the water resources of the Upper Blue Nile River Basin may not be adversely affected by climate change.

The SWAT2005 model was applied to the Lake Tana Basin for modeling of the hydrological water balance. The main objective of this study was to test the performance and feasibility of the SWAT model for prediction of stream-flow in the Lake Tana Basin. The model was calibrated and validated on four tributaries of Lake Tana; Gumara, Gilgel Abay, Megech and Rib Rivers using SUFI-2, GLUE and ParaSol algorithms and it is found that SWAT model gives good agreement with observed and simulated flows (Setegn et al, 2008).

## 2.2 Climate Change Impacts

Developing countries, particularly those in Africa are likely to be especially vulnerable to climate change as recurrent floods and droughts continue to bring misery to millions in Africa (Rizwan et.al, 2010). According to the Intergovernmental Panel on Climate Change (IPCC, 2001), African countries are more vulnerable to these changes due to lack of institutional capacity and economic development.

Water availability is highly influenced by climate variability and climate change presents many challenges for the Nile basin and Africa in general (Kigobe, 2010) such as the alteration of the hydrological cycle, which will impact on the quantity and quality of regional water resource (NYENJE, 2009). Such hydrologic changes will affect nearly every aspect of human well-being, from agricultural productivity and energy use to flood control, municipal and industrial water supply, and fish and wildlife management. The tremendous importance of water in both society

and nature underscores the necessity of understanding how a change in global climate could affect regional water supplies (Chong-yu Xu, 1999).

The climate system affects all aspects of the hydrologic cycle as it is one of the most vulnerable systems. Changes in variability, spatial patterns and seasonality of precipitation and changes in temperature will have the effect of changing the soil moisture, River runoff, groundwater recharge, and peak runoff and basin hydrology. These will consequently cause changes in hydroelectric power generation, irrigation systems, water quality, and water supply systems (Taye, 2010)

### 2.2.1 Climate scenarios

Climate scenarios are plausible representations of the future that are consistent with assumptions about future emissions of greenhouse gases and other pollutants and with our understanding of the effect of increased atmospheric concentrations of these gases on global climate. A range of scenarios can be used to identify the sensitivity of an exposure unit to climate change and to help policy makers decide on appropriate policy responses. The choice of climate scenarios and related non-climatic scenarios is important because it can determine the outcome of climate impact assessment (IPCC-TGICA, 2007).

Smith and Hulme (1998) suggests four criteria to select climate scenarios which are useful for impact researchers and policy makers i.e. consistency with global projections, physical plausibility, applicability in impact assessments and representative.

There are three main classes of climate scenario namely synthetic scenarios, analogue scenarios and scenarios based on outputs from GCMs (IPCC-TGICA, 2007).

Synthetic scenarios describe techniques where particular climatic (or related) elements are changed by a realistic but arbitrary amount, often according to a qualitative interpretation of climate model simulations for a region. The advantages of synthetic scenario are, they are simple to apply by impact analysts, capture a wide range of possible changes in climate and the same synthetic scenarios can be applied for different studies to explore the relative sensitivities of exposure units. The major drawback of synthetic scenarios is their arbitrary nature.

Analogue scenarios are constructed by identifying recorded climate regimes which may resemble the future climate in a given region. These records can be obtained either from the past (temporal analogues) or from another region at the present (spatial analogues). Scenarios from general circulation model outputs is numerical models (General Circulation Models or GCMs), representing physical processes in the atmosphere, ocean, cryosphere and land surface, are the most advanced tools currently available for simulating the response of the global climate system to increasing greenhouse gas concentrations. In this study the numerical models (General Circulation Models or GCMs) was used.

### 2.2.2 **General Circulation Models**

Climate change scenarios developed from Global Climate Models (GCMs) are the initial source of information for estimating plausible future climate (Masoud et. al, 2007). General Circulation Models (GCM), representing physical processes in the atmosphere, ocean, and land surface, are the only credible tools currently available for simulating the response of the global climate system to increasing greenhouse gas concentrations (IPCC-TGCIA, 1999).

General Circulation Models (GCMs) suggest that rising concentrations of greenhouse gases will have significant implications for climate at global and regional scales. Unfortunately, GCMs are restricted in their usefulness for local impact studies by their coarse spatial resolution (typically of the order 50,000 $km^2$) and inability to resolve important sub-grid scale features such as clouds and topography (Wilby and Dawson, 2007). Thus it is important to downscale the large scale predictors to the local scale predictands.

### 2.2.3 Downscaling Methods

Two groups of techniques have emerged as a means of relating regional scale atmospheric predictor variables to local-scale surface weather. Firstly, Regional Climate Models (RCMs) simulate sub-GCM grid-scale climate features dynamically using time-varying atmospheric conditions supplied by a GCM bounding a specified domain. Dynamical downscaling involves the nesting of a higher resolution Regional Climate Model (RCM) within a coarser resolution GCM. The RCM uses the GCM to define time–varying atmospheric boundary conditions around a finite domain, within which the physical dynamics of the atmosphere are modelled using horizontal grid spacing of 20–50 km (Wilby and Dawson, 2007). The goal of dynamic

downscaling (i.e., to extract the local-scale information from the large-scale GCM data) is achieved by developing and using limited-area models (LAMs) or regional climate models (RCMs) (Hessam et. al, 2007). The main limitation of RCMs is that they are as computationally demanding as GCMs (placing constraints on the feasible domain size, number of experiments and duration of simulations). The scenarios produced by RCMs are also sensitive to the choice of boundary conditions (such as soil moisture) used to initiate experiments (Wilby and Dawson, 2007).

Secondly, statistical downscaling is analogous to the 'model output statistics (MOS) and used for short-range numerical weather prediction (Wilby and Dawson, 2007).Statistical downscaling techniques which employs statistical relationship between the large scale climatic state and the local variations derived from historical data. Different approaches of statistical downscaling techniques are available where each method lies, generally, in one of the three categories, namely regression (transfer function) methods, stochastic weather generators and weather classification schemes (Girma, 2009). According to Wilby and Dawson (2007), Statistical downscaling methodologies have several practical advantages over dynamical downscaling approaches. In situations where low–cost, rapid assessments of localized climate change impacts are required, statistical downscaling (currently) represents the more promising option. Moreover numerous studies have also assessed the SDSM for downscaling GCM output to be used in many hydrological applications (Dile et al, 2013, Taye, 2010, Kigobe, 2010, Lijalem, 2006, Girma, 2009 etc.)

The major weaknesses of statistical downscaling methods are that the fundamental assumptions on which they are based are not verifiable, i.e. the statistical relationships developed for the present day climate also hold under different forcing conditions of plausible future climate (e.g. Wilby et al., 2004), and that they cannot explicitly describe the physical processes that affect climate.

Among the different approaches of statistical downscaling methods, regression methods are regularly used because of their ease of implementation and their low computational requirements. Thus this technique is used in this research and is briefly reviewed for clarity.

#### 2.2.3.1 Statistical Downscaling

Statistical downscaling methods involve developing quantitative relationships between large-scale atmospheric variables (predictors) and local scale surface variables (predictand) through the transfer functions (Wilby et al., 2004) which could be used as input for hydrological models (Zeryehun, 2009). SDSM develops statistical relationships, based on multiple linear regression techniques, between large-scale (predictors) and local (predictand) climate. The SDSM facilities have undergone rapid development of multiple, low cost, single-site scenarios of daily surface weather variables under the present and future climate forcing. As an addition, the tool performs ancillary tasks of data quality control and transformation, predictor variable pre-screening, automatic model calibration, basic diagnostic testing, statistical analyses and graphing of climate data (Wilby and Dawson, 2007).

The two frequently used terms in statistical downscaling are defined as follows as used in many journals. Girma (2009), the predictor is the input data used in statistical models, typically a large scale variable describing the circulation regime over a region. The predictor is also known as ’independent variable’, or simply as the ’input variable’, usually written as: Predictand = $f$ (predictors). The predictand is the output data, typically the small-scale variable representing the temperature or rainfall at a weather/climate station. The predictand, is also known as ’dependent variable’, ’response variable’, ’responding variable’, or simply as the ’output’

Statistical downscaling is based on the assumptions that (i) suitable relationships can be developed between grid- and larger-scale versus grid- and smaller-scale predictor variables; (ii) these observed, empirical relationships are valid under future climate conditions; and (iii) the predictor variables and their changes are well characterized by GCMs. If these assumptions hold, it is then possible to produce scenarios of regional and smaller-scale climate from future climate change data produced by GCMs, that are both more reliable and of finer resolution than the ‘raw’ GCM data (Wilby and Wigley, 1999).

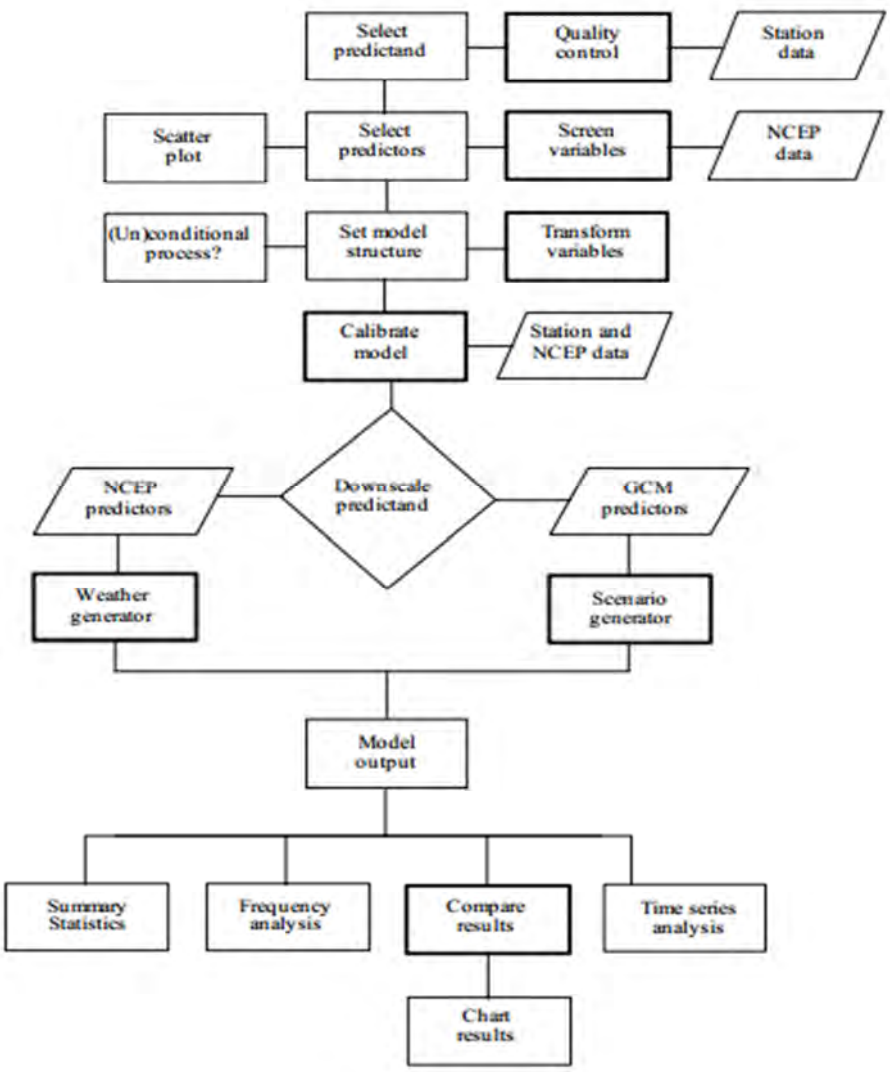


Figure 2.1: SDSM Version 4.2 climate scenario generation (adopted from Wilby and Dawson (2007) user manual)

### 2.2.4 Emissions Scenarios

Scenarios of different rates and magnitudes of climate change provide a basis for assessing the risk of crossing identifiable thresholds in both physical change and impacts on biological and human systems. In climate change research, scenarios describe plausible trajectories of different aspects of the future that are constructed to investigate the potential consequences of anthropogenic climate change. Scenarios represent many of the major driving forces - including processes, impacts (physical, ecological, and socioeconomic), and potential responses that are

important for informing climate change policy. They are used to hand off information from one area of research to another (e.g., from research on energy systems and greenhouse gas emissions to climate modeling). They are also used to explore the implications of climate change for decision making (e.g., exploring whether plans to develop water management infrastructure are robust to a range of uncertain future climate conditions). The goal of working with scenarios is not to predict the future but to better understand uncertainties and alternative futures, in order to consider how robust different decisions or options may be under a wide range of possible futures (Wayne, 2013). In order to address these issues, in 1992 the Intergovernmental Panel on Climate Change (IPCC) published the first set of climate change scenarios, called IS92. In year 2000 the IPCC released a second generation of projections, collectively referred to as the Special Report on Emissions Scenarios (SRES). These were used in two subsequent reports; the Third Assessment Report (TAR) and Assessment Report Four (AR4) and have provided common reference points for a great deal of climate science research in the last decade. The Representative Concentration Pathways (RCPs) are the latest iteration of the scenario process, and are used in the Assessment Report Five (AR5) in preference to SRES. In the new scenarios (Representative Concentration Pathways (RCPs)), there are four pathways: RCP8.5, RCP6, RCP4.5 and RCP2.6 - the last is also referred to as RCP3-PD. (The numbers refer to forcing for each RCP; PD stands for Peak and Decline). The details of RCPs are found in IPCC (2013).

But for this study the SRES scenarios are used due to the reasons that researches using the new scenarios (Representative Concentration Pathways (RCPs) are lacking and it makes difficult to validate the results of this studies with other similar works.

#### 2.2.4.1 The SRES Emissions Scenarios

The IPCC published a set of emissions scenarios in 2000 for use in climate change studies (Special Report on Emissions Scenarios – SRES). The SRES scenarios were constructed to explore future developments in the global environment with special reference to the production of greenhouse gases and aerosol precursor emissions. The SRES team defined four narrative storylines (a narrative description of a scenario (or a family of scenarios)), labeled A1, A2, B1 and B2, describing the relationships between the forces driving greenhouse gas and aerosol emissions and their evolution during the 21st century for large world regions and globally (IPCC-TGICA, 2007).

A1: a future world of very rapid economic growth, global population that peaks in mid-century and declines thereafter, and rapid introduction of new and more efficient technologies. A2: a very heterogeneous world with continuously increasing global population and regionally oriented economic growth that is more fragmented and slower than in other storylines. B1: a convergent world with the same global population as in the A1 storyline but with rapid changes in economic structures toward a service and information economy, with reductions in materials intensity, and the introduction of clean and resource-efficient technologies. B2: a world in which the emphasis is on local solutions to economic, social, and environmental sustainability, with continuously increasing population (lower than A2) and intermediate economic development.

The IPCC recommends the use of A2 (medium-high emission) and B2 (medium-low emission) for inter-comparison studies because the computing cost of all scenarios in GCM is too expensive. These two scenarios are the common to all GCM (Zeryehun, 2009).

## 2.3 Hydrological Modeling

Hydrological modeling is a powerful technique of Hydrological systems investigation for both the research hydrologist and practicing water resources engineers involved in the planning and development of integrated approach for the management of water resources. Lenhart et al, (2002, cited in Lijalem, 2006), Hydrological modeling is a great method of understanding hydrologic systems for the planning and development of integrated water resources management. The purpose of using a model is to establish baseline characteristics whenever data is not available and to simulate long-term impacts that are difficult to calculate, especially in ecological modeling.

Effective watershed management and ecological restoration require a thorough understanding of hydrologic processes in the watersheds. Spatial and temporal variations in soils, vegetation and land use practices make a hydrologic cycle a complex system, therefore, mathematical models and geospatial analyses tools are needed for studying hydrologic processes and hydrologic responses to land use and climatic changes (Dilnesaw, 2006)

Hydrological model is a mathematical model used to simulate River or stream flow and calculate water quality calculations. These models generally came in to use in the 1960s and 1970s when demand for numerical forecasting of water quality was driven by environmental legislations in

the United States and United Kingdom. At about this time computers became more widely accessible and powerful enough to significantly assist in modeling processes. There are numerous hydrological models and they can be grouped by pollutant addressed, complexity of pollutant sources, whether the model is steady state or dynamic, and the time period modeled. Also important in determining the selection of model is whether it is distributed (i.e. capable of predicting multiple points within a River) or lumped. Simple models may only address a single pollutant, whereas a complex model could have multiple runoff and point sources for pollution for more than one chemical, as well as sediment data. It could further divide the channel flow in to strata in which various biotas are modeled in relation to chemical and sediment transport. The ground water component may also be presented in a model (Kim et al, 2008).

Models often address individual steps modularly in the simulation process. Typically subroutines for surface runoff include components for a land use type, topography, soil type, vegetation cover, precipitation and land management practice (regular agricultural activities e.g. pesticide or fertilizer application).

Many different types of hydrological models have been developed. Many of these models share structural similarities because of underlying assumptions, while some of the models are distinctly different. Therefore, these models are classified according to different criteria. Hypothesis traditionally proposed two kind of modeling approaches with their strong points and limitations:

(1). physically based

(2). Conceptual lumped models

Physically based models (theoretical, white box) consist of formulation in terms of physical laws expressed in the form deterministic conservation equation for mass, momentum and energy. The equations are solved numerically by dispraising the hydrological system in to smaller entities on a square or polygonal mesh. However, accurately modeling of all processes of the hydrologic cycle becomes very complex, demands an eminent insight in hydrological behavior and is very demanding for input data. Due to these properties it is a time consuming and expensive (Abbott et al., 1986)

As an alternative to physically based distributed models, conceptual lumped models (grey box) are often used as robust tools at catchment scale. The model structures of these models are relatively simple and often are based on a series of interconnected reservoirs. Further these models are invaluable instruments for operational water management (e.g. Reservoir operation and flood forecasting). Because of the fact that the required input and output data are usually easily available, consequently these models are mostly used in rainfall-runoff modeling (Ephrem, 2011).

### 2.3.1 Hydrological Model Selection

There are numerous criteria which can be used for selecting the appropriate hydrologic model. These criteria are project dependent, since every project has its own specific requirements and needs. Further, some criteria are also user depended, such as personal preference for computer operation system, input/output management and structure.

Among the various project-depended selection criteria, Cunderlik (2003) list out four main criteria that should be considered when selecting hydrological model. These are the required model outputs important for the needed purpose and therefore to be estimated by the model (does the model predict the variables required by the project such as peak flow, event volume and hydrograph, long term flows, etc.?), Hydrologic processes that need to be modelled to estimate the desired outputs adequately (is the model capable of simulating regulated reservoir operation, snow accumulation and melt, single event or continuous processes, etc.?), Availability of input data (can all the inputs data required by the model be provided within the time and cost constraints of the project? ) and Price (does the investment appear to be worthwhile for the objectives of the project?).

In this study spatially distributed model was used to assess the climate change impact on the River flows. The choice of these models depended on their moderate input data requirement (uses readily available inputs), ability to simulate the major hydrological processes and its availability. Moreover the model was widely used in the basin for hydrological model studies and confirmed that SWAT model able to simulate flows accurately. The model structure and its description can be found in the following sections.

### 2.3.2 SWAT Model

#### 2.3.2.1 General

SWAT is an acronym for soil water assessment tool, a River basin, or watershed, scale model developed by Dr. Jeff Arnold for the USDA Agricultural Research Service (RAS). SWAT is a River basin scale, continuous time, a spatially distributed model developed to predict the impact of land management practices on water, sediment and agricultural chemical yields in large complex watersheds with varying soils, land use and management conditions over long period of time (Neitsch et al., 2009). To satisfy this objective the model is physically based: rather than incorporating regression equations to describe the relationship between input and output variables SWAT requires specific information about weather, soil properties, topography vegetation and land management practices occurring in the watershed, the SWAT model uses readily available inputs: while SWAT can be used to study more specialized processes the data required to make a run are commonly available from government agencies, is computationally efficient: simulation of very large basins or a variety of management strategies can be performed without excessive investment of time or money, enables user to study long term impacts: many of the problems currently addressed by user involve the gradual buildup of pollutants and the impact on downstream water bodies. To study these types of problems, results are needed from runs with output spanning several decades.

SWAT is a continuous time period, i.e. a long-term yield model. The model is not designed to simulate detailed, single-event flood routing.

#### 2.3.2.2 SWAT Model Simulation Processes

SWAT allows a number of different physical processes to be simulated in a watershed. For modeling purpose, a watershed may be partitioned into a number of sub watersheds or sub basins. The use of sub basins in a simulation is particularly beneficial when different areas of the watershed are dominated land use or soils dissimilar enough in properties to impact hydrology. By partitioning the watershed into sub basins the user is able to reference different of the watershed to one another spatially. Input information for each sub basin is grouped or organized in to the following categories: climate, hydrologic response unit (HRU), pond/wetlands, groundwater, and the main channel or reach draining the sub basin. Hydrologic response units

are lumped land areas within the sub basin that are comprised of unique land cover, soil, and management combinations.

No matter what type of problem studied with SWAT, water balance is the driving force behind everything that happens in the watershed. To accurately predict the movement of pesticide, sediments or nutrients, the hydrologic cycle as simulated by the model must conform to what is happening in the watershed. Simulation of the hydrology of a watershed can separated into two major divisions. The first division is the land phase of the hydrologic cycle which controls the amount of water, sediment, nutrient and pesticides loading to the main channel in each sub basin. The second division is the water or routing phase of the hydrologic cycle which can be defined as the movement of water, sediment etc. through the channel network of the watershed to the outlet (Neitsch et al., 2009).

a) **The Land Phase of the Hydrologic Cycle**: The hydrologic cycle simulated by SWAT is based on the water balance equation as follows.

$$SW_t = SW_0 + \sum_{i=1}^{t}(R_{day} - Q_{surf} - E_a - W_{seep} - Q_{gw}) \quad (2.1)$$

In which, $SW_t$ is the final soil water content (mm water), $SW_o$ is the initial soil water content in day i (mm water), t is the time (days), $R_{day}$ is the amount of precipitation in day i (mm water), $Q_{surf}$ is the amount of surface runoff in day i (mm water), Ea is the amount of evapotranspiration in day i (mm water), $W_{seep}$ is the amount of water entering the vadose zone from the soil profile in day i (mm water), and $Q_{gw}$ is the amount of return flow in day i (mm water).

The subdivision of the watershed enables the model to reflect differences in evapotranspiration for various crops and soils. Runoff is predicted separately for each HRU and routed to obtain the total runoff for the watershed. This increases accuracy and gives a much better physical description of the water balance.

Surface runoff occurs whenever the rate of precipitation exceeds the rate of infiltration. When water is initially applied to a dry soil, the infiltration rate is usually very high. However, it will decrease as the soil becomes wetter. When the application rate is higher than the infiltration rate, surface depressions begin to fill. If the application rate continues to be higher than the infiltration rate once all surface depressions have filled, surface runoff will commence.

SWAT provides two methods for estimating surface runoff: the SCS curve number procedure (USDA-SCS, 1972) and the Green & Ampt infiltration method (1911).Using daily or sub daily rainfall, SWAT simulates surface runoff volumes and peak runoff rates for each HRU (Ephrem, 2011). For this research work SCS curve number method has been used to estimate surface runoff because of the unavailability of sub daily data for Green & Ampt method.

The SCS curve number equation is (SCS, 1972).

$$Q_{surf} = \frac{(R_{day} - I_a)^2}{(R_{day} - I_a + S)} \quad (2.2)$$

Where; $Q_{surf}$ the accumulated runoff or rainfall excess (mm H2O), $R_{day}$= is the rainfall depth for the day (mm $H_2O$), $I_a$ is the initial abstractions which includes surface storage, interception and infiltration prior to runoff (mm $H_2O$), S is the retention parameter (mm). The retention parameter varies spatially due to changes in soils, land use, management and slope and temporally due to changes in soil water content. The retention parameter is defined as:

$$S = 25.4\left(\frac{1000}{CN} - 10\right) \quad (2.3)$$

Where: CN is the curve number for the day.

The initial abstraction, $I_a$ is commonly approximated as 0.2S and Eq. (2.2) becomes,

$$Q_{surf} = \frac{(R_{day} - 0.2S)^2}{(R_{day} + 0.8S)} \quad (2.4)$$

Runoff will only occur when Rday> Ia.

The SCS curve number is a function of the soil's permeability, land use and antecedent soil water conditions. SCS defines three antecedent moisture conditions: I – dry (wilting point), II – average moisture, and III – wet (field capacity). The moisture condition I curve number is the lowest value that the daily curve number can assume in dry conditions. The curve numbers for moisture conditions II and III are calculated using equations 2.5 and 2.6.

$$CN_1 = CN_2 - \frac{20(100 - CN_2)^2}{(100 - CN_2 + exp[2.533 - 0.0636(100 - CN_2)])} \quad (2.5)$$

$$CN_3 = CN_2.exp[0.00673(100 - CN_2)] \quad (2.6)$$

In which CN1 is the moisture condition I curve number, CN2 is the moisture condition II curve number, and CN3 is the moisture condition III curve number.

Typical curve numbers for moisture condition II are listed in various Tables which are appropriate to slope less than 5%. But for areas with slopes greater than 5%, the curve number is adjusted (Williams, 1995) as:

$$CN_{2s} = \frac{(CN_3 - CN_2)}{3}[1 - 2\exp(-13.86.slp)] + CN_2 \quad (2.7)$$

In which $CN_{2S}$ is the moisture condition II curve numbers adjusted for slope, $CN_3$ is the moisture condition III curve number for the default 5% slope, $CN_2$ is the moisture condition II curve number for the default 5% slope, and slp is the average percent slope of the sub basin. SWAT does not adjust curve number for slop. If the user wishes to adjust the curve number for slope effects, the adjustment must be done prior to entering the curve number in the management input file.

**Peak Runoff Rate:** The peak surface runoff rate is the maximum volume flow rate passing a particular location during a storm event. SWAT calculates the peak runoff rate with a modified rational method. In rational method it assumed that a rainfall of intensity i begins at time t = 0 and continues indefinitely, the rate of runoff will increase until the time of concentration, t = $t_{conc}$.

The modified rational method is mathematically expressed as:

$$q_{peak} = \frac{\alpha_{tc} \, . Q_{surf} . Area}{3.6 \, t_{conc}} \quad (2.8)$$

Where: $q_{peak}$ is the peak runoff rate ($m^3/s$), $\alpha_{ct}$ is the fraction of daily rainfall that occurs during the time of concentration, $Q_{surf}$ is the surface runoff (mm),Area is the sub-basin area ($km^2$), $t_{conc}$ is the time of concentration (hr), and 3.6 is a conversion factor.

SWAT estimates the value of α using the following equation:

$$\alpha_{tc} = 1 - exp[2 \, . t_{conc} \, . \ln(1 - \alpha_{0.5})] \quad (2.9)$$

Where $t_{conc}$ is the time of concentration (hr) and $\alpha_{0.5}$ is the fraction of daily rain falling in the Half-hour highest intensity rainfall.

**Time of Concentration:** The time of concentration, $t_{conc}$, is a time within which the entire sub basin area is discharging at the outlet point. It is calculated by summing up both the overland flow time of the furthest point in the sub basin to reach a stream channel ($t_{ov}$) and the upstream channel flow time needed to reach the outlet point ($t_{ch}$):

$$t_{conc} = t_{ov} + t_{ch} \tag{2.10}$$

The overland flow time ($t_{ov}$) is computed as:

$$t_{ov} = \frac{L_{slp}}{3600.\, v_{ov}} \tag{2.11}$$

Where: $L_{slp}$ is the average sub basin slope length (m), $V_{ov}$ is the overland flow velocity (m/s), and 3600 is a unit conversion factor.

The overland flow velocity for a unit width along the slope is calculated by using the Manning's equation:

$$v_{ov} = \frac{{q_{ov}}^{0.4}.\, slp^{0.3}}{n^{0.6}} \tag{2.12}$$

Where $q_{ov}$ is the average overland flow rate ($m^3/s$), Slp is the average slope of the sub basin (m/m), n is Manning's roughness coefficient of the sub basin. Assuming an average flow rate of 6.35 mm/hr and substituting the equation of $V_{ov}$ into $t_{ov}$,

$$v_{ov} = \frac{0.005.\, {L_{slp}}^{0.4}.\, slp^{0.3}}{n^{0.6}} \tag{2.13}$$

Substituting equation 2.13 into equation 2.11 gives:

$$t_{ov} = \frac{{L_{slp}}^{0.6}.\, n^{0.6}}{18.\, slp^{0.3}} \tag{2.14}$$

**Channel flow time of concentration:** Channel flow time of concentration $t_{ch}$ can computed using the equation,

$$t_{ch} = \frac{L_c}{3.6.\, v_c} \tag{2.15}$$

Where $L_c$ is the average flow channel length (km), $V_c$ is the average flow velocity (m/s), and 3.6 is a unit conversion factor.

The average flow channel length is calculated as:

$$L_c = \sqrt{L.\, L_{cen}} \tag{2.16}$$

Where L is the channel length from the furthest point to the sub basin outlet (km), $L_{cen}$ is the distance along the channel to the sub basin centroid (km).

Assuming Lcen= 0.5L, and using the Manning's equation for Vc for a trapezoidal channel with side slope of 2:1 and bottom width to depth ratio of 10:1, channel flow time becomes:

$$t_{ch} = \frac{0.62.\, L.\, n^{0.75}}{Area^{0.125}.\, {slp_{ch}}^{0.375}} \tag{2.17}$$

Where $t_{ch}$ is the time of concentration for channel flow (hr), L is channel length from the most distant point to the sub basin outlet (km), n is Manning's roughness coefficient for the channel, Area is the sub basin area (km2), and $Slp_{ch}$ is the channel slope (m/m).

**Surface Runoff Lag:** In large sub basins with a time of concentration greater than 1 day, only a portion of the surface runoff will reach the main channel on the day it is generated. SWAT incorporates a surface runoff storage feature to lag a portion of the surface runoff release to the main channel.

Once surface runoff is calculated, the amount of surface runoff released to the main channel is calculated as:

$$Q_{surf} = \left(Q'_{surf} + Q_{stor,i-1}\right).\left(1 - exp\left[\frac{-surlag}{t_{conc}}\right]\right) \tag{2.18}$$

Where $Q_{surf}$ is amount of surface runoff discharged to main channel in a day (mm), $Q'_{surf}$ is amount of surface runoff generated in a sub basin in a day (mm), $Q_{stor,i-1}$ is the surface runoff

stored or lagged from the previous day (mm), Surlag, is the surface runoff lag coefficient, and $t_{conc}$ is the time of concentration for the sub basin (hrs).

b) **Routing Phase of the Hydrologic Cycle:**

The routing phase is the second division of hydrological cycle which can be defined as the movement of water, sediments, etc. through the channel network of the watershed to the outlet.

Water is routed through the channel network using the variable storage routing method or the Muskingum River routing method. The variable storage method uses a simple continuity equation in routing the storage volume, whereas the Muskingum routing method models the storage volume in a channel length as a combination of wedge and prism storages. In the latter method, when a flood wave advances into a reach segment, inflow exceeds outflow and a wedge of storage is produced. As the flood wave recedes, outflow exceeds inflow in the reach segment and a negative wedge is produced. In addition to the wedge storage, the reach segment contains a prism of storage formed by a volume of constant cross-section along the reach length.

The variable storage routing method was developed by Williams (1969) and used in the HYMO (Williams and Hann, 1973) and (routing outputs to outlets) ROTO (Arnold et al., 1995).

For a given reach segment, storage routing is based on continuity equation:

$$\Delta V_{stored} = V_{in} - V_{out} \tag{2.19}$$

Where $V_{in}$ is the volume of inflow during the time step ($m^3$ water), $V_{out}$ is the volume of outflow during the time step (m3water), and $\Delta V_{stored}$ is the change in volume of storage during the time step ($m^3$ water).

This equation can also be written as follows:

$$V_{stored,2} - V_{stored,1} = \Delta t.\left(\frac{q_{in,1} + q_{in,2}}{2}\right) - \Delta t\left(\frac{q_{out,1} + q_{out,2}}{2}\right) \tag{2.20}$$

Where $\Delta t$ is the length of the time step (s), $q_{in,1}$ is the inflow rate at the beginning of the time step ($m^3/s$), $q_{in,2}$ is the inflow rate at the end of the time step ($m^3/s$), $q_{out,1}$ is the outflow rate at the beginning of the time step ($m^3/s$), $q_{out,2}$ is the outflow rate at the end of the time step($m^3/s$),

$V_{stored,1}$ is the storage volume at the beginning of the time step ($m^3$ water), and $V_{stored,\ 2}$ is the storage volume at the end of the time step ($m^3$ water).

The travel time is computed by dividing the volume of water in the channel by flow rate.

$$TT = \frac{V_{stored}}{q_{out}} = \frac{V_{stored,1}}{q_{out,1}} = \frac{V_{stored,2}}{q_{out,2}} \quad (2.21)$$

Where TT is the travel time (s), $V_{stored}$ is the storage volume ($m^3$ water), and $q_{out}$ is the discharge rate ($m^3/s$).

The storage coefficient can be defined as:

$$SC = \frac{2\Delta t}{2TT + \Delta t} \quad (2.22)$$

Where SC is the storage coefficient, TT is the travel time (s) and Δt is the length of the time step (s).

#### 2.3.2.3 Potential Evapotranspiration (PET)

As Neitsch et al. (2009) stated, Potential evapotranspiration (PET) was a concept originally introduced by Thorns Waite (1948) as part of a climate classification scheme. He defined PET is the rate at which evapotranspiration would occur from a large area uniformly covered with growing vegetation that has access to an unlimited supply of soil water and that was not exposed to advection or heat storage effects. Because the evapotranspiration rate is strongly influenced by a number of vegetative surface characteristics, Penman (1956) redefined PET as “the amount of water transpired by a short green crop, completely shading the ground, of uniform height and never short of water”. Penman used grass as his reference crop, but later researchers (Jensen, et al., 1990) have suggested that alfalfa at a height of 30 to 50 cm may be a more appropriate choice.

Numerous methods have been developed to estimate PET. Three of these methods have been incorporated into SWAT, Penman-Monteith (Monteith 1965, Allen 1986, Allen et al.1989), Priestley-Taylor (Priestley and Taylor 1972), and Hargreaves (Hargreaves et al.1985) methods..

The model will also read in daily PET values if the user prefers to apply a different potential evapotranspiration method. The three PET methods included in SWAT vary in the amount of required inputs. The Penman-Monteith method requires solar radiation, air temperature, relative humidity and wind speed. The Priestley-Taylor method requires solar radiation, air temperature and relative humidity. The Hargreaves method requires air temperature only (Neitsch et al., 2009). Equations for the three methods are described below:

**Penman Monteith method:** the Penman-Monteith method combines components that account for energy needed to sustain evaporation, the strength of the mechanism required to remove the water vapor and aerodynamics and surface resistance terms. The penman-Monteith equation is:

$$\lambda E = \frac{\Delta.(H_{net} - G) + \rho_{air}.c_p.{}^{[e_z{}^o - e_z]}/_{r_a}}{\Delta + \gamma.\left(1 + {}^{r_c}/_{r_a}\right)} \quad (2.23)$$

Where $\lambda E$ is the latent heat flux density (MJ $m^{-2}$ $d^{-1}$), E is the depth rate evaporation (mm $d^{-1}$), $\Delta$ is the slope of the saturation vapor pressure-temperature curve, de/dT (kPa $C^{-1}$), $H_{net}$ is the net radiation (MJ $m^{-2}$ $d^{-1}$), G is the heat flux density to the ground (MJ $m^{-2}$ $d^{-1}$), $\rho_{air}$ is the air density (Kg $m^3$), $c_p$ is the specific heat at constant pressure (MJ $kg^{-1}$ $C^{-1}$), ${e_z}^o$ is the saturation vapor pressure of air at height z (kPa), $e_z$ is the water vapor pressure of air at height z (kPa), $\gamma$ is the psychometric constant (kPa $C^{-1}$), $r_c$ is the plant canopy resistance (s $m^{-1}$) and $r_a$ is the diffusion resistance of the air layer (aerodynamic resistance) (s $m^{-1}$).

The most accurate estimate of evapotranspiration with penman-Monteith equation are made when evapotranspiration is calculated on an hourly basis and summed to obtain the daily values. Mean daily parameter values have been shown to provide reliable estimates of daily evapotranspiration values and this is used in SWAT.

**Priestley Taylor method:** Priestley and Taylor (1972) developed a simplified version of the combination equation for use when surface areas are wet. The aerodynamic component removed and the energy component was multiplied by a coefficient $\alpha_{pet} = 1.28$ when the general surroundings are wet or under humid conditions.

$$\lambda E_o = \alpha_{pet}.\frac{\Delta}{\Delta+\gamma}.(H_{net} - G) \quad (2.24)$$

Where $\lambda$ is the latent heat flux density (MJ $m^{-2}$ $d^{-1}$), $E_o$ is potential evapotranspiration (mm $d^{-1}$), $\alpha_{pet}$ is the coefficient, $\Delta$ is the slope of the saturation vapor pressure-temperature curve, de/dT (kPa $C^{-1}$), $H_{net}$ is the net radiation (MJ $m^{-2}$ $d^{-1}$), G is the heat flux density to the ground (MJ $m^{-2}$ $d^{-1}$), $\gamma$ is the psychometric constant (kPa $C^{-1}$.

The Priestley-Taylor equation provides potential evapotranspiration estimates for low advective conditions. In Semiarid and arid areas where the advection component of the energy balance is significant, the Priestley-Taylor equation will under estimate the potential evapotranspiration.

**Hargreaves method:** According to Neitsch et al. (2009) the Hargreaves method was originally derived from eight years of cool season Alta fescue grass lysimeter data from Davis, California (Hargreaves, 1975). Several improvements were made to the original equation (Hargreaves and Samani, 1982 and 1985) and the form used in SWAT was published in 1985 (Hargreaves et al., 1985):

$$\lambda E_o = 0.0023.H_o.(T_{mx} - T_{mn})^{0.5}.(T_{av} + 17.8) \quad (2.25)$$

Where λ is the latent heat transfer of vaporization (MJ$Kg^{-1}$), $E_o$ is the potential evapotranspiration (mm$d^{-1}$), $H_o$ is the extraterrestrial radiation (MJ$m^{-2}d^{-1}$), $T_{max}$ is the maximum air temperature for a given day (°C), $T_{min}$ is the minimum air temperature for a given day (°C), $T_{av}$ is the mean air temperature for a given day (°C).

#### 2.3.2.4 Ground Water System

Ground water is water in the saturated zone of earth materials under pressure greater than atmospheric, i.e. positive pressure (Neitsch et al., 2009).

Water in the saturated zone is the only underground water that is available to supply wells and springs and is the only water to which the name ground water is correctly applied .Recharge of the saturated zone occurs by percolation of water from the land surface through the unsaturated zone .The unsaturated zone is, therefore, of great importance to ground-water hydrology (RALPH C. HEATH, 1987).

Streams may be categorized by their relationship to the ground water system. A stream located in a discharge area that receives ground water flow is a gaining or effluent stream. This type of stream is characterized by an increase in discharge downstream. A stream located in a recharge area is a losing or influent stream. This type of stream is characterized by a decrease in a discharge downstream (Neitsch et al., 2009).

SWAT simulates two aquifers in each sub basin. The shallow aquifer is an unconfined aquifer that contributes to flow in the main channel or reach of the sub basin. The deep aquifer is a confined aquifer. Arnold et al. (1993 cited in Neitsch et al., 2009) described, Water that enters the deep aquifer is assumed to contribute to stream flow somewhere outside of the watershed

**I. Shallow Aquifer:** the water balance in shallow aquifer is**:**

$$aq_{sh,i} = aq_{sh,i-1} + w_{rchrg,sh} - Q_{gw} - w_{revap} - w_{pump,sh} \quad (2.26)$$

Where $aq_{sh,i}$ is the amount of water stored in the shallow aquifer on day i (mm), $aq_{sh,i-1}$ is the amount of water stored in the shallow aquifer on day i-1 (mm), $w_{rchrg,sh}$ is the amount of recharge entering the aquifer on day i (mm), $Q_{gw}$ is the groundwater flow, or base flow, into the main channel on day i (mm), $w_{revap}$ is the amount of water moving into the soil zone in response to water deficiencies on day i (mm), and $w_{pump,sh}$ is the amount of water removed from the shallow aquifer by pumping on day i (mm).

Recharge: Water that moves past the lowest depth of the soil profile by percolation or bypass flow enters and flows through the vadose zone before becoming shallow and/or deep aquifer recharge. The lag between the time that water exits the soil profile and enters the shallow aquifer will depend on the depth to the water Table and the hydraulic properties of the geologic formations in the vadose and ground water zone.

The recharge to both aquifers on a given day is calculated as:

$$w_{rchrg,i} = \left(1 - exp\left[\frac{-1}{\delta_{gw}}\right]\right).w_{seep} + exp\left[\frac{-1}{\delta_{gw}}\right].w_{rchrg,i-1} \quad (2.27)$$

Where $w_{rchrg,I}$ is the amount of recharge entering the aquifer on day i (mm), $\delta_{gw}$ is the delay time or drainage time of the overlying geologic formations (days), $w_{seep}$ is the amount of water

exiting the bottom of the soil profile on day i (mm water), $w_{rchrg,i-1}$ is the amount of recharge entering the aquifer on day i-1 (mm).

Groundwater/ Base flow: The shallow aquifer contributes base flow to the main channel or reaches within the sub basin. Base flow is allowed to enter the reach only if the amount of water stored in the shallow aquifer exceeds a threshold value specified by the user.

The steady state response of groundwater flow recharge is:

$$Q_{gw} = \frac{8000.K_{sat}}{{L_{gw}}^2}.h_{wtbl} \quad (2.28)$$

Where $Q_{gw}$ is the groundwater flow, or base flow, into the main channel on day i (mm), $K_{sat}$, is the hydraulic conductivity of the aquifer (mm/day), $L_{bw}$ is the distance from the ridge or sub basin divide for the groundwater system to the main channel (m), and $h_{wtbl}$, is the water Table height (m).

Assuming that variation in groundwater flow is linearly related to the rate of change in water Table height the groundwater flow/base flow is computed as:

$$Q_{gw,i} = Q_{gw,i-1}.exp\left[-\alpha_{gw}.\Delta t\right] + w_{rchrg,sh}.\left(1 - exp\left[-\alpha_{gw}.\Delta t\right]\right) \quad \text{If } aq_{sh} > aq_{shthr,q} \quad (2.29)$$

$$Q_{gw,i} = 0 \qquad \text{If } aq_{sh} \leq aq_{shthr,q}$$

Where $Q_{gw}$ is the groundwater flow, or base flow, into the main channel on day i (mm water), $Q_{gw-1}$ is the groundwater flow, or base flow, into the main channel on day i-1 (mm water), $a_{gw}$ is the base flow recession constant, Δt is the time step (1day), $w_{rchrg,sh}$ is the amount of recharge entering the shallow aquifer on day i (mm water), $aq_{sh}$ is the amount of water stored in the shallow aquifer at the beginning of day i (mm water) and $aq_{shthr,q}$ is the threshold water level in the shallow aquifer for groundwater contribution to the main channel to occur (mm water).

The base flow recession constant, $a_{gw}$, is a direct index of groundwater flow response to changes in recharge (Smedema and Rycroft, 1983). Values vary from 0.1-0.3 for land with slow response to recharge to 0.9-1.0 for land with a rapid response.

When the shallow aquifer receives no recharge equation 2.27 simplified to:

$$Q_{gw} = Q_{gw,0}.exp[-\alpha_{gw}.t] \text{ If } aq_{sh} > aq_{shthr,q} \quad (2.30)$$

$$Q_{gw,i} = 0 \quad \text{If } aq_{sh} \leq aq_{shthr,q}$$

Where $Q_{gw}$ is the groundwater flow, or base flow, into the main channel on day i (mm water), $Q_{gw,o}$ is the groundwater flow, or base flow, into the main channel at the beginning of the recession (time, t =0 ) (mm water), $\alpha_{gw}$ is the base flow recession constant, $aq_{sh}$ is the amount of water stored in the shallow aquifer at the beginning of day i (mm water), t is the time elapsed since the beginning of recession (days) and $aq_{shthr,q}$ is the threshold water level in the shallow aquifer for groundwater contribution to the main channel to occur (mm water).

**REVAP**: water may move from the shallow aquifer into the overlying unsaturated zone. In periods when the material overlying the aquifer is dry, water in the capillary fridge that separates the saturated and unsaturated zone will evaporate and diffuse upward. As water is removed from the capillary fridge by evaporation, it is replaced by water from the underlying aquifer (Neitsch et al., 2009). SWAT models the movement of water into the overlying unsaturated layer as a function of water demand for evapotranspiration.

The maximum amount of water that will be removed from the aquifer via, revap, on a given day is:

$$w_{revap,mx} = \beta_{rev}.E_o \quad (2.31)$$

Where $w_{revap,mx}$ is the maximum amount of water moving into the soil zone in response to water deficiencies (mm water), $\beta_{rev}$ is revap coefficient, and $E_o$ is the potential evapotranspiration for the day (mm water).

II. **Deep aquifer:** The water balance for the deep aquifer is;

$$aq_{dp,i} = aq_{dp,i-1} + w_{deep} - w_{pump,dp} \quad (2.32)$$

where $aq_{dp,i}$ is the amount of water stored in the deep aquifer on day i (mm), $aq_{dp,i-1}$ is the amount of water stored in the deep aquifer on day i-1 (mm), $w_{deep}$ is the amount of water percolating from the shallow aquifer into the deep aquifer on day i (mm), and $w_{pump,dp}$ is the amount of water removed from the deep aquifer by pumping on day i (mm). If the deep aquifer is

specified as the source of irrigation water or water removed for use outside the watershed, the model will allow an amount of water up to the total volume of the deep aquifer to be removed on any given day.

## 2.4 Hydrological Model evaluation

In order to evaluate the model's performance relative to the observed data, the following three performance measures were mostly used: Percent difference between simulated and observed data (D), Correlation coefficient ($R^2$) and Nash and Sutcliffe simulation efficiency ($E_{ns}$) (Nash and Suttcliffe, 1970).

The percent difference measures the average difference between the simulated and measured values for a given quantity over a specified period (usually the entire calibration or validation period in the study). The percent difference can be calculated using the following equation.

$$D = 100\left[\frac{\sum_{i=1}^{n} q_{si} - \sum_{i=1}^{n} q_{oi}}{\sum_{i=1}^{n} q_{oi}}\right] \quad (2.33)$$

Where, $D$ is the percent of difference, $q_{si}$ is the simulated values in each model time step, $q_{oi}$ is the measured values in each model time step. The monthly time step was applied in this study. A value close to 0% is best for D.

The regression coefficient ($R^2$) is the square of the Pearson product–moment correlation coefficient and describes the proportion of the total variance in the observed data that can be explained by the model. The closer the value of $R^2$ to 1, the higher is the agreement between the simulated and the measured flows. It is calculated as using the following equation:

$$R^2 = \frac{[(\sum_{i=1}^{n} q_{si} - \overline{q_s})(\sum_{i=1}^{n} q_{oi} - \overline{q_o})]^2}{\sum_{i=1}^{n}(q_{si} - \overline{q_s})^2 \sum_{i=1}^{n}(q_{oi} - \overline{q_o})^2} \quad (2.34)$$

Where, $R^2$ is the regression coefficient, $q_{si}$ is the simulated values, $\overline{q_s}$ is the average simulated value, $q_{oi}$ is the measured value, $\overline{q_o}$ is the average measured value, n is the number of computed values.

Nash and Sutcliffe simulation efficiency ($E_{Ns}$) indicates the degree of fitness of observed and simulated data. The value of $E_{NS}$ ranges from 1.0 (best) to negative infinity. $E_{NS}$ value of 0.0

means the model predictions are just as accurate as using the measured data average to predict the measured data. $E_{NS}$ values less than 0.0 indicate the measured data average is a better predictor of the measured data than the model predictions while a value greater than 0.0 indicates the model is a better predictor of the measured data than the measured data average (Dilnesaw, 2006). It is calculated as follows with the same variables defined above:

$$E_{NS} = 1 - \frac{\sum_{i=1}^{n}(q_{oi} - q_{si})^2}{\sum_{i=1}^{n}(q_{oi} - \overline{q_o})^2} \quad (2.35)$$

Where, $E_{NS}$ is the Nash and Sutcliffe simulation efficiency, $q_{si}$ is the simulated values, $q_{oi}$ is the measured value, $\overline{q_o}$ is the average measured value, n is the number of computed values.

As Dilnesaw (2006) stated, SWAT developers in Santhi et al., (2001) assumed an acceptable calibration for hydrology at a D<15%, $R^2$ >0.6 and $E_{NS}$> 0.5.

## 2.5 Hydrological Model Calibration, Validation

Calibration is test of a model with known input and output information that is used to adjust or estimate factors for which data are not available. Lijalem (2006) described Calibration as, it is tuning of model parameters based on checking results against observations to ensure the same response over time. This involves comparing the model results, generated with the use of historic meteorological data, to recorded stream flows. In this process, model parameters varied until recorded flow patterns are accurately simulated.

In order to utilize any predictive watershed model for estimating the effectiveness of future potential management practices one need to select values for the model parameters so that the model closely simulates the behavior and performance characteristics of the study site.

Refsgaard and Storm (1996) distinguished three types of calibration methods: the manual trial-and-error method, automatic or numerical parameter optimization method; and a combination of both methods. According to Refsgaard (1996) the first method is the most common, and especially recommended for the application of more complicated models in which a good graphical representation is a prerequisite. However, it is very cumbersome, time consuming, and requires experience. Alternatively, an automatic calibration involves the use of a numerical algorithm, which finds the optimum of a given numerical objective function. This is carried out

by applying the model to numerous combinations and permutations of parameter levels, in order to find the best parameter set in terms of satisfying the criterion of accuracy. The combination means that the manual method is placed at the beginning of the procedure in order to delineate rough orders of magnitude, which is followed by the automatic calibration for fine adjustment. The reverse procedure is also possible, whereby the automatic method is used as a kind of sensitivity analysis to find the most important parameters, which are afterwards manually calibrated.

Validation is comparison of the model outputs with an independent data set without making further adjustments. Model validation confirmed the applicability of the watershed-based hydrologic parameters derived during the calibration process.

Model calibration determines the best or at least a reasonable, parameter set while validation ensures that the calibrated parameters set performs reasonably well under an independent data set (Dilnesaw, 2006).

### 2.6.SDSM Bias Correction

Bias correction compensates for any tendency to over– or under–estimate the mean of conditional processes by the downscaling model (Wilby & Dawson, 2007). Despite to the continuous efforts to improve GCM's capability of simulating historical climates, the use of bias-correction methods is essential for the impact assessment studies of climate change. In assessing potential hydrologic impacts of climate change, a suitable correction of biases in climate model projected temperature and precipitation is the principal focus due to its significant influence on the hydrologic response (Watanabe et al, 2012).

There are different bias correction methods i.e. Linear Scaling (LS), LOCal Intensity scaling (LOCI), Power transformation (PT), Variance scaling (VARI), Distribution mapping (DM) and Quantile Mapping (QM). Different researches were carried out to compare these bias correction methods. Fang et al (2014) conducted researches to compare the different bias correction methods in downscaling meteorological variables for hydrologic impact study in an arid area in China and they found that for temperature correction all bias correction methods are equally plausible in correcting raw temperature whereas for precipitation Distribution mapping (DM) and Quantile Mapping (QM) performed equally best. Moreover the study showed that Linear

Scaling (LS) method is the simplest way of bias correction both for temperature and precipitation which perfectly match the monthly mean of corrected values with that of observed ones. For this study the simplest way (linear correction method) was applied due to its simplicity and the objective of the study mainly focuses on mean differences. In LS method, Precipitation is typically corrected with a multiplier and temperature with an additive term on a monthly basis.

$$P_{cor,m,d} = P_{raw,m,d} . \frac{\mu(P_{obs,m})}{\mu(P_{raw,m})} \quad 2.36$$

$$T_{cor,m,d} = T_{raw,m,d} + \mu(T_{obs,m}) - \mu(T_{raw,m}) \quad 2.37$$

Where $P_{cor,m,d}$ and $T_{cor,m,d}$ are corrected precipitation and temperature on the d$^{th}$ day of m$^{th}$ month and $P_{raw,m,d}$ and $T_{raw,m,d}$are the raw simulated precipitation and temperature on the d$^{th}$ day of m$^{th}$ month. μ(.) represents the expectation operator (e.g. $\mu(T_{obs,m})$) rep-resents the mean value of observed temperature at given month m).

# 3. MATERIALS AND METHODS

In this chapter the detail description of the study area, the general methodologies and materials required to achieve the specific objective of this study were precisely described.

## 3.1 Description of the Study Area

### 3.1.1 General

Gumara watershed, drained by Gumara Rivers, is located in south Gonder zone of the Amhara National Regional State, at 624 KM North of Addis Ababa. This watershed is part of the Abay Basin and more particularly part of Lake Tana sub-basin which is situated on the North Eastern side of Lake Tana and contributes significant inflows to the Lake Tana. It drains Dera, Farta, Fogera and some part of Estie Woredas and the gauged part covers 1394 $km^2$. The geographical location of the watershed is between $11^0$ 34' 41.41" N and $11^0$ 56' 36.95" N latitude to $37^0$ 29' 30.48" E and $38^0$ 10' 58.01" E longitude. River originates on the high plateau to the east, which is characterized by mountainous, highly rugged and dissected topography with steep slopes and drains to the plain in the west, characterized by valley floor with flat to gentle slopes where the River overflows its bank during the rainy season (Yibeltal, 2008). The elevation of the watershed ranges from 1800 m.a.s.l. at the lake to 3704 m.a.s.l. at the highlands, with slopes (Maria, 2012) ranging from 0% to more than 70%.

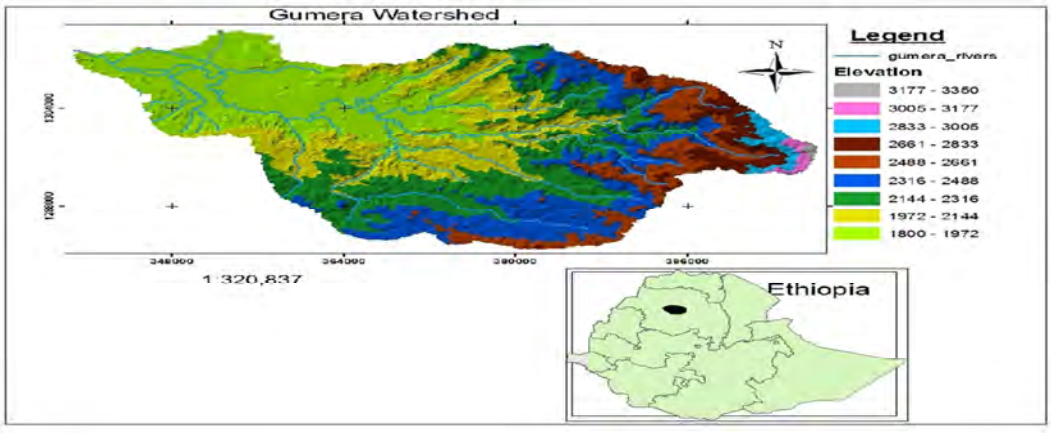


Figure 3.1: Location Map of Watershed

### 3.1.2 Land use and Land Cover

The dominant land use of the watershed is rain fed agriculture and cultivated land is in a various forms including intensively cultivated, cultivated land with scattered trees, cultivated land with trees and shrubs and seasonally cultivated lands. More than three quarter of all land in the watershed has already been brought under cultivation. The major crops grown in the watershed are Teff, maize, Barley, Wheat and other cereals. Teff is the main staple food crop in the area. Bush or shrub land, grazing land, forest/wood land and wetland/swap are other land cover types in the watershed (WWDSE, 2007). Wetlands/swamp areas are commonly existent on the lower banks of Rivers, mainly of River and near Lake Tana. As it can be shown in the figure 3.2, the majority of the catchment is covered by crop land (cultivated), while the remaining are covered by leafy forests, shrubs, grasses and some are bar land and wet land.

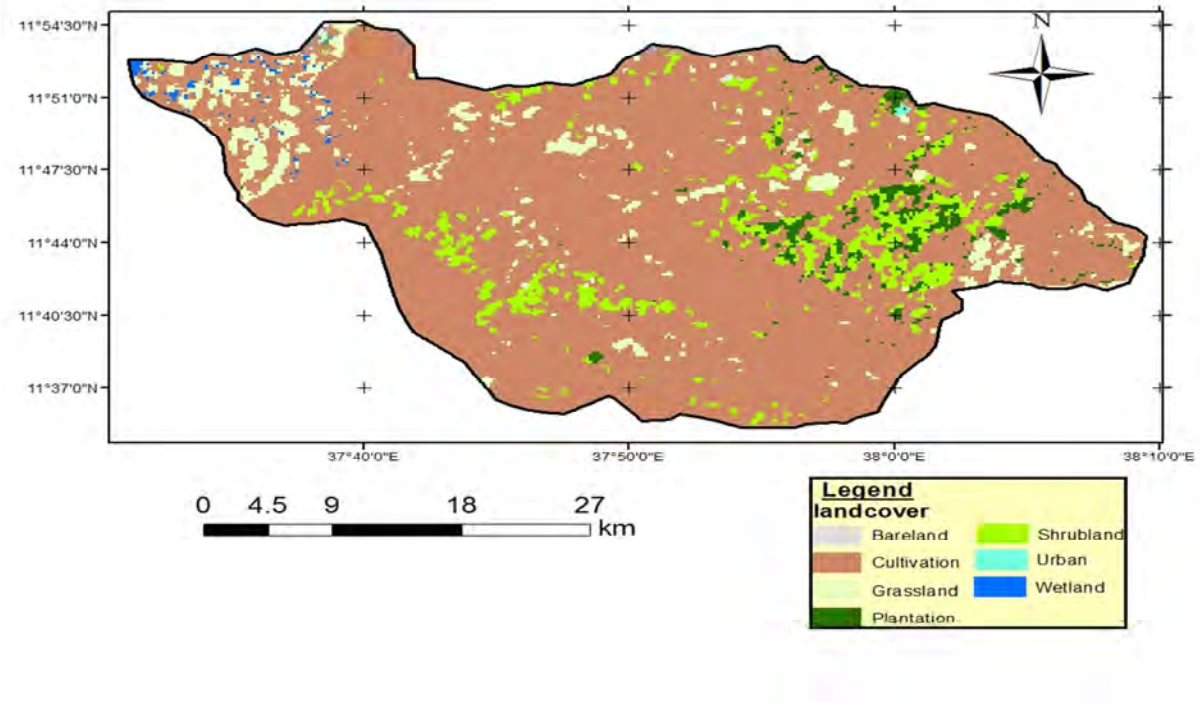


Figure 1.2: land cover map of Gumara catchment (obtained from Bahir Dar University)

### 3.1.3 Soil Type of the Study Area

Soil data information as per FAO soil group is available at the ministry of water resource GIS department. The data was compiled during master plan study of the Abay River basin

study. Based on the data acquired from the ministry water resources GIS department and as per FAO soil classification, the catchment is dominantly covered by haplic luvisols, eutric vertisols, eutric fluvison, eutric leptosols and chronic luvisols.

### 3.1.4 Climate of the Study Area

There are about some meteorological stations within the study area and its surroundings such as Bahir Dar, Debre Tabor, Amedber, Woreta, Amde Genet, Nifas Mewucha, Wanzaye and Gassay which are monitored by Ethiopian Meteorological Agency. Out of which Bahir Dar and Debre Tabor are first classes while others are second and third class stations.

The annual climate may be divided in to two, rainy and dry season. The rainy season may be divided into a minor rainy season in March to May (Belg) and a major rainy season from June through September (Kiremit). The dry season occurs between October and February (Bega). According to WWDSE (2007) the four wettest months cover 85percent of the total annual rainfall. While the remaining months, being from October to May has a total rainfall of about 15% of the mean annual rainfall. The mean annual rainfall and temperature of the area varies spatially from station to station. Based on the data obtained from Ethiopian Meteorological Agency, the mean annual rainfall is 1528mm (1986-2005) at Debre Tabor station, 1288mm (1992-2008) at Woreta and 1279mm (1986-2005) at Bahir Dar station while the maximum (minimum) temperature are $27.02^{o}$c($9.51^{o}$c), $27.5^{o}$c($9.6^{o}$c) and $27.95^{o}$c($11.97^{o}$c) at Debre Tabor, Bahir Dar and Woreta stations respectively.

### 3.1.5 Hydrology

Gumara is one of the major Rivers which contributes significant amount of inflow to Lake Tana. For this reason the Ethiopian ministry of water resources installed gauging station downstream of the River. The gauging station is located at $11^{0}$ 50’ 0” N and $37^{0}$ 38’ 0” E and measures daily instantaneous flows of the River since 1959 and covers the area of 1394 $km^2$. According to Ephrem (2011) Gumara River has 21 tributaries and the total length of the River is 99.6 km.

Based on the recorded flow data obtained from Ethiopian Ministry of Water Resources hydrology department, the average daily flow of the River is 34.12$m^3$/s (1986-2005).

## 3.2 Modeling Approach

The modeling approaches were divided in to two major parts. The first part was climate change modeling approach and the second was hydrological modeling approach.

### 3.2.1 Climate Change Modeling Approach

#### 3.2.1.1 General Circulation Model (GCM) outputs

Global Circulation Model (GCM) derived scenarios of climate change were used for predicting the future climates of the study area based on criteria proposed by the Intergovernmental Panel on Climate Change (IPCC). Among the wide range of GCM models HadCM3, (Hadley Centre for Climate Prediction and Research, England), ECHAM4 (Max Plank Institute, Hamburg, Germany), CGCM2 (Canadian Centre of Climate Modeling and Analysis), GFDL_R30 (Geophysical Fluid Dynamics Laboratory & NOAA), and CCSR/NIES (Centre for Climate Systems Research & Japanese National Institute for Environmental Studies) are commonly used. Use of average outputs of different GCMs can minimize the uncertainties associated with each GCMs and can result in plausible future climates for impact studies (Lijalem, 2006).

However, as this study was carried out within a very short period of time, only the HadCM3 model was selected for the impact study. Besides, the HadCM3 GCM output is chosen since the model is widely used for climate change impact assessment and the results of HadCM3 can be easily downscaled using SDSM (Dile et al., 2013).

For HadCM3 the model result is available for A2 (medium-high) and B2 (medium-low) emission scenarios. For this study the ensemble “a” is considered for A2a and B2a experiments (the “a” in A2a and B2a refers the ensemble member in the HadCM3 A2 and B2 experiments).

#### 3.2.1.2 Downscaling Techniques

There are different down scaling methods used to relate regional scale atmospheric predictor variables to local-scale surface weather and the detail of each are described in section 2.2.3. According to Wilby and Dawson (2007), Statistical downscaling methods have several practical advantages over dynamical downscaling approaches. In situations where low–cost, rapid assessments of localized climate change impacts are required, statistical downscaling (currently) represents the more promising option. Thus for this study SDSM 4.2- a decision support tool for

the assessment of regional climate change impacts developed by Wilby and Dawson (2007) was used to downscale large scale predictors and it was freely downloaded from http://www.sdsm.org.uk

SDSM develops statistical relationships, based on multiple linear regression techniques, between large-scale (predictors) and local (predictand) i.e. precipitation and maximum and minimum temperature for this study which could be used as input for hydrological modeling.

### 3.2.1.3 Predictor Variables

Large-scale predictor variable informations are freely obtained from the Canadian climate impact scenario group with web address of: http://www.cics.uvic.ca/scenarios/sdsm/select.cgi/. The National Center for Environmental Prediction (NCEP_1961-2001) reanalysis data and HadCM3 predictor variables for the A2a and B2a are obtained on a grid by grid box basis from a resolution of 2.5° latitude by 3.75° longitude. The geographical location of the watershed is between $11^0$ 34' 41.41" N and $11^0$ 56' 36.95" N (average $11^0$ 45'40" N) to $37^0$ 29' 30.48" E and $38^0$ 10' 58.01" E (average $37^0$ 20' 45" E). Hence the required predictor data that represents the watershed were downloaded from the nearest average location of the watershed.

The predictor data files downloaded from the grid of interest consists of the following three directories:

NCEP_1961-2001: This directory contains 41 years of daily observed predictor data, derived from the NCEP reanalysis, normalized over the complete 1961-1990 period. .

H3A2a_1961-2099: This directory contains 139 years of daily GCM predictor data, derived from the HadCM3 A2 (a) experiment, normalized over the 1961-1990 period.

H3B2a_1961-2099: This directory contains 139 years of daily GCM predictor data, derived from the HadCM3 B2 (a) experiment, normalized over the 1961-1990 period.

Large-scale predictor variable information i.e. National Center for Environmental Prediction (NCEP_1961-2001) reanalysis data set were used for the calibration and validation of SDSM with the observed precipitation, maximum and minimum temperature at Debre Tabor station and

HadCM3 (Hadley centre Climate Model 3) GCM (H3A2a_1961-2099 and H3B2a_1961-2099 data were used for the baseline and climate scenario generation.

#### 3.2.1.4 Quality Control

Few meteorological stations have 100% complete and/or fully accurate data sets. Handling of missing and imperfect data is necessary for most practical situations. Simple Quality Control checks in SDSM enable the identification of gross data errors, specification of missing data codes and outliers prior to model calibration (Wilby and Dawson, 2007).

The precipitation and maximum and minimum temperature at Debre Tabor, Bahir Dar station, Woreta, Amde Genet, Nifas Mewucha, Wanzaye and Amedber were collected from the Ethiopian National Meteorological Agency. However, there are higher missed values in most weather stations except Bahir Dar and Debre Tabor in which the predictand variables are comparatively consistent and lower missed values. After visual inspection and correlation analysis was done Debre Tabor station was selected for downscaling due to their long-term and high-quality data and hence the predictand variables from Debre Tabor weather station was used in this study.

#### 3.2.1.5 Screening Predictor Variables

Identifying the empirical relationships between gridded predictors and single site predictands (such as station precipitation, maximum and minimum temperature) is central to all statistical downscaling methods and is often the most time consuming step in the process (Wilby and Dawson, 2007). The main purpose of the Screen Variables operation is to assist the user in the selection of appropriate downscaling predictor variables for model calibration. The decision process is also complicated by the fact that the explanatory power of individual predictor variables varies both spatially and temporally.

Screening is identifying the downscaling predictors which have high correlation with the actual climate variables. The model correlates each predictands (observed precipitation, maximum and minimum temperature) at Debre Tabor with National Center for Environmental Prediction (NCEP) downloaded predictor data. Annual analysis period was used which provides the predictor-predictand relationship all along the months of the year.

Table 3.1: List of Predictor variables derived from African window for the grid on the study area (Twenty six predictor variables)

| predictor variable | description | predictor variable | description |
|---|---|---|---|
| mslpaf | men sea level pressure | p5 Zha | 500hpa divergence |
| p_faf | surface air flow strength | p8_faf | 850hpa airflow strength |
| p_uaf | surface zonal velocity | p8_uaf | 850hpa zonal velocity |
| p_vaf | surface meridinal velocity | p8_vaf | 850 hpa meriodinal velocity |
| p_zaf | surface vorticity | p_zaf | 850 hpa vorticity |
| p_thaf | surface wind direction | p850af | 850hpa geopotential height |
| p_zhaf | surface divergence | p8thaf | 850hpa wind direction |
| p5_faf | 500hpa air flow strength | p8zhaf | 850 hpa divergence |
| p5_uaf | 500pa zonal velocity | r500af | relative humidity at 500 hpa |
| p5_vaf | 500hpariodinal velocity | r850af | relative humidity at 850 hpa |
| p5_zaf | 500hpa vorticity | rhumaf | near surface relative humidity |
| p500af | 500hpa geopotential height | shumaf | surface specific humidity |
| p5thaf | 500hpa wind direction | tempaf | mean temperature at 2 m |

SDSM model has two processes to be specified before the analysis takes place i.e. Conditional and unconditional processes. In case of daily temperature where the predictand-predictor process is not regulated by intermediate process unconditional process was used, whereas for daily precipitation where the amounts depend on the occurrence of wet-day, the conditional process was chosen. Significance value is used to test the significance of predictor–predictand correlations and it was set as the default of ($p<0.05$ (5%)).

Several analyses were made by selecting a maximum of 6 out of 26 predictor variables at a time till best predictor-predictand correlations were found even though up to 12 predictors (Wilby and Dawson 2007) are possible to select at a time.

The strength of the individual predictors varies on a month by month basis. Hence the most appropriate combination of the predictors with the predictand was chosen by looking the analysis output of all months.

The Correlation matrix was done to investigate inter–variable correlations for annual sub–periods to identify the amount of explanatory power that is unique to each predictor.

#### 3.2.1.6 SDSM Calibration

The Calibration Model process constructs downscaling models based on multiple regression equations, given daily weather data (the predictand i.e. observed precipitation, maximum and minimum temperature at Debre Tabor station and regional–scale, atmospheric predictor variables which were derived from the NCEP re-analysis data set.

The model type should be checked to determine the temporal resolution of the downscaling model i.e. either Monthly, Seasonal or annual. In Monthly models, different model parameters are derived for each month. In Seasonal models, all months in the same season (e.g., December, January and February for winter) have the same model parameters. In Annual models, all months have the same parameters (i.e., there is no attempt to specify intra–annual variations in parameter values) (Wilby & Dawson, 2007). Hence, for this study, the calibration was done for the period of 10 years (1986-1995) at a monthly model type in order to see the monthly temporal variations.

The downscaling process is Unconditional for daily temperature value and Conditional for precipitation. Since for conditional processes in which the distribution of predictand values is skewed, the Fourth root transformations were applied.

#### 3.2.1.7 Weather Generator and Validation

Ensembles of synthetic daily weather series were produced using NCEP re–analysis atmospheric predictor variables and regression model weights produced by the Calibrate Model operation. The Weather Generator enables the verification of calibrated models (assuming the availability of independent data) as well as the synthesis of artificial time series representative of present climate conditions. The Weather Generator can also be used to reconstruct predictands or to infill missing data.

Ensemble members, up to a maximum of 100 are possible, and hence in this research the ensemble size of 20 (default) were used. Individual ensemble members are considered equally plausible local climate scenarios realized by a common set of regional-scale predictors. (Wilby and Dawson, 2007) noted that the extent to which ensemble members differ depends on the relative significance of the deterministic and stochastic components of the regression models used for downscaling. Hence local temperatures are largely determined by regional forcing and

the difference between the ensemble members is similar looking whereas precipitation series display more “noise” arising from the local factors and show larger differences between individual ensemble members.

An independent predictand variables from 1996-2000 at Debre Tabor station were used for model validation.

#### 3.2.1.8 Scenario Generation

The Scenario Generator operation produces ensembles of synthetic daily weather series given daily atmospheric predictor variables supplied by a GCM (either under present or future greenhouse gas forcing) (Wilby and Dawson, 2007).

The IPCC recommends the use of A2 (medium-high emission) and B2 (medium-low emission) for inter-comparison studies because the computing cost of all scenarios in GCM is too expensive. These two scenarios are common to all GCM (Zeryehun, 2009). Hence for this study, the HadCM3A2a and HadCM3B2a were the two GCM output files used for the scenario generation. The regression weights produced during the calibration process were applied to the time series outputs of the GCM model. This is based on the assumption that the predictor-predictand relationships under the current condition remain valid for future climate conditions. Twenty ensembles of synthetic daily time series data were produced for each of the two SRES scenarios for a period of 139years (1961 to 2099). Finally the mean of the twenty ensembles for the specified period was produced for maximum and minimum temperature and precipitation. The period from 1986-2000 were considered as a base period whereas the period from 2001-2099 were considered as future periods. The future periods were divided into four time horizons from 2001-2025, 2026-2050, 2051-2075 and 2076-2099 and analyses were made for each time horizons.

#### 3.2.1.9 Bias Correction Methods

For this study Linear Scaling (LS) method was adapted to correct the model errors due to its simplicity and the objective of the study mainly focuses on mean differences. It operates with monthly correction values based on the differences between observed and raw data (GCM-

simulated data in this case). Precipitation is typically corrected with a multiplier and temperature with an additive term on a monthly basis.

In bias correction methodology, the bias behavior of the model does not change with time i.e. the transfer function is time independent and thus applicable in the future (Hagemann and Haerter, 2011). The correction factors derived during the base period (1986-2000) were applied for the future period (2001-2099). First the SDSM model simulates the reanalysis and GCM data using the default bias correction factor of 1.0.The default value of 1.0, indicating no bias correction. Then after the simulated results were corrected based on linear scaling method and the changing factor were also applied for the future periods.

For future scenarios, the climate signal (difference between future and baseline climates) was first removed before the correction is adjusted. Then the future simulated results were added (temperature) and multiplied (precipitation) with the changing factor obtained in the baseline correction for each month. Then, the climate signal is added back to create a precipitation and temperature scenario for the future.

### 3.2.2 SWAT Hydrological Modeling Approach

SWAT is a River basin scale, continuous time, a spatially distributed model developed to predict the impact of land management practices on water, sediment and agricultural chemical yields in large complex watersheds with varying soils, land use and management conditions over long period of time. The model can be used to simulate a single watershed or a system of multiple hydrologically connected watersheds (Neitsch et al., 2009).

The main reasons for the selection of SWAT model for this study are due to the model's moderate input data requirement (uses readily available inputs), ability to simulate the major hydrological processes and its availability. Moreover the model is physically based, spatially distributed, and belongs to the public domain. SWAT can also simulates hydrological outputs based on a changed climate if the changes in the climate parameters are given as an input to the model.

Here, the methodological steps which were carried out in SWAT model were described in the following section.

#### 3.2.2.1 Watershed Delineation

The watershed delineation carries out advanced GIS functions to aid the user in segmenting watersheds into several hydrologically connected sub-watersheds for use in watershed modeling with SWAT (M. Winchell et al., 2010). Gumara watershed was delineated based on the automatic procedure using digital elevation models (DEM) data. A digital elevation model (DEM) tile of 30m resolution for latitude 11º 45' 39"N and longitude 37º 38' 44" E respectively was obtained from Bahir Dar university geography department and hence used for delineating the Gumara Sub-watershed.

The initial stream network and sub basin outlets were defined based on a drainage area threshold (DEM- based). After creating initial stream networks and sub basin outlets were defined, the final stream network and outlet configuration used for modeling were refined by deleting and adding outlets. Based on the manually added outlets the Gumara watershed was partitioned into sixteen hydrologically connected sub basins and the final outlets found at the gauging station was used for comparison of measured and predicted flows.

#### 3.2.2.2 Hydrological Response Unit (HRU) Definition

After watershed delineation of Gumara watershed was completed, the Hydrologic Response Units (HRU) were defined in ArcSWAT by overlaying soils, land use and slope classes that enables the model to reflect differences in evapotranspiration and other hydrologic conditions for different land covers/crops and soils which increases (Neitsch et al., 2009) the accuracy of load predictions and provides a much better physical description of the water balance.

The HRUs were determined by assigning multiple HRUs for each subwatershed by considering the sensitivity of the hydrologic processes based on a certain threshold values of soil/land use combinations as it better describes the heterogeneity within the watershed and accurately simulates the hydrologic processes.

The final HRU were defined based on a threshold percentage, i.e. Only those land use classes, soil units and slope classes in a sub-catchment were taken into account, which were larger than the respective threshold value. For most applications, the default setting for land use threshold (20%), soil threshold (10%) and slope threshold (20%) are adequate (Neitsch et al.,

2009). Hence in this research the threshold values of 5% for land use, 5% for soils and 15% for slope classes were used to reduce those very small HRU. Based on the threshold percentage values, the Gumara watershed was partitioned into 102 HRUs.

#### 3.2.2.3 Weather Generation

Long periods of daily weather data are required for hydrological models simulation. But in many areas such data are either incomplete or records may not have sufficient length, which is the case in this study.

SWAT requires daily values of precipitation, maximum and minimum temperature, solar radiation, relative humidity and wind speed. The weather data collected from seven stations in the study area have; however, missing data. As SWAT has a built in weather generator that is used to fill the gaps, all the missing values were filled with a missing data identifier, -99 and the weather generator first independently generates missed values of the day. Therefore, in order to fill the missing data, daily rainfall, temperature, wind speed, solar radiation and relative humidity data from, Bahir Dar, Woreta and Debre tabor weather stations were used as an input to calculate statistical monthly weather generator parameters which are calculated by Weather parameter calculator program. Using thus three stations the SWAT model generates representative weather variables for Gumara watershed using Thiesen polygon method for and fills the missed values.

The weather generator input parameters contains statistical data needed to generate representative daily climate data for the sub basin. and thus parameters for this study are found in appendix B.

#### 3.2.2.4 Surface Runoff Volume and Peak Runoff Rate

SWAT provides two methods for estimating surface runoff: the SCS curve number method (SCS 1972) and the Green & Ampt infiltration method (1911). Even though the latter method is better in estimating runoff volume accurately, unavailability of sub-daily time step data makes it difficult to be used for this study. Hence, for this study the SCS curve number method was adopted.

SWAT calculated the peak runoff rate with a modified rational method. In rational method it assumed that a rainfall of intensity i begins at time t = 0 and continues indefinitely, the rate of runoff will increase until the time of concentration, t = $t_{conc}$.

### 3.2.2.5 Potential Evapotranspiration Estimation

Penman (1956) defined PET as "the amount of water transpired by a short green crop, completely shading the ground, of uniform height and never short of water". Penman used grass as his reference crop.

Numerous methods have been developed to estimate PET. Three of these methods have been incorporated into SWAT: Penman-Monteith (Monteith 1965, Allen 1986, Allen et al.1989), Priestley-Taylor (Priestley and Taylor 1972), and Hargreaves (Hargreaves etal.1985) methods. The model will also read in daily PET values if the user prefers to apply a different potential evapotranspiration method. The three PET methods included in SWAT vary in the amount of required inputs. The Penman-Monteith method requires solar radiation, air temperature, relative humidity and wind speed. The Priestley-Taylor method requires solar radiation, air temperature and relative humidity. The Hargreaves method requires air temperature only (Neitsch et al., 2009).

For this study the Penman-Monteith method was applied for Gumara watershed and able to simulate potential evapotranspiration near to the measured values.

### 3.2.2.6 Ground Water

SWAT assumes two layers of aquifers while simulating the ground water balance i.e. shallow-unconfined aquifer, and a deep-confined aquifer. The unconfined shallow aquifer contributes to flow in the main channel or reach of the sub basin, whereas the deep confined aquifer assumed to contribute to stream flows outside the watershed. The volume of water available in the shallow aquifer is governed by the recharge from the top soil profile (recharge), the flow into the main stream channels or reach (base flow), the movement into the overlying unsaturated zone (revap),and the flow to the deep aquifer (deep percolation).

Base flow occurs only when the amount of water stored in the shallow aquifer exceeds a threshold volume of water. In SWAT model, the threshold water depth in the shallow aquifer between 0-5000mm is considered.

In this study the threshold water depth was identified as one of the sensitive parameters that affect the base flow. Hence, the threshold water depth used for calibration of SWAT model was obtained by varying the depth of water within the allowable ranges. First the Swat model was run using the default values of threshold water depth. Then after, the values were adjusted with in the tolerable ranges until the fitted value was obtained. The final fitted value was used further for validation of the SWAT model.

#### 3.2.2.7 Flow Routing

The second phase of the SWAT hydrologic simulation, the routing phase, consists of the movement of water, sediment and other constituents (e.g. nutrients, pesticides) in the stream network.

Two options are available to route the flow in the channel networks: the variable storage and Muskingum methods. Both are variations of the kinematic wave model. While calculating the water balance in the channel flow, the transmission and evaporation are also well considered by the model.

For this study, the variable storage method was used which is based on a simple continuity equation in routing the storage volume.

#### 3.2.2.8 SWAT Model setup, calibration and validation Approach

##### 3.2.2.8.1 Base Flow Separation

For calibration of simulated flows, the total gauged stream flow data was separated into surface and base flow components. Both the base flow and surface runoff were used during the model calibration to compare the observed with the simulated values at Gumara gauge station. This provided insight into the components that needed to be adjusted further for better results. The stream flow data from 1991-2005 obtained from Ethiopian Ministry of Water Resources hydrology department were separated in to base flow and surface flow using the automated

digital filter methods. The automated filter method is (Arnold etal. 1995) fast and objective method of continuous base flow separation and that is why it was adopted for this research.

As Arnold, etal (1995) stated, Nathan and McMahon (1990) described that the automated base flow separation and recession analysis technique is developed based on the recursive digital filter techniques. The filter can be passed over the stream flow data three times (forward (Base flow Fr1), backward (Base flow Fr2), and forward (Base flow Fr3)). Each pass results in less base flow as a percentage of total flow and in general, the fraction of water yield contributed by base flow should fall somewhere between the value for base flow Fr1 and base flow Fr2. Hence, for this study the fraction of water yield contributed by base flow between the value for Base flow Fr1 and Base flow Fr2 was adopted for calibration of simulated flows.

#### 3.2.2.8.2 SAWT Sensitivity Analysis

Sensitivity analysis is a method of minimizing the number of parameters to be used in the calibration step by making use of the most sensitive parameters largely controlling the behavior of the simulated process.

The sensitivity analysis was undertaken by using a built-in tool in SWAT that uses the Latin Hypercube One-factor-At-a-Time (LH-OAT) design method.

The LH-OAT sensitivity analysis method combines thus the robustness of the Latin Hypercube sampling that ensures the full range of all parameters has been sampled with the precision of an OAT designs assuring that the changes in the output in each model run can be unambiguously attributed to the input changed in such a simulation leading to a robust and efficient sensitivity analysis method (Ann van Griensven, 2005).

After running the sensitivity analysis, the mean relative sensitivity (MRS) of the parameters were used to rank the parameters, and their category of sensitivity were also defined based on the Lenhart et al. (2002) classification i.e. small to negligible ($0 \leq MRS < 0.05$), medium ($0.05 \leq MRS < 0.2$), high ($0.20 \leq MRS < 1.0$), and very high ($MRS \geq 1.0$).

Based on these classifications, sensitive parameters with mean relative sensitivity value of medium to very high were selected for calibration of the simulated flows for Gumara Rivers. The higher the value of mean relative sensitivity, the higher will be the influence on the run off.

#### 3.2.2.8.3 SWAT Model Calibration

Refsgaard and Storm (1996) distinguished three types of calibration methods: the manual trial-and-error method, automatic or numerical parameter optimization method; and a combination of both methods. According to Refsgaard (1996) the first method is the most common, and especially recommended for the application of more complicated models in which a good graphical representation is a prerequisite.

For this research work, the manual calibration was adopted until the model objective functions reached a satisfactory level (i.e. D<15%, $R^2$ >0.6 and $E_{NS}$> 0.5). The procedure for manual calibration of the SWAT model for flow is as it is recommended by SWAT developers in Santhi et al. (2001). Initially, base flow was separated from surface flow for both observed and simulated stream flows using an automated digital filter technique. After separation of the base flow and surface flow, The surface runoff was calibrated by adjusting sensitive parameters that affect surface runoff which were identified during sensitivity analysis until a satisfactory objective function was achieved (i.e. D<15%, $R^2$ >0.6 and $E_{NS}$> 0.5).

Thereby, with the same criteria calibration of base flow parameters followed by adjusting the sensitive parameters which affects groundwater contribution and surface runoff was continually rechecked as the base flow calibrating variables also affect surface runoff simulation.

Stream flows measured at Gumara River gage station from 1991-2000, were used for calibrating of the model including the first two years warm up period.

#### 3.2.2.8.4 SAWT Model validation

Validation of Gumara River flows were done with an independent data set without making further adjustments of the calibration parameters. The process continued till simulation of validation-period stream flows confirm that the model performs satisfactorily. Model validation confirmed the applicability of the watershed-based hydrologic parameters derived during the calibration process.

For this study Stream flows measured at Gumara River gage station from 2001-2005 were used for the validation process to evaluate the model accuracy.

### 3.2.2.9 Input Data for SWAT Hydrological Modeling

The major spatially distributed and temporally varied data that are collected for hydrological modeling are digital elevation model (DEM) data, weather data, soil data, land use data and River flow data.

#### 3.2.2.9.1 Digital Elevation Model (DEM) Data

The Digital Elevation Model (DEM) is any digital representation of a topographic surface and specifically to a raster or regular grid of spot heights. It is the basic input of SWAT hydrologic model to delineate watersheds and River networks.

The first step in creating the model input is the watershed delineation accomplished using digital elevation data. DEM is the first input of SWAT model for delineating the watershed to be modeled. Based on threshold specifications and the DEM, the SWAT Arc View interface was used to delineate the watershed into sub basins and subsequently, sub basins were divided into Hydrologic Response Units (HRU)

The DEM was also used to analyze the drainage patterns of the land surface terrain. Sub basin parameters such as slope gradient, slope length of the terrain, and the stream network characteristics such as channel slope, length, and width were derived from the DEM.

For this study, a digital elevation model (DEM) tile of 30m resolution for latitude 11º 45’ 39”N and longitude 37º 38’ 44” E respectively was obtained from Bahir Dar University geography department and hence used for delineating the Gumara watershed.

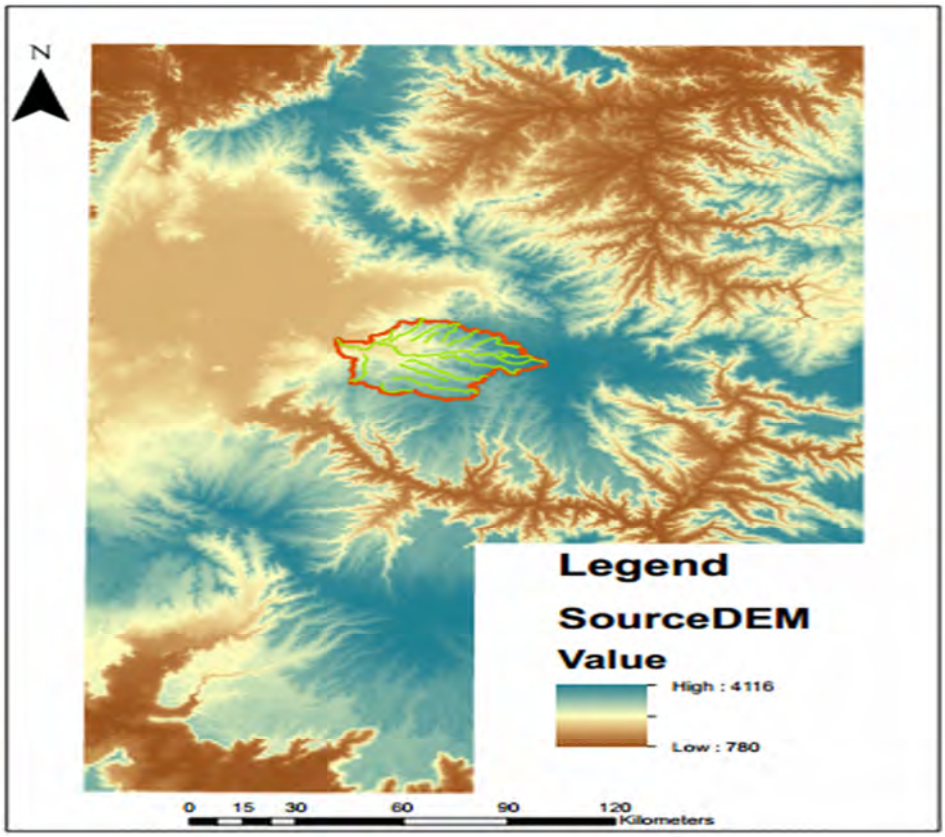


Figure 3.3: Source DEM used for Delineation (obtained from Bahir Dar University)

**3.2.2.9.2 Land Use Land Cover Data**.

The Land use of the Gumara catchment is one of the most important factors that affect surface erosion, runoff, and evapotranspiration in a watershed.

SWAT requires the land use land cover data to define the Hydrological Responses Units (HRU). The land use land cover map of the study area was obtained from the ministry of water resources GIS department and from Bahir Dar University Geography department. Moreover Mequanint (2008) used Updated land use land cover map of Gumara watershed obtained from WWDSE (2007) and it is also adopted for this study. Based on these data the SWAT major land use land cover map was produced by overlying the land use shape files. Then after the major land use land cover classification were sub divided into sub classes mainly based on dominant crops for cultivated lands. As it can be shown in the figure 3.4 the majority of the catchment is covered by crop land (cultivated), while the remaining are covered by leafy forests, shrubs, grasses and some are bar land and wet land.

Table 3.2: SWAT Major Land Use Classes, Codes and Areal Coverage

| Land use | SWAT code | Area (ha) | % watershed area |
|---|---|---|---|
| Agricultural Land-Close-grown | AGRC | 27480 | 21.63 |
| Agricultural Land-Generic | AGRL | 62742.3 | 49.39 |
| Agricultural Land-Row Crops | AGRR | 17552.8 | 13.82 |
| Range-Grasses | RNGE | 2754.52 | 2.17 |
| Range-Brush | RNGB | 3140.7 | 2.47 |
| Wetlands-Non-Forested | WETN | 33.42 | 0.03 |
| Pasture | PAST | 9525.64 | 7.5 |
| Residential | URBN | 69.8023 | 0.05 |
| Forest-Mixed | FRST | 3732.04 | 2.94 |

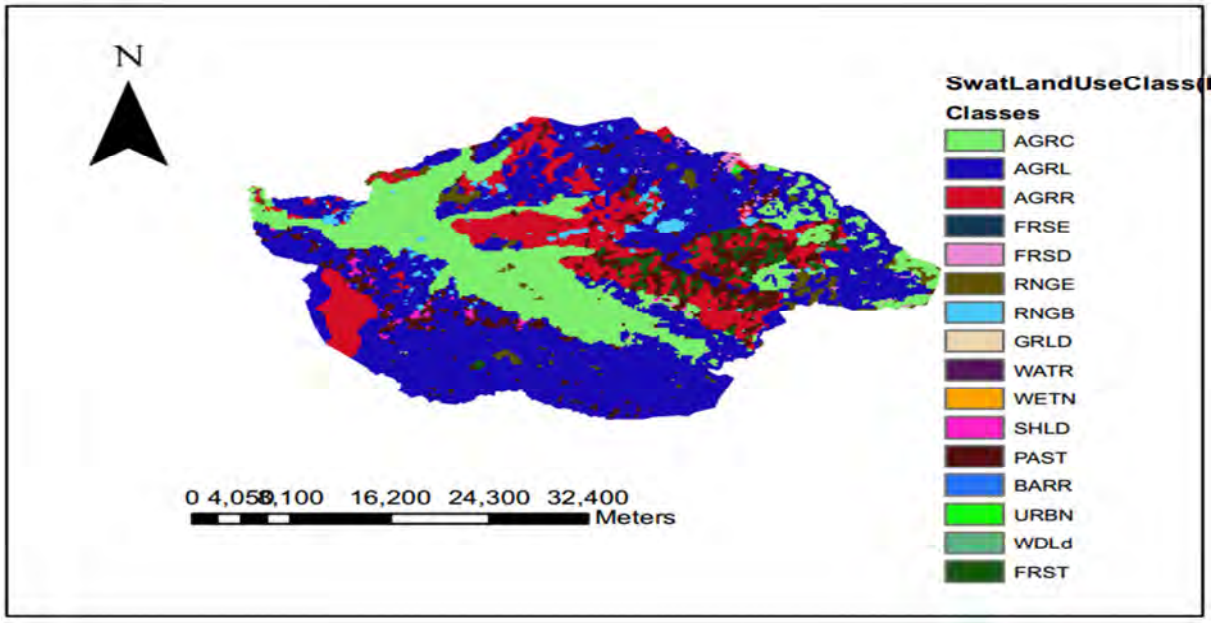


Figure 3.4: SWAT land use classes of Gumara watershed

### 3.2.2.9.3 Soil Data

Soil physical and chemical properties are other inputs required by SWAT's soil data base. Soil data information as per FAO soil group is available at the ministry of water resource GIS department. The data was compiled during master plan study of the Abay River basin study. Beside to this the soil map of Gumara watershed was obtained from Bahir Dar University geography department. Based on the data acquired, the soil map of the watershed was developed by overlying the soil map shape file during HRU definitions. As shown in the figure 3.5, the

catchment is dominantly covered by haplic luvisols, eutric vertisols, eutric fluvison, eutric leptosols and chronic luvisols. Table 3.3 shows the major soil types and their percentage of area coverage obtained during overlying of soil maps.

Table 3.3: Major Soil types in Gumara Watershed and their areal coverage used for SWAT input

| Major Soil Type | Area (ha) | % Watershed Area |
|---|---|---|
| Chromic Luvisols | 28734.46 | 22.62 |
| Eutric Fluvisols | 3506.06 | 2.76 |
| Eutric Leptosols | 9540.04 | 7.51 |
| Haplic Luvisols | 77133.34 | 60.72 |
| Eutric Vertisols | 7621.87 | 6 |
| Urban | 241.36 | 0.19 |

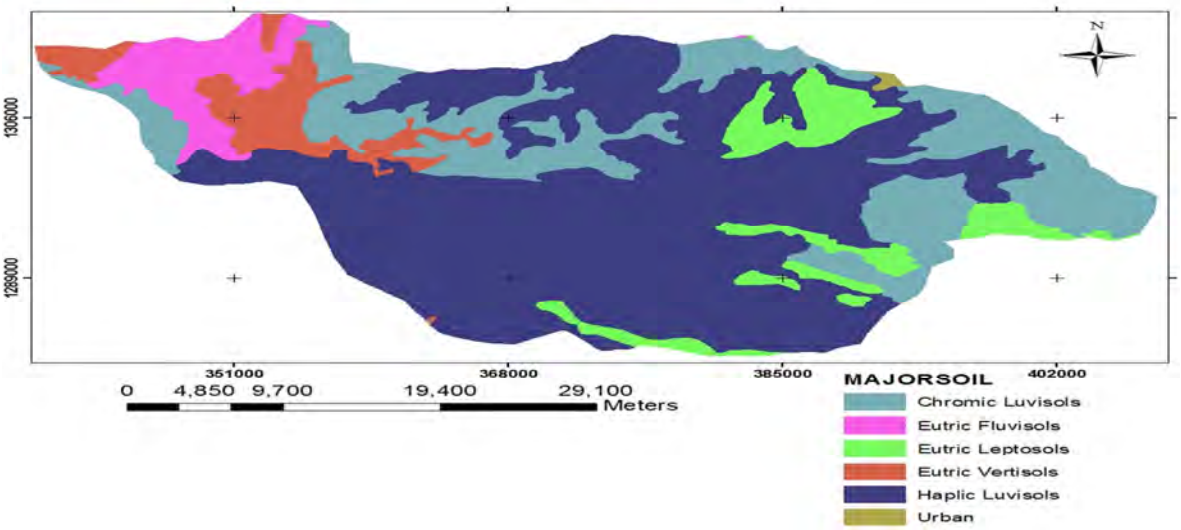


Figure 3.5: Major soil groups for Gumara watershed

### 3.2.2.9.4 Meteorological Data

SWAT requires daily weather inputs such as daily precipitation, maximum and minimum temperature, solar radiation data, relative humidity, and wind speed data, which can be read from measured records and/or generator by weather generator embedded in SWAT. The measured daily meteorological data in and around Gumara watershed were collected from Ethiopian Meteorological Agency. Although all stations have missed data value, all the missing data were filled with a missing data identifier of -99 and the weather generator first independently

generates missed values of the day. To fill the missing data and generate representative areal weather variables, daily rainfall, temperature, wind speed, solar radiation and relative humidity data from, Bahir Dar, Woreta and Debre tabor weather stations were used as an input to calculate statistical monthly weathered generator parameters which are calculated by Weather parameter calculator program.

#### 3.2.2.9.5 Hydrological Data

Daily measured discharge data of Gumara River were collected from Ethiopian Ministry of Water Resources hydrology department.

The historical observed flows of the River between 1986 and 2005 which were obtained from MoWR hydrology department and these data were used for calibration and validation of SWAT model. Summary of Historically recorded River flows at Gumara River gauge station are found in the in the Appendix D

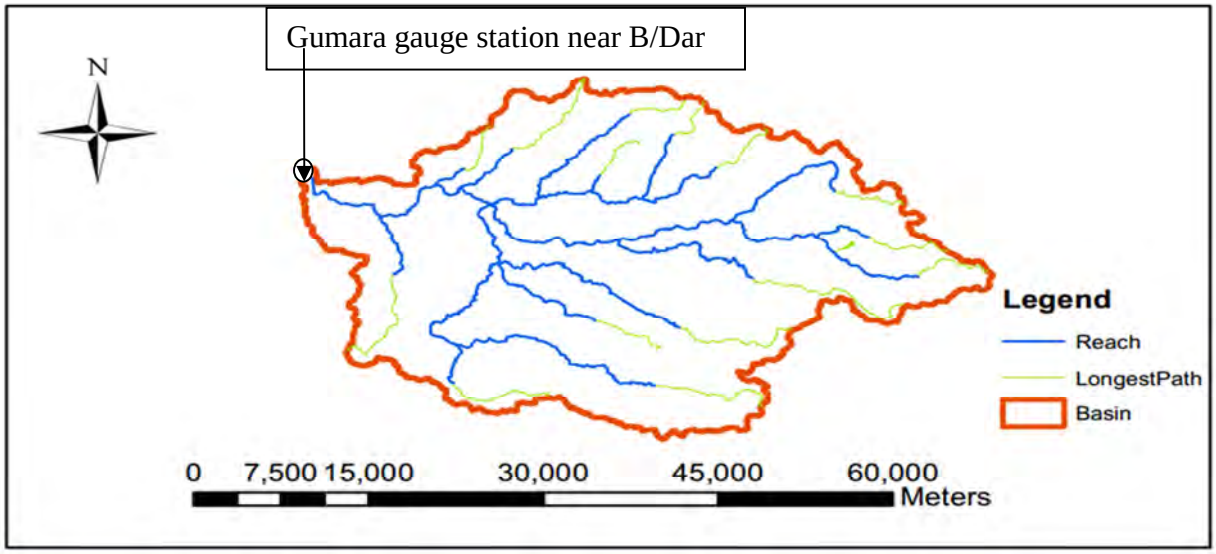


Figure 3.6: Gauged Gumara Watershed

### 3.3. Sources of Uncertainty in Climatological and Hydrological Modeling Approach

Different models and model outputs are involved in this study, which are based on simplified assumptions and hence uncertainties are obvious in each of the models and model outputs. The

types of uncertainties can be due to data quality, the GCMs and SRES scenarios selected, the downscaling method used, and the hydrologic modeling applied.

Data availability and reliability are the common problems in countries like Ethiopia. The time serious data are not fully recorded. Even though it was tried to fill the missed data, it is true that certain level of uncertainty existed which makes the calibration and validation task more difficult.

Only single output of the GCM (HadCM3) and two emission scenarios (A2a and B2a) were used for this study though other output of GCM and emission scenarios are also existed used for impact studies and it is another source of uncertainty. On the other hand, the coarser resolutions of GCMs outputs are not used directly for impact studies. “Downscaling” is a solution towards narrowing the temporal and spatial resolution disparity and hence the SDSM techniques involved in this study were the source of uncertainty because if its difficulties to find good predictors-predictand correlation which is the important part of downscaling process. Meanwhile, SDSM is based on the assumption that the predictor-predictand relationships under the current condition remain valid for future climate conditions too, which might not be the case and hence another source of uncertainty.

Related to hydrological modeling approach the uncertainty is due to the assumption that the climatic variables other than precipitation and temperature such as wind speed, sunshine hour, relative humidity and non-climatic variables as land use changes remain constant even though it is not true.

# 4. RESULTS AND DISCUSSION

The results and discussion part divided into two major parts i.e. the climate change model results and discussion and the hydrological modeling results and discussion. The results of each part were shown using both statistically and graphically and discussed in detail accordingly. Moreover, the hydro-climatological conditions of the catchment from the period 1986 to 2005 were analyzed using observed hydrological and meteorological data.

## 4.1 Comparison of Observed Data at Various Climate Stations.

All meteorological stations in and around the Gumara catchment are found within the same grid boxes in climate change impact assessment. Hence, meteorological data screening for the different stations in the study area were carried out through correlation matrix and only one station was selected to downscale the large scale predictors. The daily precipitation, maximum and minimum temperature from the period 1986-2000 were averaged on monthly basis to calculate the correlation coefficient of each stations as shown in the Table 4.1 and 4.2.

The correlation of precipitation data among seven stations was done (Table 4) and the correlation coefficients were found between 0.68 and 0.85. This reveals that the agreements between stations are good. Among other stations, the precipitation at D.Tabor station showed very good agreements in which the correlation coefficient ranges from 0.87 to 0.95. Hence the precipitation at D.Tabor station was used for this study.

Table 4.1: Correlation between average monthly precipitations of seven stations on matrices basis

| Station | D.Tabor | B/Dar | Woreta | Wanzaye | N.Mewucha | A.Genet | Amedber |
|---|---|---|---|---|---|---|---|
| D.Tabor | 1 | 0.95 | 0.88 | 0.93 | 0.87 | 0.9 | 0.94 |
| B/Dar | | 1 | 0.82 | 0.88 | 0.68 | 0.72 | 0.89 |
| Woreta | | | 1 | 0.9 | 0.82 | 0.82 | 0.85 |
| Wanzaye | | | | 1 | 0.77 | 0.83 | 0.9 |
| N.Mewucha | | | | | 1 | 0.85 | 0.81 |
| A.Genet | | | | | | 1 | 0.86 |
| Amedber | | | | | | | 1 |

Similarly, the correlation analysis of the average monthly temperature was carried out among four stations (Table 4.2) and the result of correlation coefficients ranges from 0.66 to 0.96 for maximum temperature, and from 0.21 to 0.75 for minimum temperature. The maximum temperature still shows good correlations across the stations while the minimum temperature shows relatively poor correlations particularly between B/Dar and Wanzaye stations and D.tabor and B/Dar stations in which the correlation coefficient is 0.21 and 0.46 respectively.

Table 4.2: Correlation coefficient on maximum and minimum temperature of four stations

| | maximum temperature | | | | | | Minimum temperature | | | |
|---|---|---|---|---|---|---|---|---|---|---|
| Station | (1) | (2) | (3) | (4) | | Station | (1) | (2) | (3) | (4) |
| D.Tabor (1) | 1 | 0.77 | 0.96 | 0.85 | | D.Tabor (1) | 1 | 0.46 | 0.55 | 0.75 |
| B/Dar (2) | | 1 | 0.82 | 0.66 | | B/Dar (2) | | 1 | 0.57 | 0.21 |
| Woreta (3) | | | 1 | 0.82 | | Woreta (3) | | | 1 | 0.5 |
| Wanzaye (4) | | | | 1 | | Wanzaye (4) | | | | 1 |

In general both maximum and minimum temperature at D.Tabor station resulted good correlation and hence used for this study. The average temperature differences from the base-period values (deltas) and the average monthly precipitation change factors (precipitation multipliers) developed for this station can then be applied for the other stations too. Consequently, the climate scenarios were only developed for Debre Tabor Station.

## 4.2 Hydro-Climatological Conditions of Gumara Catchment from 1986-2005

The observed daily precipitation at Debre Tabor station showed that the maximum amount of precipitation occurred within the major parts of the rainy season (June-September) except in the year 1997 and 1998 in which the maximum daily precipitation were recorded in May and October respectively. In most of the year, the average monthly precipitations are found between 3.5 mm and 5 mm as shown in the figure 4.1. However in the year 1996 and 1997 the most extreme events were occurred i.e. 12.7 mm, 12.75 mm respectively. The lowest value of average monthly precipitation was recorded in the year 1987 (3.2 mm).

Moreover, the trend line of observed average monthly precipitation from 1986-2005 shows slight increments.

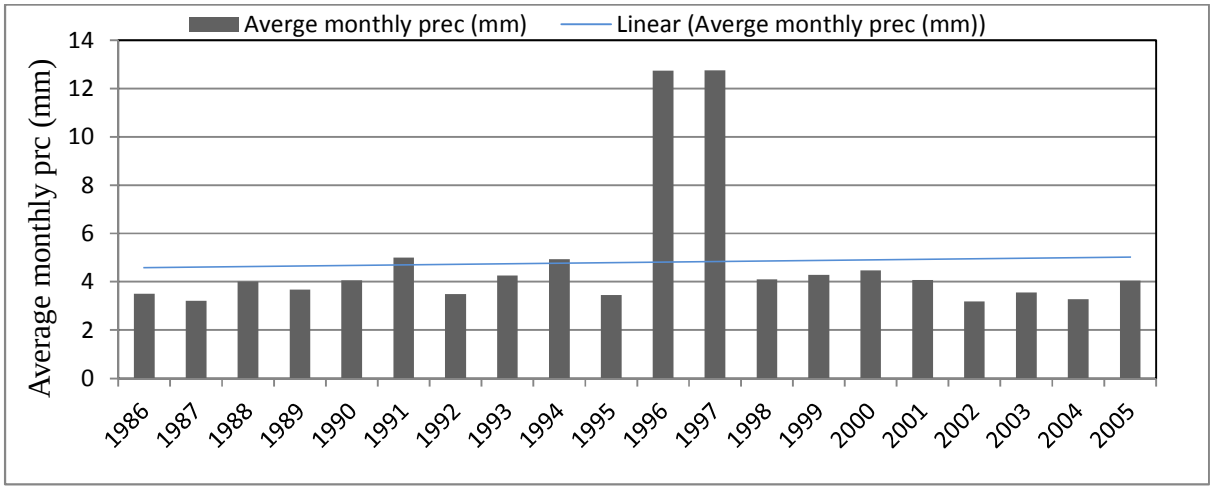


Figure 4.1: Observed Average Monthly Precipitation at Debre Tabor Station (1986-2005) (mm)

Unlike that of precipitation, the observed average monthly maximum and minimum temperature did not show large variation from year to year. Figure 4.2 showed that, in most of the year the average monthly maximum temperature are found between 21.5$^{o}$c (1987) and 22.6$^{o}$c (2005) while for minimum temperature the average monthly values are more or less similar (9.5$^{o}$c). In the year 1986 the lowest average monthly maximum temperature was observed (20$^{o}$c). The trend line of maximum temperature showed slight increments while it is constant for minimum temperature.

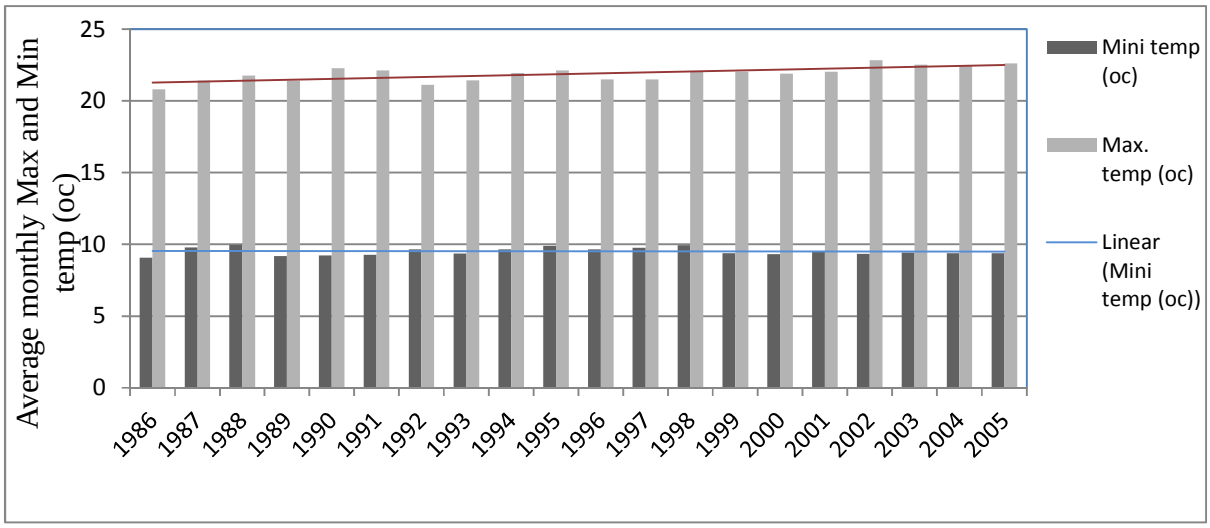


Figure 4.2: Observed Average Monthly Max and Min temperature at Debre Tabor Station (1986-2005) ($^{o}$c)

Figure 4.3 shows the average monthly flows of Gumara River. As it can be shown from the figure the flow patterns of the flow corresponds with the pattern of average monthly precipitation (figure 4.1). In most of the year the average monthly flows are found between 25$m^3$/s and 38$m^3$/s. However in the year 1996 and 1997 the most extreme flows were occurred in which the average monthly flow reaches to a maximum of 53.11$m^3$/s and 52.5$m^3$/s respectively. These two extreme values occurred due to the corresponding high values of precipitation (figure 4.1) in the same years. The lowest flow of the River was recorded in the year 1987 (20 $m^3$/s) and this also corresponds with the lowest value of precipitation within the same year. The trend line of the average monthly flow of the River also shows slight increments.

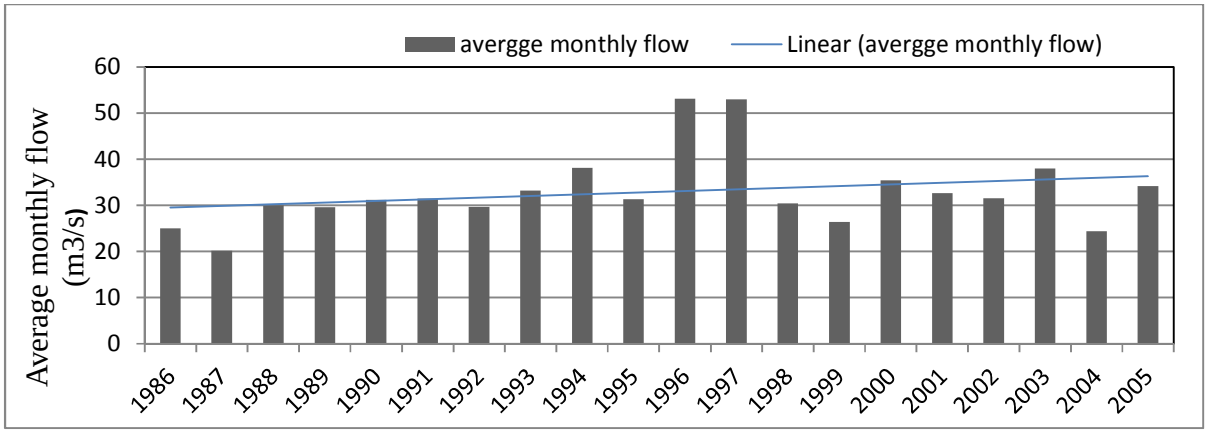


Figure 4.3: Observed Average Monthly Flows at Gumara River Gauge Station (1986-2005) ($m^3$/S)

## 4.3 Climate Change Model Outputs

The results of Comparisons of observed data among different stations for quality control, the calibration and validation of SDSM model, selection of predictor variables and scenario generations for base period and for the future time period were discussed.

### 4.3.1 Predictor Variables Selection

The first step in the downscaling procedure using SDSM was to establish the empirical relationships between the predictand variables (minimum temperature, maximum temperature, and precipitation) collected from stations and the predictor variables obtained from the NCEP re-analysis data for the current climate. It involves the identification of appropriate predictor

variables that have strong correlation with the predictand variable. The correlation matrix between predictor variables were used to investigate the association strength between them. Higher value of correlation static's indicates strong association. Therefore, in the screening of predictor variables the partial correlation coefficients was used as selection criteria. Up to six predictors were selected at a time and analyzed to investigate the percentage of variance explained by specific predictand–predictor pairs, then those predictors that have high explained variance was selected. Then after using the selected predictors the correlation matrix was done to investigate inter variable correlations for annual sub periods. Finally, predictors with better spatial and temporal correlations were selected.

Predictor variables that have better spatial and temporal correlation with the predictand at Debre Tabor weather station at significance level of less than 0.05 were presented in Table 4.3.

The application of these empirical predictor-predictand relationships of the observed climate is to downscale ensembles of the same local variables for the future climate. This is based on the assumption that the predictor-predictand relationships under the current condition remain valid under future climate conditions.

Table 4.3: List of predictor variables that have better spatial and temporal correlation with the predictands at Debre Tabor station at significant level of less than 0.05($p<0.05$)

| Predictands | Predictors(NCEP reanalysis data) | Notation | Partial r |
|---|---|---|---|
| Precipitation | Surface Meridian Velocity | ncepp_vaf | -0.053 |
| | 850 hpa divergence | ncepp8zhaf | +0.118 |
| | Relative Humidity at 850hpa | ncepr850af | +0.348 |
| Maximum Temperature | Mean Temperature at 2 M | nceptempaf | +0.383 |
| | Surface Specific Humidity | ncepshumaf | +0.109 |
| | Surface Vorticity | ncepp_zaf | +0.303 |
| Minimum temperature | Mean Temperature at 2 M | nceptempaf | +0.444 |
| | Surface Specific Humidity | ncepshumaf | +0.300 |
| | 500hpa geo-potential height | ncepp500af | +0.109 |
| | 850 hpa meriodinal velocity | ncepp8_vaf | +0.014 |

The partial correlation coefficient (r) shows the explanatory power that is specific to each predictor. All are significant at p = 0.05, hpa – is a unit of pressure, 1 hPa = 1 mbar = 100 Pa = 0.1 kPa

The Partial correlations indicate that on average relative humidity at 850 hPa has the strongest association with local precipitation once the influence of all other predictors has been removed, whereas maximum and minimum temperatures are strongly correlated with mean temperature at 2m, which shows their heavy dependence on regional temperatures.

### 4.3.2 SDSM Calibration and Validation Outputs

The calibration was done for the period of 10 years (1986-1995) at a monthly model type in order to see the monthly temporal variations. Monthly precipitation, maximum temperature, and minimum temperature values were generated based on the above selected predictor variables of the NCEP data. Twenty ensembles (runs) were generated and the average of these ensembles was taken as a simulated result for each predictand variable. The conditional and unconditional processes were selected for daily rainfall and daily temperature (maximum and minimum) values respectively and since for conditional processes in which the distribution of predictand values is skewed, the Fourth root transformations were applied. The calibration and validation statistics for all the three predictand variables before and after bias correction are shown in Table 4.4.

These results show that the simulated precipitation, maximum temperature and minimum temperature have good agreements with the observed results. Precipitation is a conditional process (dependent on other intermediate processes like on the occurrence of humidity, cloud cover, and/or wet-days) and high spatial variability. Due to this reason the calibration and validation results are comparatively less than the maximum and minimum temperature (Lijalem, 2006, Dile et al, 2013). However for this study a good agreement between generated and observed precipitation was resulted ($R^2$ =0.7) during calibration and this might be due to less spatial variability of precipitation on Gumara watershed. Hence the SDSM model resulted in satisfactory multiple regression equation parameters for precipitation, maximum and minimum temperature (Table 4.4). Thus, it may be inferred that future projections may also be well replicated. However, the calibration results before bias corrections showed good agreements for all the three predictands, the model under estimates in some months and over estimates in some other months as shown in the figure 4.4 and 4.5. To correct this under/over estimation, a linear scaling bias correction method was applied and it perfectly matches the observed predictands with generated values as shown in (table 4.4).

Table 4.4: Calibration statistics of daily precipitation, maximum temperature, and minimum temperature before and after bias correction at Debre Tabor Station with the Reanalysis data

| | uncorrected | | Bias corrected | |
|---|---|---|---|---|
| | $R^2$ | | $R^2$ | |
| Predictands | Calibration | Validation | Calibration | Validation |
| precipitation | 0.70 | 0.62 | 0.99 | 0.99 |
| Maximum temperature | 0.69 | 0.65 | 0.98 | 0.99 |
| Minimum temperature | 0.72 | 0.77 | 0.99 | 0.99 |

Figure 4.4 (a, b) also shows the calibration results between observed and generated mean daily maximum and minimum temperature before and after bias correction.. As it can be shown in the figure, the generated values of both maximum and minimum temperature have the same trends as the observed values. For maximum temperature, the model slightly over estimates from month May-July and slightly under estimates in month January, February, September, October and November. While in the remaining months the generated and observed values are more or less similar. The model also over estimates the minimum temperature from June-December and over estimates from January-April. After bias correction, the generated and observed values showed similar patterns.

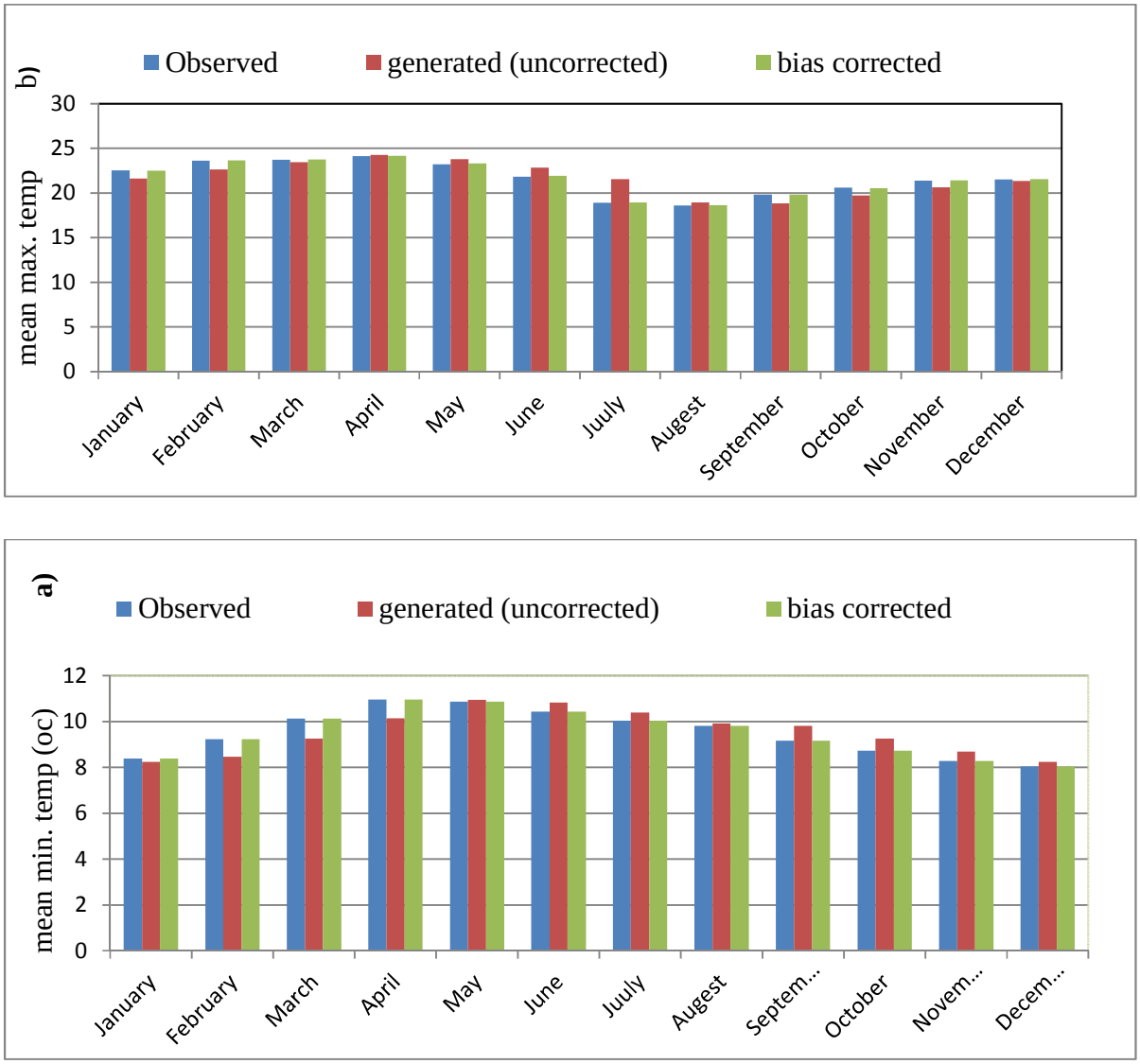


Figure 4.4: Calibration results before and after bias correction between observed and generated mean daily maximum temperature ($^{o}$c) (a) and mean daily minimum temperature ($^{o}$c) (b), in the time step for the Debre Tabor station

Figure 4.5 shows the calibration results of precipitation. As shown in the figure, the model highly overestimates in some months and underestimates in some other months. However, the overall agreement was good (Table 4.4)

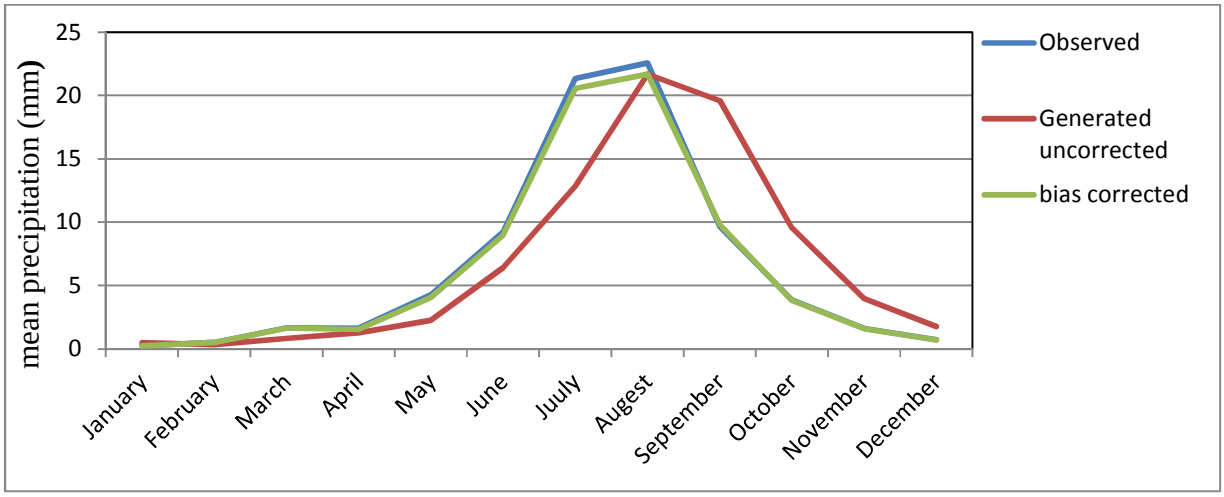


Figure 4.5: Calibration results before and after bias correction between observed and generated mean daily precipitation (mm) in the time step for the Debre Tabor station.

Validation was done using an independent observed data for the period of five year from 1996 to 2000. Here also twenty ensembles (runs) of daily values were generated and the averages of these ensembles were taken for the comparison. The correlation coefficients before bias correction that were found during the calibration are also maintained during the validation as shown in the Table 4.4. A good agreement was also found between the observed and simulated precipitation ($R^2$=0.62) though it is a conditional process and for minimum temperature ($R^2$ =0.77) during validation. The model over estimates the precipitation during validation in the month of June through December as compared to the observed data as shown in the figure 4.7 but the overall agreement between simulated and observed is good. From the month of August-November the simulation results were exceptional in which the model results were highly deviated from the measured values. But this might be due to the conditional process of precipitation and its high temporal and spatial variability. However as that of calibration, the validation results also found to be good agreements between generated and observed precipitation, maximum and minimum temperature which proofs the SDSM models ability to generate weather variables for Gumara watershed under a given set of model parameters. As that of calibration, to correct the model errors the bias correction was applied and it perfectly matches the observed and generated values.

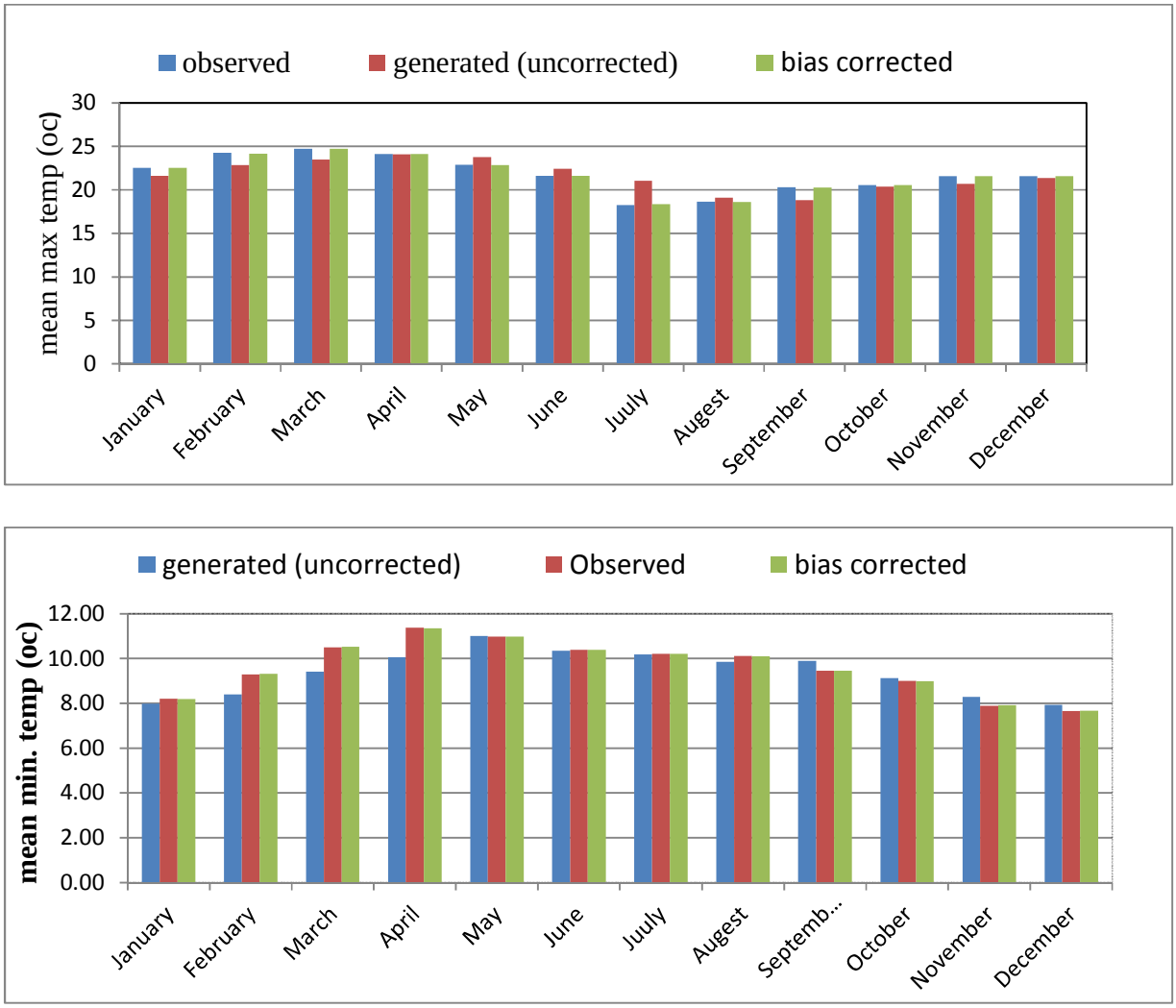


Figure 4.6: Validation results before and after bias correction between observed and generated mean daily maximum temperature ($^{o}$c) (a) and mean daily minimum temperature ($^{o}$c) (b)

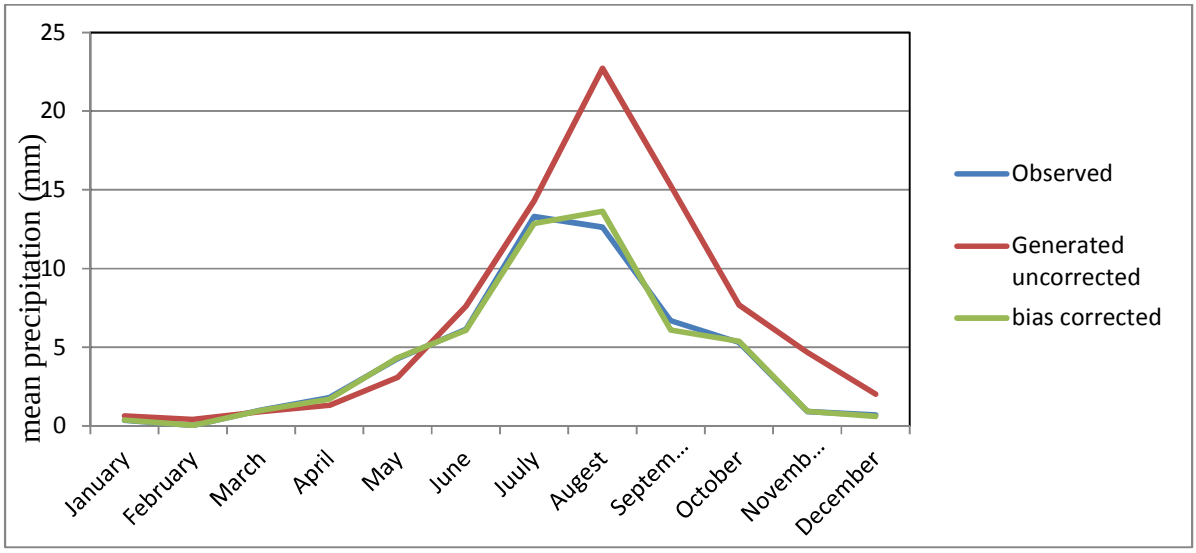


Figure 4.7: validation results before and after bias correction between observed and generated mean daily precipitation (mm) in the time step for the Debre Tabor station.

### 4.3.3 Scenarios Generated

One of the criteria commonly used in evaluating the performance of any useful method is whether the historic (observed) condition can be replicated or not. For this study, the HadCM3A2a and HadCM3B2a were the two GCM output files used for the scenario generation. The regression weights produced during the calibration process were applied to the time series outputs of the GCM model based on the assumption that the predictor-predictand relationships under the current condition remain valid for future climate conditions. Twenty ensembles of synthetic daily time series data were produced for each of the two SRES scenarios for a period of 139years (1961 to 2099). Finally, the mean of the twenty ensembles for the specified period was produced for maximum and minimum temperature and precipitation.

The climate scenario for the future period was developed from statistical down scaling using the GCM predictor variables for the two emission scenarios for 100 years based on the mean of 20 ensembles and the analysis was done based on 25 years period from 2001-2025, 2026-2050, 2051-2075 and 2076-2099. The IPCC recommends 1961-1990 as a climatological base period in impact assessment. Hence, for this research the period from 1986-2000 was taken as a base period with in which the comparison was made. The observed climatological data collected from Ethiopian meteorological stations contains more consistent time series records from the period

1986 and onwards than the period before 1986 and this is why the period from 1986-2000 were taken as a base period. Moreover, (Wilby and Dawson, 2007) suggested that Station meteorological data prior to 1st January 1961 or after 31st December 2000 will have no pre-prepared predictor variables. Thus, data that lie outside the standard period 1961 to 2000 can't be used as observational data.

#### 4.3.3.1 Scenarios Developed for the Base Period (1986-2000)

For the sake of comparison with the observed values, the generated values of the base period were averaged to a monthly time step and the bias correction was also applied.

**I. Maximum Temperature**

The downscaled monthly, seasonal and annual average maximum temperature resulted in good agreement with the observed temperature before bias correction for the baseline period in both A2a ($R^2$ = 0.7) and B2a ($R^2$ = 0.78) emission scenarios except slight Variations between observed and downscaled maximum temperature for the months of June, July, September and October for A2a emission scenarios and in the month September and October for B2a emission scenarios as shown in figure 4.8. The overall agreement confirms that the SDSM is able to produce synthetic maximum temperature series given daily atmospheric predictor variables supplied by a GCM (either under present or future greenhouse gas forcing). To correct under/over estimations of the model, the bias correction was applied and after bias correction the simulated and observed values showed a very good agreements i.e. $R^2$ = 0.99 (A2a) and $R^2$ = 0.98 (B2a)

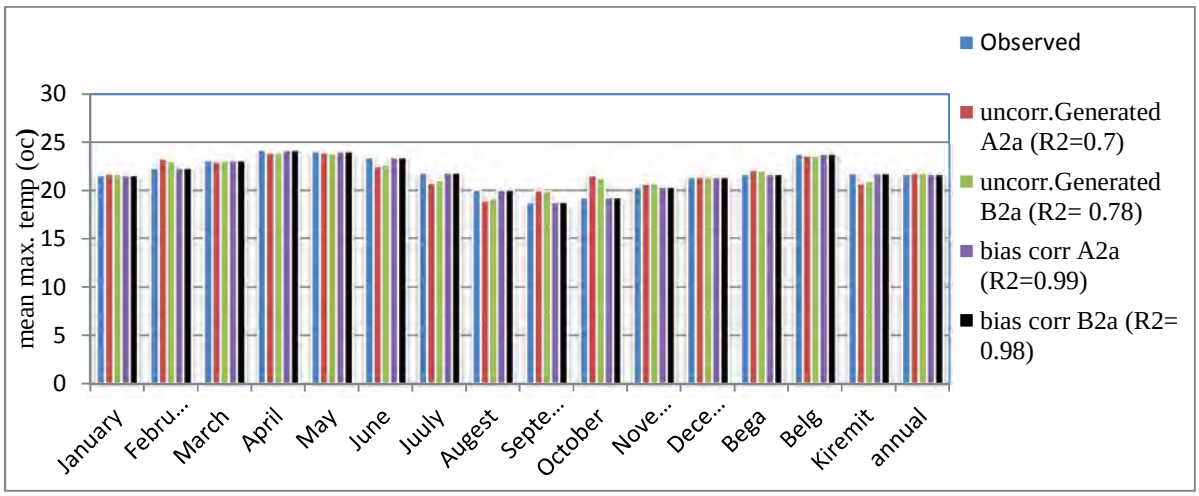


Figure 4.8 Pattern of Observed and downscaled mean monthly, seasonal and annual maximum temperature before and after bias correction for the base period (1986-2000)

## II. Minimum Temperature

The downscaled mean monthly minimum temperature before and after bias correction for A2a and B2a emission scenario for the base period are shown in the figure 4.9.

As shown in the figure 4.9 the downscaled monthly, seasonal and annual mean minimum temperature before bias correction resulted a good agreements with the observed mean monthly, seasonal and annual minimum temperature in both A2a ($R^2$ = 0.81) and B2a ($R^2$ = 0.82) emission scenarios. For the month of June, October and November the observed value is slightly higher than the downscaled values but the general trend shows similar patterns. Moreover in Kiremit season, the model underestimates the minimum temperature as compared to the observed one. As compared to the maximum temperature, a better agreement was found in minimum temperature. After bias correction the generated minimum temperature perfectly agreed with the observed minimum temperature i.e. $R^2$= 1 for both A2a and B2a scenarios.

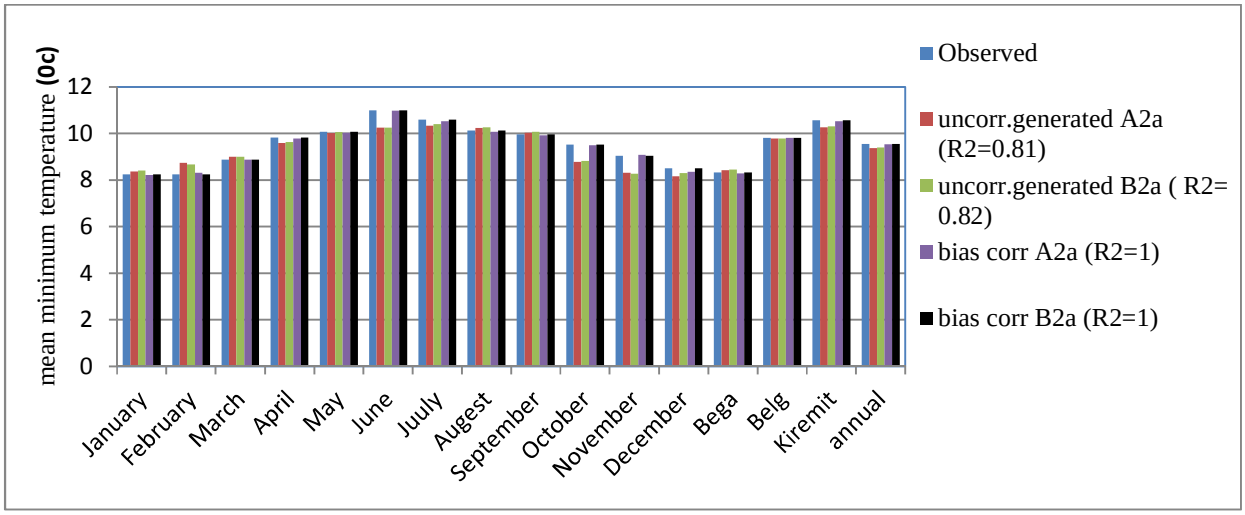


Figure 4.9: Pattern of Observed and downscaled mean monthly, seasonal and annual minimum temperature before and after bias correction for the base period (1986-2000)

### III. Precipitation

As compared to the minimum and maximum temperature the precipitation could not able to replicate the observed data. This is due to complicated nature of precipitation processes and its distribution in space and time (Habtom, 2009). This might be due to the conditional process (dependent on other intermediate processes like on the occurrence of humidity, cloud cover, and/or wet-days) and high variability in space and so the relatively coarse spatial resolution of the current generation of climate models is not adequate to fully capture that variability.

As it can be seen from the figure 4.10 the mean monthly generated value in both A2a and B2a scenario is over estimated from April to August and under estimated from September to December. The largest monthly variation occurs from month of July to September. The largest seasonal variation occurs in Kiremit in which the generated values for both scenarios are over estimated. These indicate that the SDSM model over estimates the precipitation in the major parts of rainy season. The annual mean values are more or less similar with the observed value. The correlation results before bias correction, however, shows good agreements between the down scaled and observed precipitations for both A2a ($R^2$ = 0.81) and B2a ($R^2$ = 0.79) scenarios. Meanwhile, the general monthly, seasonal and annual patterns are similar with observed precipitations. But to correct over/under estimation of the model, bias correction was applied and

after correction the observed and simulated precipitations were perfectly matched i.e. $R^2$=0.99 both for A2a and B2a scenarios.

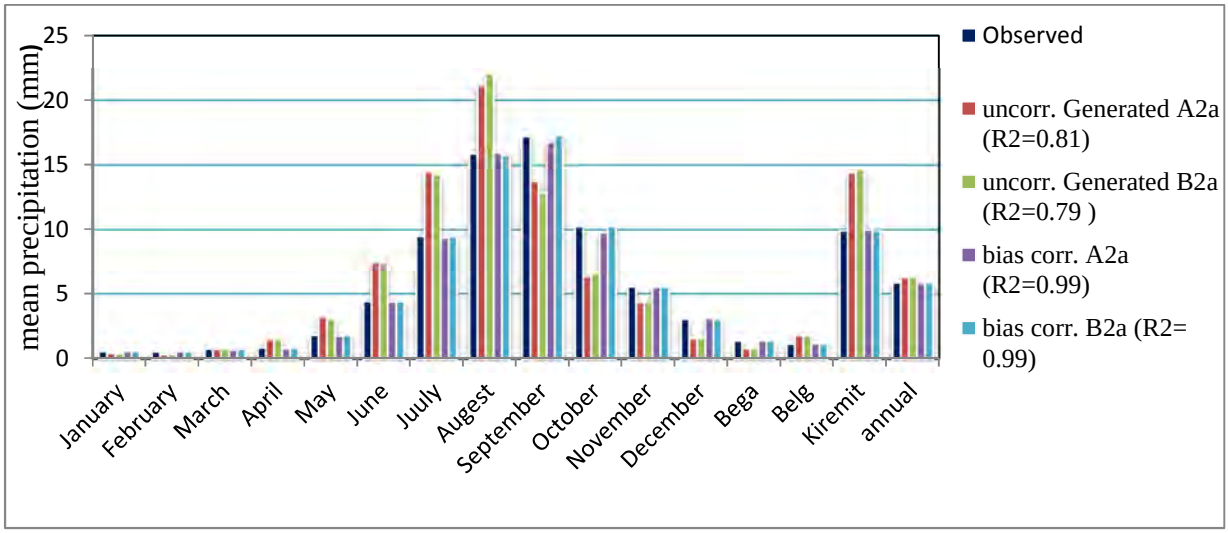


Figure 4.10: Pattern of Observed and downscaled mean monthly, seasonal and annual precipitation before and after bias correction for the base period (1986-2000)

#### 4.3.3.2 Scenarios Developed for the Future periods (2001-2099)

For future scenarios, the climate signal (difference between future and baseline climates) was first removed before the correction is adjusted. Then the future simulated results were added (temperature) and multiplied (precipitation) with the changing factor obtained in the baseline correction for each month. Then, initially removed climate signal is added back to create a bias corrected precipitation and temperature scenario for the future.

**I. Maximum Temperature**

The mean monthly, seasonal and annual change in maximum temperature for the future period (2001-2099) for both A2a and B2a emission scenarios are shown in the figure 4.11 (a, b). As it can be seen from figure, the overall results (2001-2099) for annual mean maximum temperature showed an increasing trend for both scenarios (A2a and B2a). during 2001-2099 the mean annual increment of maximum temperature ranges between $0.14^0$c (2001-2025) and $1.01^0$c (2076-2099) for A2a emission scenarios as compared to the base period while for B2a emission scenarios, it ranges between $0.2^o$c (2001-2025) and $0.77^o$c (2076-2099) and the increment is not worth for

both scenarios based on IPCC-TGICA (2007) in which the globally averaged surface air temperature is projected to warm 1.4 °C to 5.8°C by 2100.

Moreover, on monthly basis, the maximum temperature increases from January- February (2001-2099), September- November (2001-2099) and June-August (2051-2099) for both scenarios and the increment was highest in September by 2.92$^{o}$c (2076-2099) for A2a scenario whereas for B2a scenario the highest increment was found in October by 2.53$^{o}$c (2051-2075). In March and April, maximum temperature shows a decreasing trend from 0.32$^{o}$c (2001-2025) to 0.71$^{o}$c (2076-2099) for A2a scenario and 0.25$^{o}$c (2001-2025) to 0.56$^{o}$c (2076-2099) for B2a scenario. During June-August, the maximum temperature also shows decreasing trend from period 2001-2025 and 2026-2050. The maximum temperature increases almost in equal proportions in December for all future periods.

The Seasonal maximum temperature increases in Bega (October–February) and the increment ranges between 0.42$^{o}$c (2001-2025) to 0.77$^{o}$c (2076-2099) for A2a scenario and 0.44$^{o}$c (2001-2025) to 0.7$^{o}$c (2076-2099) for B2a scenario. In Belg *(*March–May) the maximum temperature decreases in the future periods (2001-2099) and the decrease during 2026-2050 for A2a scenario was exceptional (1.26$^{o}$c) though it is difficult to reason out. In Kiremit (June–September) season the maximum temperature increases up to a maximum of 1.74$^{o}$c (A2a) and 1.05$^{o}$c (B2a) between 2051-2075 and 2076-2099 and shows decreasing trend between 2001-2025 and 2026-2050 in both scenarios.

Monthly, seasonal and annual increase in maximum temperature for A2a scenario is greater than B2a scenario because A2a scenario represents medium to high scenario which produces more $CO_2$ concentration than B2a scenario which represents low to medium emission scenarios.

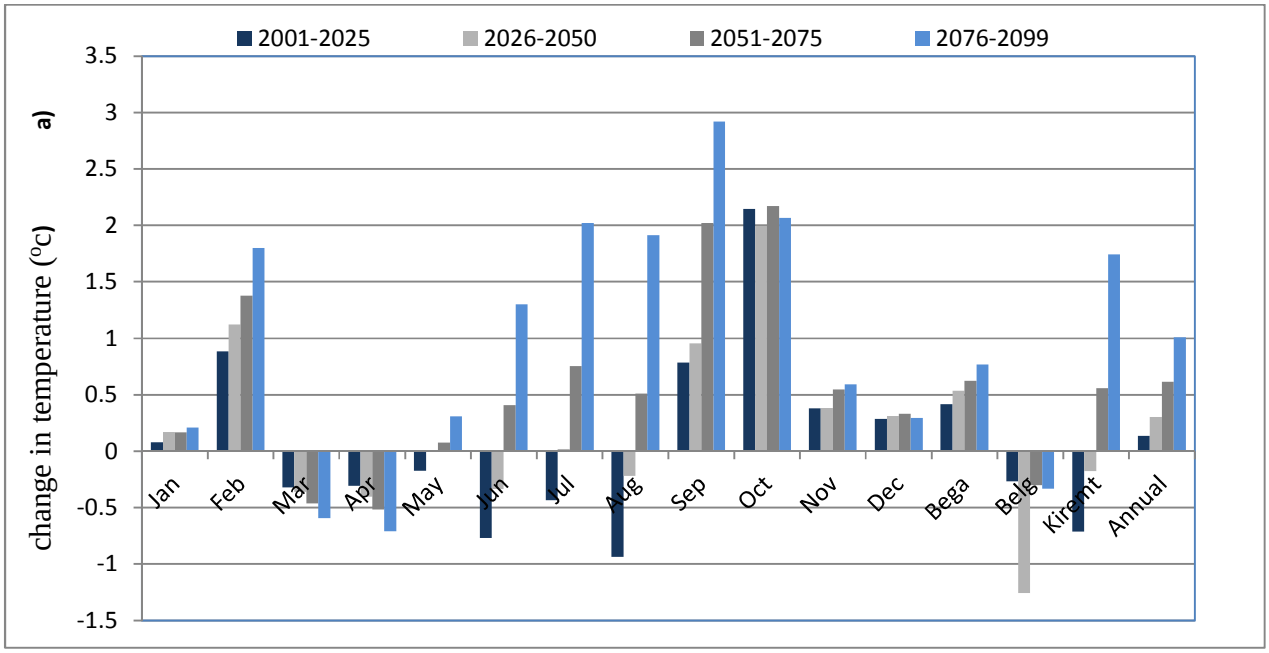


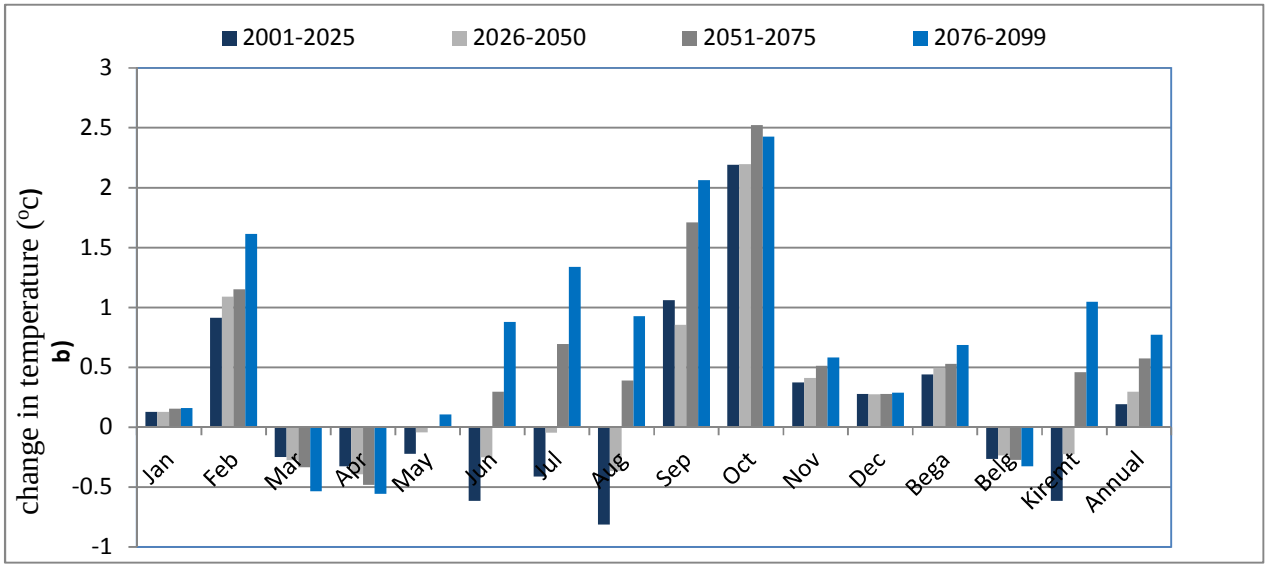


Figure 4.11: Change in average monthly, seasonal and annual maximum temperature in the future (2001-2099) for A2a scenario (a) and B2ascenario (b) from the base period.

Figure 4.12 shows the general trend of maximum temperature for the future periods as compared to the base period. The figure 4.12 reveals that even though the increase or decreases of maximum temperature are not systematic on monthly and seasonal basis (figure 4.11, a & b), the average annual maximum temperature shows an increasing trend for the future period for both A2a and B2a scenarios and the trend line shows positive relation.

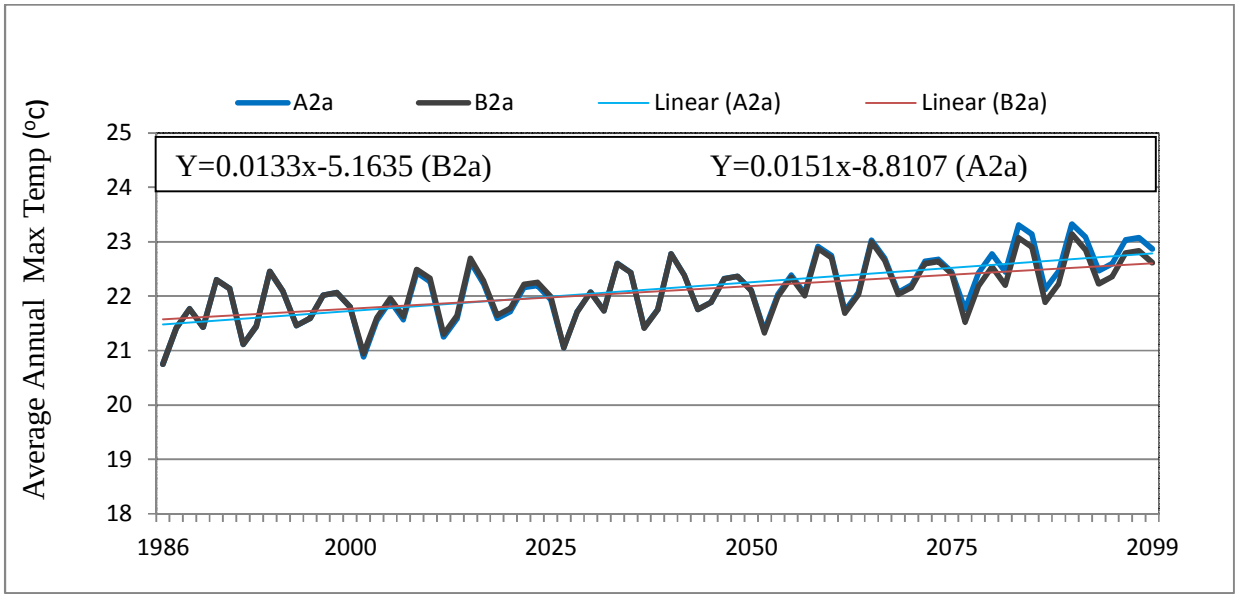


Figure 4.12: Trend of downscaled maximum temperature (1986-2099)

### III. Minimum Temperature

Figure 4.13 (a, b) shows the mean monthly, seasonal and annual changes of minimum temperature for the future periods (2001-2099) for the two emission scenarios (A2a and B2a) as compared to the base period. The minimum temperature shows increasing trends for the future periods (2001-2099) from January-march and July- September for both A2a and B2a emission scenarios except in July in which the temperature shows slight decreases from the period 2001-2025. The increment of minimum temperature varies from $0.17^0$c in January (2001-2025) to $2.33^0$c in March (2076-2099) and from $0.23^0$c in July (2026-2050) to $2.36^0$c in August (2076-2099) for A2a scenario. For B2a scenario it ranges from $0.22^0$c in January (2001-2025) to $1.8^0$c in March (2076-2099) and from $0.206^0$c in July (2026-2050) to $1.79^0$c in August (2076-2099). In January and September the increment is higher for the period 2026-2050 than the period 2051-2075 for B2a scenarios. From April-June and October-December the minimum temperature decreases within the range $0.23^0$c in December (2001-2025) to $2.16^0$c in May (2076-2099) as compared to the base period for both scenarios. Seasonally the minimum temperature increases in Bega (October–February) and Kiremit (June–September) for both A2a and B2a emission scenarios except in Kiremit in which the temperature shows slight decreases from the period 2001-2025. The overall results (2001-2099) for annual mean minimum temperature decreases for

both scenarios (A2a and B2a) except slight increments ($0.05^0$c) in A2a scenario for the period 2076-2099.

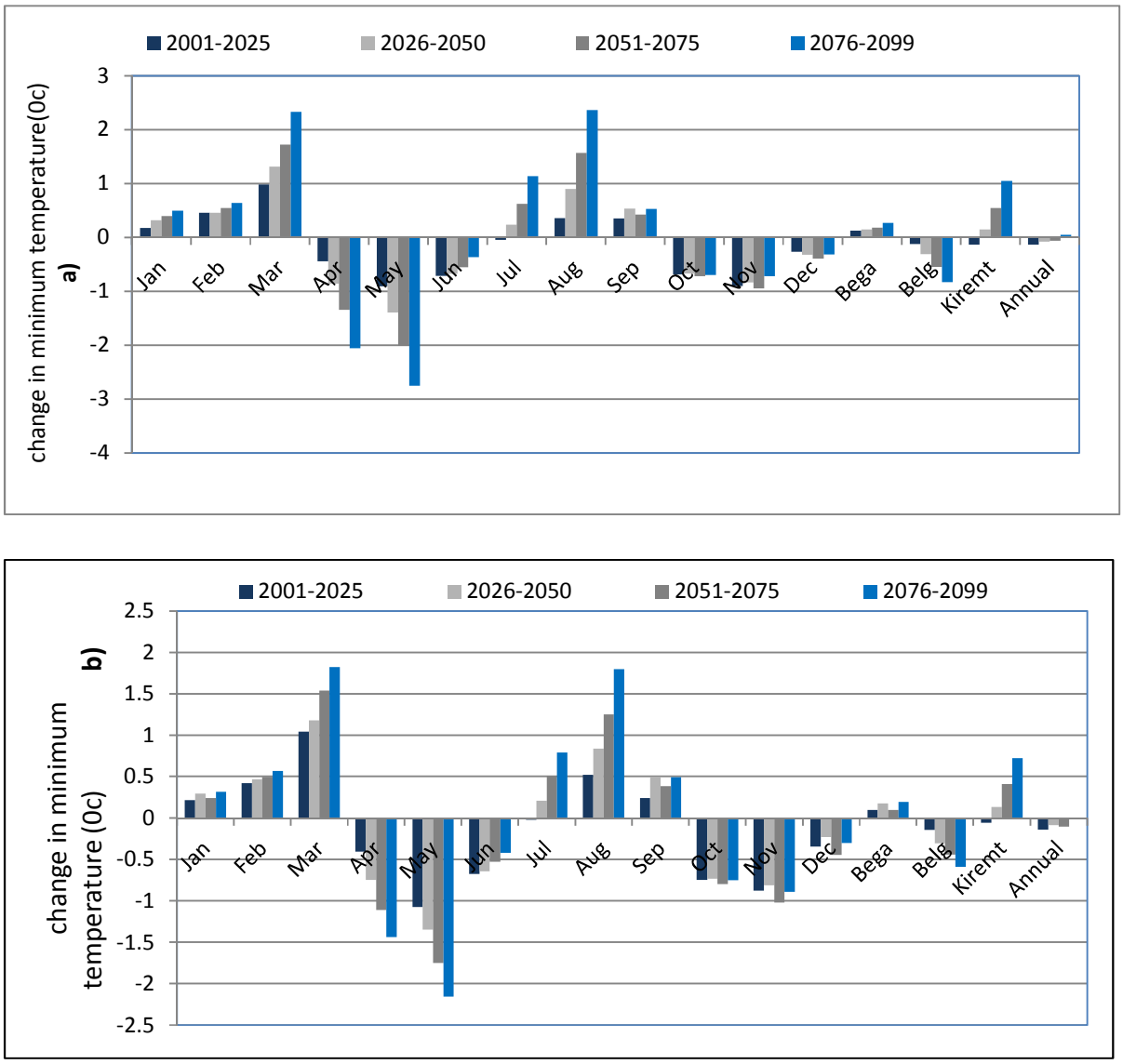


Figure 4.13: Change in average monthly, seasonal and annual minimum temperature in the future (2001-2099) for A2a scenario (a) and B2ascenario (b) from the base period.

Figure 4.14 shows the future trend of minimum temperature. As shown in the figure, there are high fluctuation of minimum temperatures for both A2a and B2a scenarios. However, the overall average annual minimum temperature shows a slight increasing trend line for the future time period.

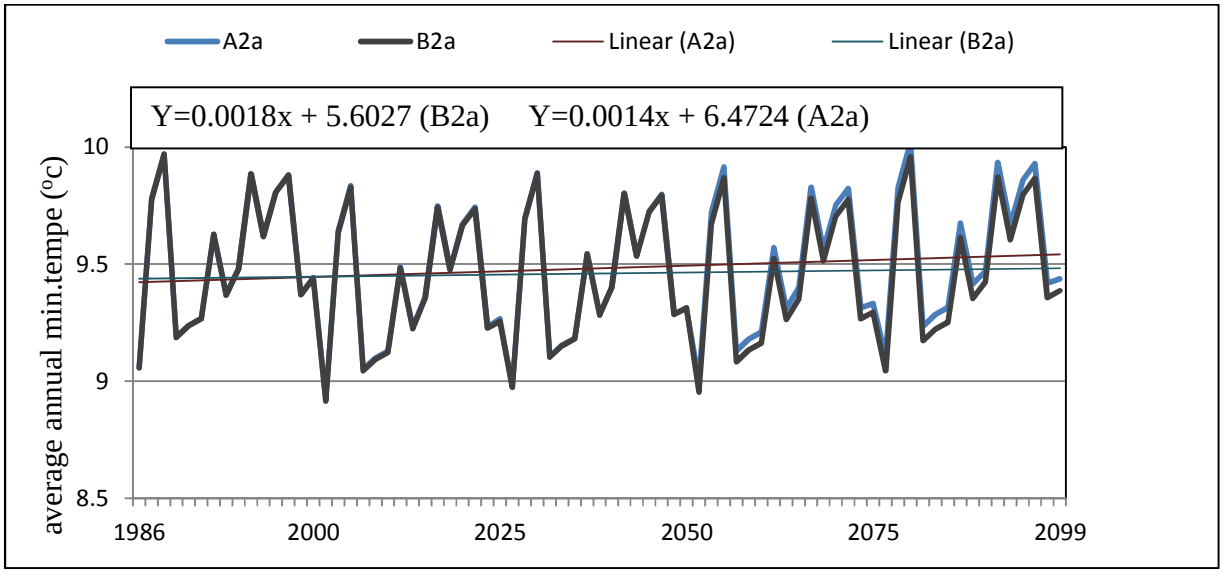


Figure 4.14: Trend of downscaled minimum temperature (1986-2099)

## IV. Precipitation

As it can be seen from the figure 4.15 (a, b) the overall results (2001-2099) for annual percentage change in precipitation showed an increasing trend for both scenarios (A2a and B2a). The increment of annual percentage change of precipitation ranges from 10.49% (2001-2025) to 13.7% (2076-2099) for A2a scenario and for B2a scenario the increment ranges between 6.46% (2001-2025) and 13.72% (2076-2099). The results of this study was thus in line with the previous researches done on Tana basin, upper Blue Nile basin (Taye (2010) and Kim *et al*. (2008)). Moreover, UNFCCC (2007) assessed regional impacts and vulnerabilities to climate change in four regions including Africa and the results showed that annual mean rainfall increases in East Africa due to climate change.

On monthly basis, the percentage change in precipitation is not systematic i.e. precipitation increases in some months and decreases in some other months. The percentage changes in precipitation increases from April-August and decreases from January-March and from September-December for the future (2001-2099) periods as compared to the base period. The increment is most dramatic in April from the period 2026-2050 for both A2a and B2a scenarios in which the precipitation increases by 90.85 % and 86.32% respectively. The decrease in

precipitation reaches to a maximum of 47.5% (2001-2025) for A2a scenario and 46.3% (2076-2099) for B2a scenario.

Seasonally, the precipitation increases in Belg (March–May) and Kiremit (June–September) in which the precipitation increases up to a maximum of 59.33% (2026-2050) for A2a scenario and 56.6% (2026-2050) for B2a scenario. A study done by Rizwan et al., (2010) on Blue Nile based on HadCM3 model also showed that, the mean precipitation from June-September increases for both A2 and B2 scenarios. Moreover, in Kiremit season the average precipitation projections for the entire Nile basin ( 2020 and 2080 ) by Beyene et al (2010) and Dile et al (2013) on Gilgel Abay River (2020, 2050 and 2080) showed increasing trends. The increment of precipitation in Belg and Kiremit season may have positive implications since these two seasons are the cropping season in Ethiopia. Precipitation decreases in Bega (October–February) season for both scenarios by 43% (2001-2025) and 41.2% (2001-2025) for A2a and B2a scenarios respectively.

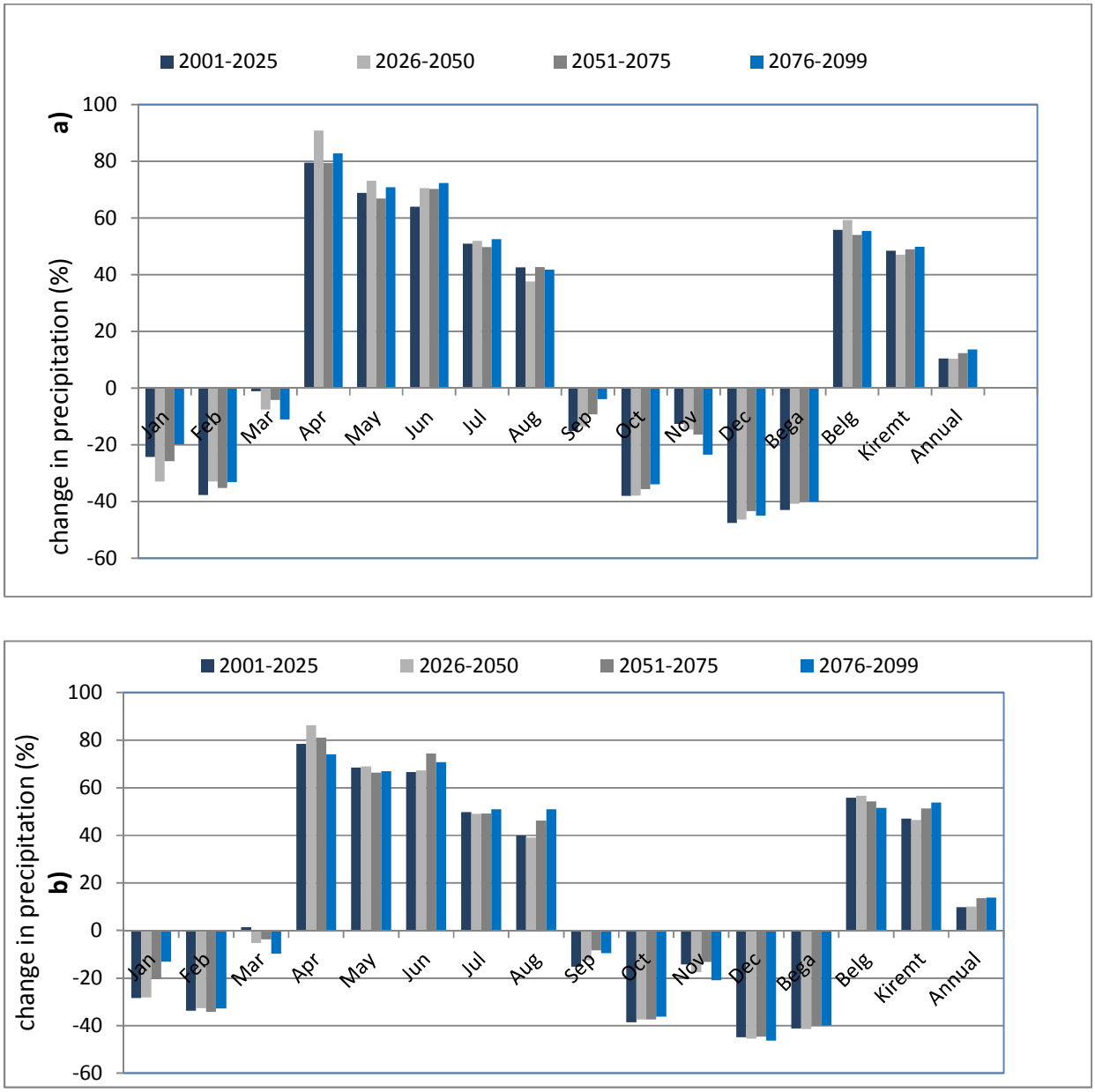


Figure 4.15: percentage Change monthly, seasonal and annual precipitations in the future (2001-2099) for A2a scenario (a) and B2ascenario (b) from the base period.

The generated future scenarios for annual precipitation generally show an increasing trend with respect to the base period and this is also in line with the previous study reports and research's done by Siri Eriksen et al., (2008) and Bates et al., (2008) in which the projected changes in precipitation increases over parts of eastern Africa.

## 4.4 SWAT Hydrological Model outputs

In SWAT hydrological modeling, identifying the most sensitive parameter that highly influences the surface runoff and ground water flows, calibration and validation of SWAT model applicability and the hydrological responses of Gumara catchment under changing climatic variables due to climate change were discussed.

### 4.4.1 Base Flow Separation at Gumara River Gauge Station

Base flow and surface flow was separated using the automated digital filter methods based on the daily flow data measured at the outlet of the Gumara watershed showed that 64% of the flow is contributed by the base flow and the rest by the surface runoff. This shows that the total stream flow is largely contributed by flow from the shallow aquifer. The base flow recession constant (alpha factor), which is the rate at which groundwater is returned to the stream, was found to be 0.05. Base flow days, which are the number of days for the base flow recession to decline through one log cycle, has a value of about 95.8 days.

### 4.4.2 Sensitivity Analysis Outputs

Sensitivity analysis is the process of identifying the model parameters that exert the highest influence on model calibration or on model predictions. Even though 19 parameters were used for the sensitivity analysis, only 8 of them revealed meaningful effect on the daily flow simulation of the Gumara River. Curve number (CNII), available water capacity (SOL_AWC), Channel effective hydraulic conductivity (CH_K2), and soil evaporation compensation factor (ESCO) were relatively high sensitive parameters that significantly affect surface runoff while the threshold water depth in shallow aquifer for flow (GWQMN), base flow Alpha factor (ALPHA_BF), Groundwater delay (GW_DELAY) and Groundwater "revap" coefficient (GW_REVAP) were other parameters that mainly influence base flow.

Table 4.5: Flow sensitive parameters and their Category of Sensitivity

| No | Sensitive parameters | Code | lower and upper bound | Relative Sensitivity | Category of sensitivity |
|---|---|---|---|---|---|
| 1 | Initial SCS CN II value | CN2 | ±25% | 3.35 | V. high |
| 2 | Available water capacity [mm WATER/mm soil] | SOL_AWC | ±25% | 0.94 | high |
| 3 | Threshold water depth in the shallow aquifer for flow [mm] | GWQMN | 0-5000 | 0.25 | high |
| 4 | Groundwater delay [days] | GW_DELAY | 0-500 | 0.23 | high |
| 5 | Channel effective hydraulic conductivity [mm/hr] | CH_K2 | 0-150 | 0.18 | medium |
| 6 | Base flow alpha factor [days] | ALPHA_BF | 0-1 | 0.17 | medium |
| 7 | Soil evaporation compensation factor | ESCO | 0-1 | 0.15 | medium |
| 8 | Groundwater "revap" coefficient | GW_REVAP | 0.02-0.2 | 0.08 | medium |

### 4.4.3 Flow Calibration Outputs

Flow calibration was performed for a period of ten years from 01/01/ 1991 to 31/12/2000 using the sensitive parameters identified. However, flow was simulated for eight years from January1$^{st}$, 1993 to December 31$^{st}$, 2000, within which the first two year were considered as a warm up period in order to set hydrologic processes to reach into equilibrium. The manual calibration method was used to calibrate the model using the observed stream flow. Observed daily stream flows were adjusted on the monthly basis and Simulations runs were conducted on monthly basis to compare the modeling output with the measured daily discharge at the outlet of Gumara watersheds. Manipulation of the identified parameter values were carried out within the allowable ranges recommended by SWAT developers. The value of the selected sensitive parameters were changed so many times within the acceptable ranges until satisfactory results were met between the monthly simulation runs and monthly measured discharges and it was a very challenged tasks to get the fitted parameter values used for calibration.

Table 4.6: Flow sensitive parameters and their fitted values used for calibration

| No | Sensitive parameters | Code | lower and upper bound | Initial value | Calibrated Value |
|---|---|---|---|---|---|
| 1 | Initial SCS CN II value | CN2 | ±25% | default | -25% |
| 2 | Available water capacity [mm WATER/mm soil] | SOL_AWC | ±25% | default | -25% |
| 3 | Threshold water depth in the shallow aquifer for flow [mm] | GWQMN | 0-5000 | 100 | 96 |
| 4 | Groundwater delay [days] | GW_DELAY | 0-500 | 30 | 21 |
| 5 | Channel effective hydraulic conductivity [mm/hr] | CH_K2 | 0-150 | 0 | 0.75 |
| 6 | Base flow alpha factor [days] | ALPHA_BF | 0-1 | 0.7 | 0.05 |
| 7 | Soil evaporation compensation factor | ESCO | 0-1 | 0.5 | 0.85 |
| 8 | Groundwater "revap" coefficient | GW_REVAP | 0.02-0.2 | 0.02 | 0.2 |

The calibration results in Table 4.7 show that there is a good agreement between the simulated and measured monthly flows. Percent of error of the observed and simulated monthly flows at Gumara gauge station is 1.2% which is well within the acceptable range of ±15%. Further a good agreement between observed and simulated monthly flows are shown by the coefficient of determinations ($R^2$=0.9) and the Nash-Suttcliffe simulation efficiency ($E_{NS}$=0.89) and thus fulfilled the requirements suggested by Santhi et al. (2001) for $R^2$ >0.6 and $E_{NS}$> 0.5.

Table 4.7: Calibration statistics for measured and simulated flows at Gumara flow gauge station.

| period | Total Flow(m3/s) | | Mean Monthly Flow (m3/s) | | % Error | $R^2$ | $E_{NS}$ |
|---|---|---|---|---|---|---|---|
| | observed | simulated | Observed | Simulated | | | |
| 1993-2000 | 3565.29 | 3522.95 | 37.14 | 37.7 | 1.2 | 0.9 | 0.89 |

The graphical representation of the simulated and observed monthly flows (figure 4.16) shows a reasonable agreement. Even though the model slightly over estimates the peak values in the year 1994 and 1999 and under estimates in remaining part of the calibration period, the overall flow is well simulated and the trend shows good patterns. Figure 17 also shows the scatter plots between observed and simulated flows and the equations showed positive relations between observed and simulated flows.

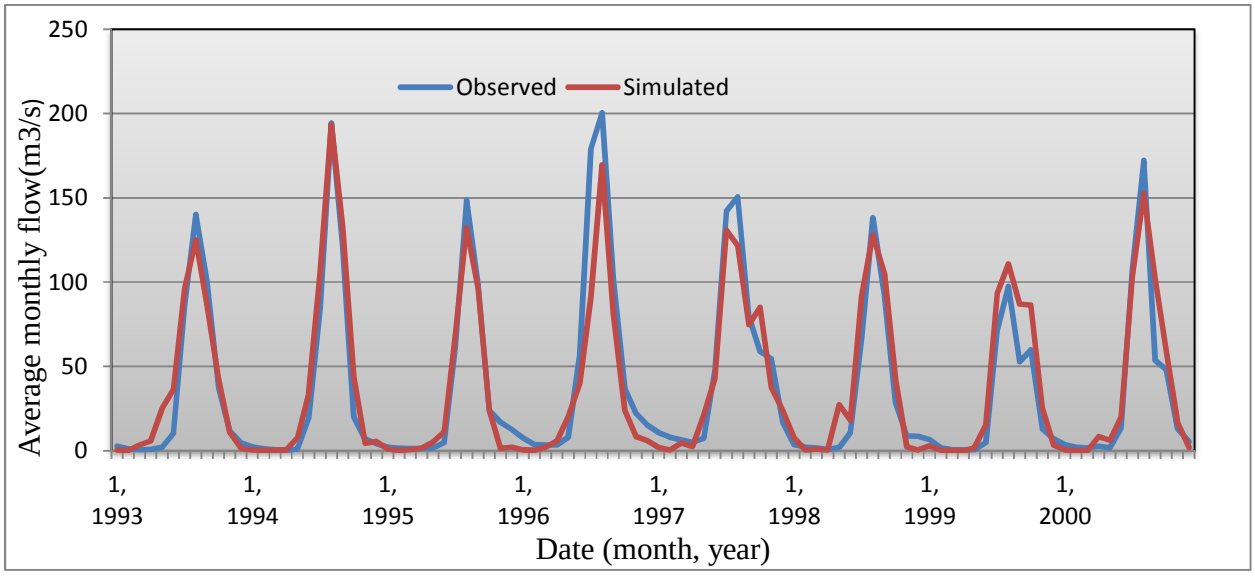


Figure 4.16: Calibration results of average monthly simulated and observed flows at Gumara River gauge station

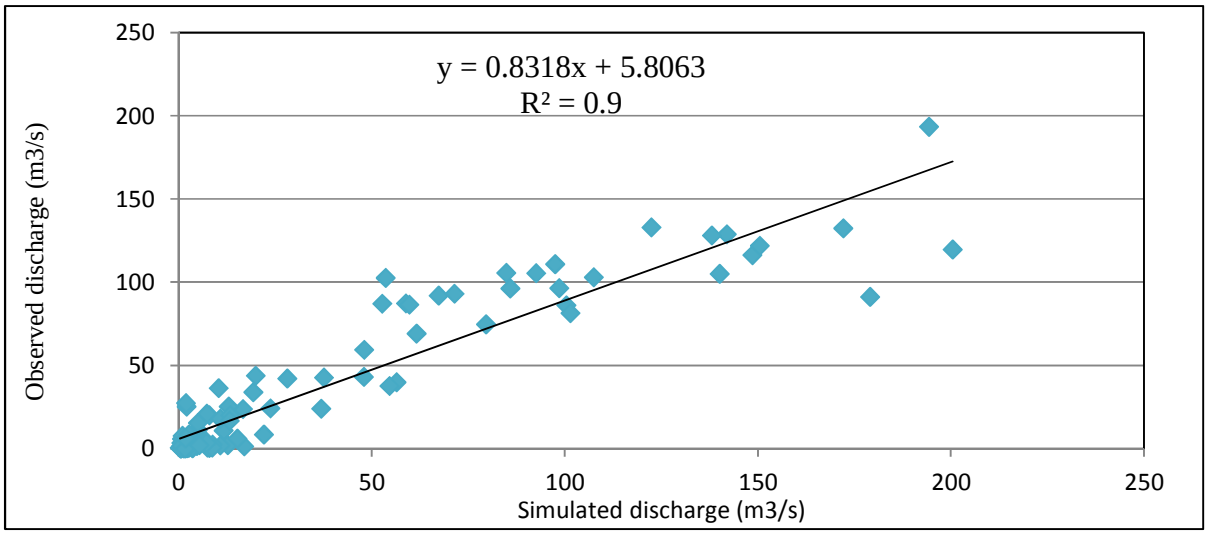


Figure 4.17: Scatter plots of monthly simulated versus observed flow at Gumara River gauge station after calibration

### 4.4.4 Flow Validation Outputs

Validation of the model was carried out using an independent data set for five years from 2001-2005 without making further adjustments of sensitive parameters. The validation results are shown in the Table 4.8.

Table 4.8: validation statistics for measured and simulated flows at Gumara flow gauge station

| Period | Total Flow(m3/s) | | Mean Monthly Flow (m3/s) | | | | |
|---|---|---|---|---|---|---|---|
| | Observed | Simulated | Observed | Simulated | % Error | $R^2$ | ENS |
| 2001-2005 | 1976.72 | 2130.89 | 32.95 | 35.13 | 6.63 | 0.89 | 0.86 |

As it can be seen from the Table 4.8 there is good agreement between monthly observed and simulated flows at Gumara River gauge station. The percent of error between the observed and simulated monthly flow is 6.63% and it is found within the tolerable range of ±15%.The coefficient of determinations ($R^2$) and Nash-Suttcliffe simulation efficiency ($E_{NS}$) were found to be 0.89 and 0.86 respectively and these shows a very good correlation of the simulation results with the observed values.

Furthermore, figure 4.18 shows the hydrograph of monthly observed and simulated flows. Even though the model slightly overestimates the peak values from the year 2001-2003 and under estimates in the year 2004 and 2005, the general trend is more or less similar. The scatter plots between simulated and observed flows also showed positive relations (figure 4.19)

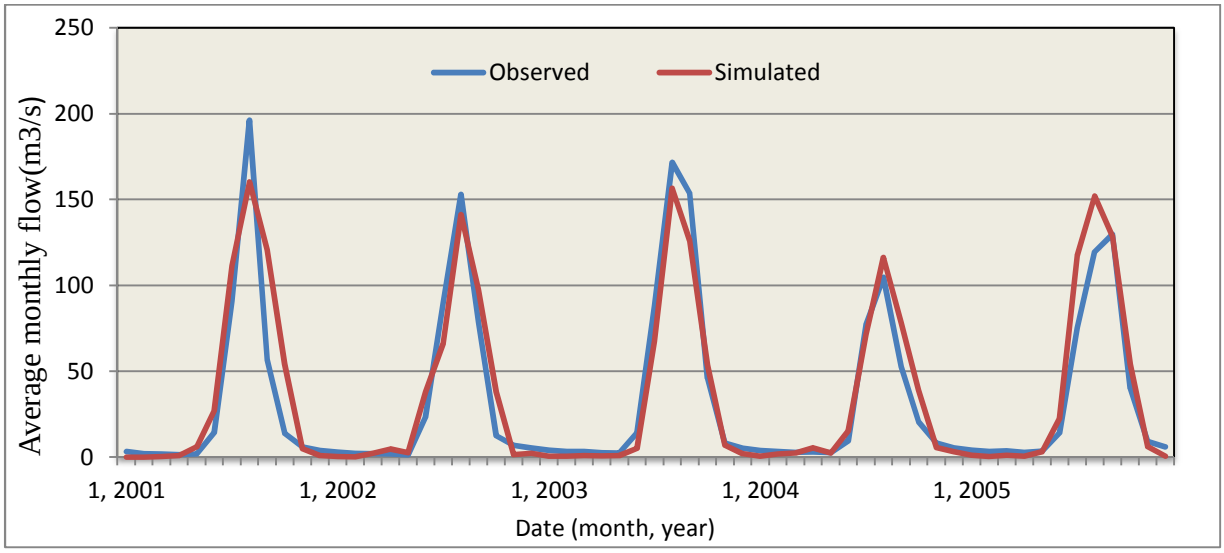


Figure 4.18: Validation results of average monthly simulated and observed flows at Gumara River gauge station

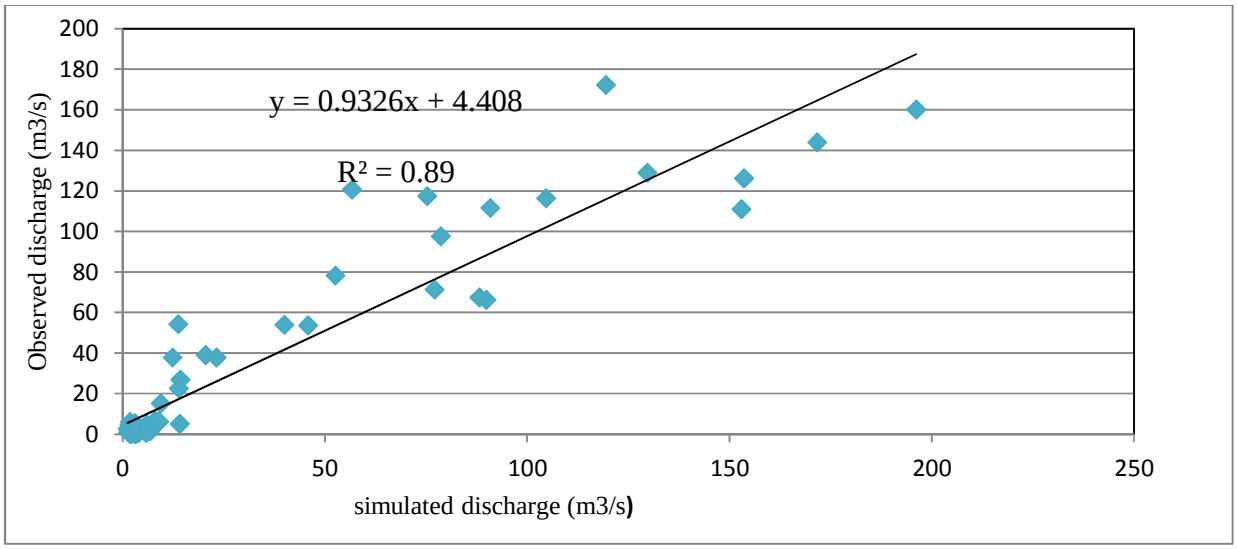


Figure 4.19: Scatter plots of monthly simulated versus observed flow at Gumara River gauge station after Validation

Thus, the validation check illustrates the accuracy of the model for simulating time-periods outside of the calibration period. The model performed as good in the validation period (2001-2005), as for the calibration period (1993-2000) at Gumara gauge station as indicated in Table 4.8. Hence, the set of optimized parameters used during calibration process can be taken as the representative set of parameter to explain the hydrologic characteristic of the Gumara watershed

and further simulations using SWAT model can be carried out by using these parameters for any period of time.

## 4.5 Impact of Climate Change on Gumara River flow Volume

The objective of downscaling is to generate an estimate of meteorological variables corresponding to a given scenario of the future climate and these meteorological variables were used as a basis for hydrological impact assessment. Stream flow is largely depends on the amount of precipitation falling on the catchment, and the amount of evapotranspiration released from that catchment. The change in the amount of precipitation and minimum and maximum temperature obviously changes Gumara River flow volumes.

The period from 1986 – 2000 were used as a base period against which the climate change impact was assessed. The daily precipitation and minimum and maximum temperature used for impact assessment were adjusted using bias corrected SDSM model results for the future four data periods of 25 years (2001-2025, 2026-2050, 2051-2076, and 2076-2099) and SWAT hydrologic model was re-run for each data periods and the SWAT parameters identified during the calibration period also remains valued.

Other climate variables such as wind speed, solar radiation, and relative humidity were assumed constant throughout the future simulation periods, which are not possible in actual case. Even though it is definite that in the future land use changes will also take place, this was also assumed constant. However, the main objective of this study is to get an indicative possible effect of climate change on the stream flow assuming changes only in the two main drivers (Temperature and precipitation).

Thus, for this study the impact of climate change on stream flow was predicted based on conditional temperature and rainfall changes on a monthly, seasonal, and annual basis.

The simulation results for the future four time horizons in terms of monthly, seasonal and annual average total flow volume and percentage change of these average total flow volumes as compared to the base period are summarized in the Table 4.9 (A and B) and figure 4.20 (A and B) for the two scenarios

Table 4.9: Monthly, Seasonal and Annual Average Total Flow volumes (MCM)

A) A2a scenarios

| Month, Season & Annual | Base Period (1986-2000) | 2001-2025 | 2026-2050 | 2051-2075 | 2076-2099 |
|---|---|---|---|---|---|
| January | 2.5 | 1.42 | 1.31 | 1.41 | 1.5 |
| February | 1.47 | 0.81 | 0.83 | 0.85 | 0.89 |
| March | 6.83 | 6.17 | 5.54 | 5.68 | 5.28 |
| April | 10.7 | 22.8 | 25 | 22.8 | 23.4 |
| May | 46.6 | 102 | 106 | 99.3 | 103 |
| June | 112 | 237 | 255 | 250 | 248 |
| July | 413 | 742 | 754 | 744 | 754 |
| August | 622 | 948 | 931 | 955 | 950 |
| September | 461 | 555 | 548 | 567 | 570 |
| October | 260 | 253 | 250 | 261 | 262 |
| November | 99.3 | 77.7 | 75.9 | 79.1 | 79.9 |
| December | 31.1 | 17.9 | 17 | 17.6 | 16.5 |
| Bega | 387 | 460 | 460 | 468 | 481 |
| Belg | 63.8 | 151 | 156 | 147 | 148 |
| Kiremit | 1602 | 2607 | 2604 | 2588 | 2648 |
| Annual | 2051 | 2318 | 2321 | 2356 | 2416 |

B) B2a scenarios

| Month, Season & Annual | **Base Period (1986-2000)** | **2001-2025** | **2026-2050** | **2051-2075** | **2076-2099** |
|---|---|---|---|---|---|
| January | 2.5 | 1.39 | 1.36 | 1.54 | 1.62 |
| February | 1.47 | 0.84 | 0.86 | 0.9 | 0.89 |
| March | 6.83 | 6.58 | 5.54 | 5.95 | 5 |
| April | 10.7 | 23.1 | 24.3 | 23.2 | 21 |
| May | 46.6 | 101 | 101 | 98.7 | 97.1 |
| June | 112 | 241 | 245 | 245 | 235 |
| July | 413 | 737 | 733 | 733 | 833 |
| August | 622 | 933 | 928 | 968 | 1026 |
| September | 461 | 545 | 548 | 572 | 591 |
| October | 260 | 247 | 251 | 262 | 270 |
| November | 99.3 | 76.3 | 76.4 | 82.5 | 84.7 |
| December | 31.1 | 17.5 | 16.6 | 18.4 | 18.7 |
| Bega | 387 | 410 | 407 | 426 | 440 |
| Belg | 63.8 | 129 | 127 | 125 | 120 |
| Kiremit | 1602 | 2528 | 2518 | 2596 | 2651 |
| Annual | 2051 | 2300 | 2314 | 2394 | 2410 |

As it can be seen from Table 4.9 (A and B) the overall results (2001-2099) for average annual total flow volume showed an increasing trend for both A2a and B2a scenarios as compared to the base period. The percentage increment of total average annual flow volume ranges from 13.04% (2001-2025) to 17.8% (2076-2099) for A2a scenario and for B2a scenario the increment ranges between 12.13% (2001-2025) and 17.5% (2076-2099) as shown in the figure 4.20 (A and B). Increase in average total annual flow volume is observed for the periods which show a corresponding increase in mean annual precipitation during scenario developments. As compared to the base period the mean annual flow volume results of this study confirmed the previous researches done by Beyene et al. (2010) on Hydrologic Impacts of Climate Change on the Nile River Basin in which the mean annual stream flow increases in the upper Blue Nile basin as compared to the base period. Dile et al ((2013) also showed that the annual inflow volume on Gilgel Abay River (one tributary to lake Tana as Gumara River) increases in the future periods. The highest increment is observed in the early century (2010-2039) in contrast with this study which is occurred in the late century (2076-2099). But this Might be due to high special variability and different hydrological modeling approaches.

On monthly basis in the month of January, February, March, November and December the average monthly total flow volume decreases throughout the future four time horizon for both A2a and B2a scenarios as compared to the base period. In the month January the total flow volume decreases by 47.44 % (2026-2050) which is the highest percentage change while in the month of March it decreases by 9.58% (2001-2025) and it is the lowest percentage change for A2a scenario and for B2a scenario the percentage decrease ranges between 3.67% (2001-2025) in the of month March to 46.62% (2026-2050) in the month of December. In the month October the average monthly total flow volume also decreases during the period 2001-2025 and 2026-2050 for A2a and B2a scenarios. The decrease in percentage of average monthly total flow volume corresponds to the decrease in precipitations which was shown during scenario development. From April to September it was found to be increasing in average monthly total flow volumes for future four time horizons and the increment is most dramatic from April to August, which is the major part of Belg and rainy seasons that contributes the biggest portion of inflow volumes. The range of increment lies between 18.82% (2026-2050) in the month of September and 134.54% (2026-2050) in the month of April for A2a scenario. Moreover, for B2a scenario it ranges between 18.02% (2001-2025) in the month of September and 127.52% (2026-

2050) in the month of April. The largest increment in percentage of average monthly total flow volume occurred within the same months (April) and time horizons (2026-2050) for the two emission scenarios while the smallest increment was found to be with in the same month (September) but different time periods (2026-2050 for A2a scenario and 2001-2025 for B2a scenario). Slight increment was also found in the month October from 2051-2075 and 2076-2099 for both scenarios. The percentage increment of the flow volume here also corresponds to the increment of precipitations for all of these months (April-August) except in the month of September, which shows a decrease in precipitation and increases in the average monthly total inflow volumes. However, in September the flow volume increment might be due to high increment of precipitation in the previous months and groundwater lag time effects.

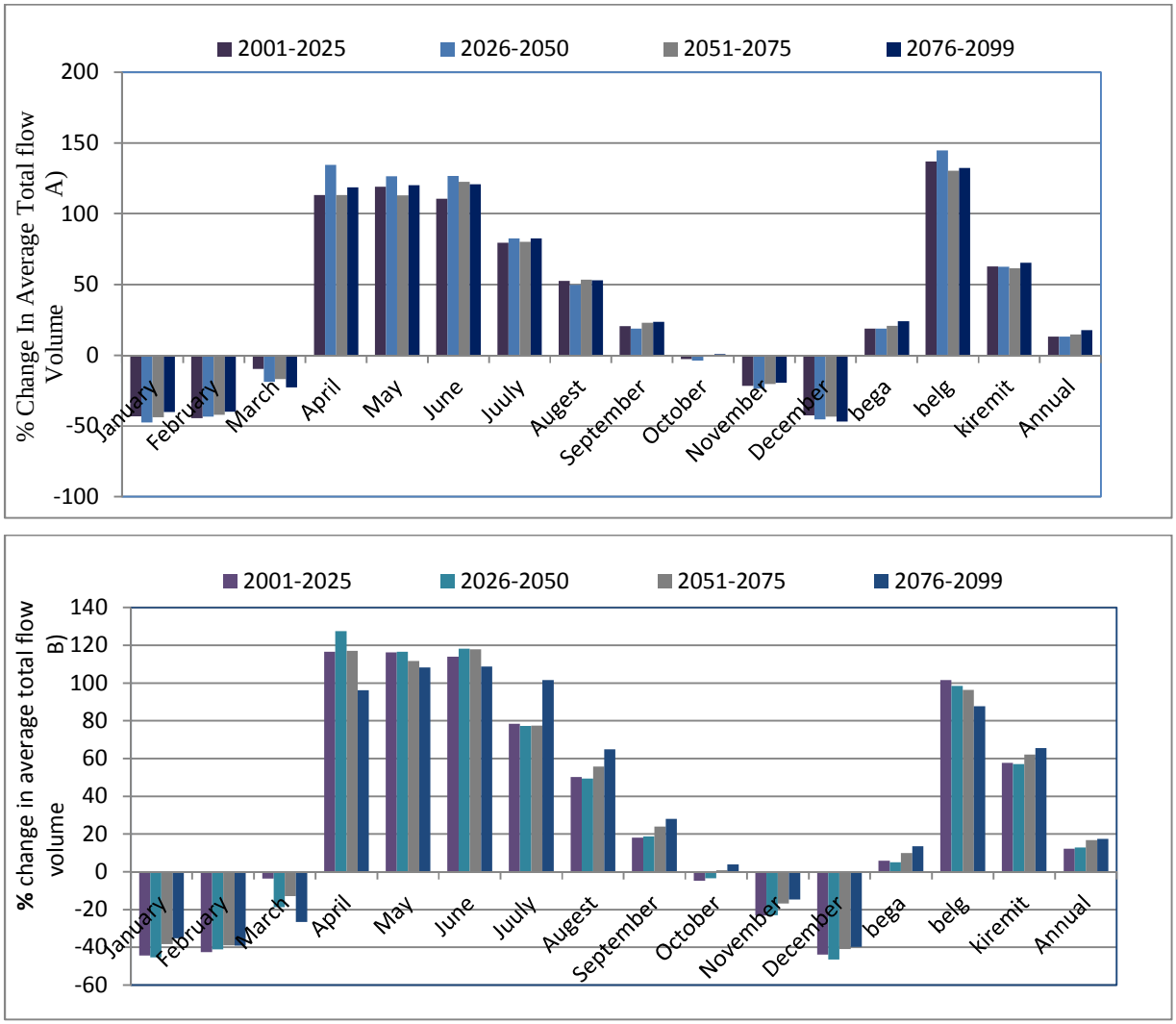


Figure 4.20: Percentage change in average monthly, seasonal, and annual total flow volume for the period 2001-2099 as compared to the baseline period (1986-2000) at Gumara River gauge station for (A) A2a scenario and (B) B2a scenario

Seasonally the average total flow volume increases in all the three seasons (Bega, Belg and Kiremit) for future four time horizons. However, the highest increment is shown in Belg season (March-May) in which the percentage change ranges between 130.33% (2051-2075) and 144.65% (2026-2050) for A2a scenario and for B2a scenario, the flow volume increases between 87.76% (2076-2099) and 101.58% (2001-2025). The percent of increment for B2a (low – medium emission) scenario lower than A2a (medium-high emission) scenario. Significant changes of average flow volume were also found in Kiremit (Jun-September) season. From the period of 2001-2025 and 2026-2050, the increment is more or less similar (62.7%) for A2a

scenario and in B2a scenario the increment is 57.45% for the same time periods. From the period 2051-2075 and 2076-2099, the average flow volume increases by 61.6% and 65.33% respectively for A2a scenario while it increases by 62.1% and 65.5% respectively for B2a scenario. Rizwan et al (2010) carried out researches on the upper Blue Nile using different GCM out puts including HadCM3 and the results showed that the runoff increases in the future in the major rainy seasons (June-September) which causes the possibility of flood occurrences in the future due to the extreme runoff. This study also reveals the increment of runoff in Kiremit season in line with Rizwan et al (2010). The increment of average seasonal total flow volume corresponds to the increase in percentage of seasonal precipitations except in Bega season. In Bega season even though the precipitation in the future four time horizons decreases as compared to the base period, the average total flow volume increases between 17.75% (2026-2050) and 24.18% (2076-2099) for A2a scenario. Moreover, for B2a scenario it increases between 5.02% (2026-2050) and 13.53% (2076-2099). This might be due to a significant increase of precipitations in Belg and Kiremit season which contributes more to the groundwater recharges and this in turn maintain the flow high in Bega season.

In general climate change results in an increase in flow volumes on Gumara River which is one of the major tributaries of Lake Tana. The increase in flow volume might have positive as well as negative implication on socio economic conditions of the sub basin. The surplus water can be used for irrigation activities in dry season. Meanwhile, the increase in flow will feed significant amount of inflows for the proposed irrigation Dam on Gumara River. However, the increase in flow volume of Gumara River is more Significant in (Belg and Kiremit) which may causes flooding problems. In general With climate change, the runoff of Gumara river may become much more seasonal and as a result the flow of the River may highly reduce in some months and season while the flow highly increases in some part of the year.

# 5. CONCLUSION AND RECOMMENDATION

## 5.1 Conclusions

The tremendous importance of water in both society and nature underscores the necessity of understanding how a change in global climate could affect the availability and reliability of water resources at a catchment scale. Human beings, at the larger scale, are vulnerable to climate change as recurrent floods and droughts continue to bring misery and keep on claiming many lives all over the world. Regarding to the design and management of water resource systems, it is required to make indicative predictions of the impacts of climate change on the spatial and temporal variability of rainfall and temperature and their influences on stream flows. Understanding the problem is part of the solution and predicting the level of climate change impact on water resources is a prerequisite for planners and decision makers to reduce, prevent and/or to find the possible adaptation measures. Hence, the impact of climate change on Gumara River was carried out to address part of the global problem by showing the possible indicative predictions of climate changes.

The study confirmed that the Statistical downscaling Model (SDSM) is able to simulate climatic events. The calibration and validation results of SDSM showed that the model is able to simulate the climatic variables (precipitation and temperature) which follow the same trend with the observed one. Even though, the precipitation is a conditional process and high special variability, the overall result from SDSM is well correlated with the observed precipitations. Hence, SDSM can predict the future climatic events under changing conditions based on the assumption that the predictor-predictand relationships under the current condition remain valid for future climate conditions.

The results of the statistical down scaling model for the future scenario (A2a and B2a) on monthly and seasonal basis indicate that precipitation and temperature do not show systematic increase or decrease. Precipitation and temperature increases in some months and decreases in some other months for both Aa2 and B2a scenarios. For A2a scenario the maximum increment of maximum temperature reaches up to $2.92^0$c (monthly) and $1.74^0$c (seasonally) and the maximum reduction reaches up to $0.92^0$c (monthly) and $1.26^0$c (seasonally) while the Monthly and seasonal minimum temperature increases by a maximum of $2.36^0$c and $1.05^0$c respectively and decreases by $2.76^0$c and $0.83^0$c. For B2a scenario the maximum increment of maximum

temperature reaches up to 2.53$^0$c (monthly) and 1.05$^0$c (seasonally) and the maximum reduction reaches up to 0.82$^0$c (monthly) and 0.62$^0$c (seasonally) while the Monthly and seasonal minimum temperature increases by a maximum of 1.82$^0$c and 0.72$^0$c respectively and decreases by 2.16$^0$c and 0.59$^0$c. Regarding to the annual temperature, the maximum temperature shows an increasing trend for A2a and B2a scenarios with an increment of 1.01$^0$c and 0.77$^0$c respectively at the end of 21$^{st}$ century. The minimum temperature indicates very minor changes.

The results of down scaled precipitation reveal that precipitation increases for the future time horizons mainly in the major parts of the rainy season (April to August) up to a maximum of 90.86% for A2a and 86.33% for B2a and decreases in the remaining months up to a maximum of 47.55% (A2a) and 46.3% (B2a). Seasonally, the precipitation increases in Belg and Kiremit season while it decreases in Bega season. The percent of increment reaches a maximum of 59.33% and 56.65% for A2a and B2a scenarios. The annual precipitation shows increasing trend for both A2a and B2a scenario with the percent increment of up to 13.7% (A2a and B2a) at the end 21$^{st}$ century.

The results of the hydrological model calibration and validation indicate that SWAT model is able to accurately explain the hydrological characteristic of Gumara watershed. The statistics of the model performance criteria (Nash–Sutcliffe model efficiency (ENS), coefficient of determination ($R^2$) and percentage deviation of simulated mean from measured one (D)) indicates that monthly simulated flow by SWAT corresponded very well with the measured values at Gumara River gauge station.

Following to the calibration and validation, the SWAT model was re-run using the downscaled precipitation and maximum and minimum temperature to predict the impact of climate changes on the hydrology of Gumara River. Results show that average monthly, seasonal and annual inflow volume changes mainly corresponding to the change in precipitation except in month of September and Bega season in which the flow volume increases even though the precipitation decreases. The average flow volume decreases from January-March and from October-December except a slight increment in a month of October during the period of 2051-2075 and 2076-2099 for both A2a and B2a scenarios. The maximum reduction of the average monthly flow volume reaches up to 47.44% and 46.62% for A2a and B2a scenarios respectively within the same time horizons (2026-2050). Dramatic increase of flow volume were occurred in the main parts of the

rainy season (April-September) in which the average flow volume increases to a maximum of 134.54% for A2a and 127.52% for B2a with in the same time period (2026-2050). Average Seasonal flow volume also increases in all the three seasons and the increment is more significant in Belg season (144.65% for A2a scenario and 101.58% for B2a scenario).

Annually, the average flow volume showed an increasing trend and the maximum increment is almost equal for the two scenarios, which are 17.65% (average) (2076-2099).

In conclusion, the hydrology of Gumara River is highly vulnerable to climate change, especially in the temporal variation of average monthly and seasonal flow volumes but the impact is moderate on average annual flow volumes for the future four time horizons.

## 5.2 Recommendation

Results of impact studies are mainly depend on the quality of input data. As mentioned above, lack of meteorological and hydrological data were the major challenges of this study. Hence, any of the concerned bodies should give due attention for data handling and recording of reliable data.

The models and model outputs used in this study possessed a certain level of uncertainty. The model simulation considered land use changes and other climatic variables such as wind speed, sunshine hours, and relative humidity remain constant for the future time horizons although it is not true in the actual case. Hence, the results of this research should be taken carefully and be considered as indicative prediction of the future and further researches should be extended by considering the future land use changes and other climatic variables.

The results of this study are based on the outputs of a single GCM and only two emission scenarios (A2a and B2a). However, it is recommended to use different GCM outputs and emission scenarios to compare the results of different models and explore a wide range of climate change scenarios that would result different hydrological impacts. Meanwhile, the GCM was downscaled to a catchment level only using statistical downscaling model which is a regression based model, even though other methods exists which are used for impact assessment. Thus, this research should be extended in the future considering other downscaling methods.

Water resources are vulnerable and have the potential to be strongly impacted by climate change, with wide-ranging consequences for human societies and ecosystems. Precipitation and temperature are highly affected by climate changes and in turn, the change of these climatic variables affects the stream flows, the recurrent floods and droughts. Hence, it is recommended to intensify such kind of researches at the catchment level to give insight for decision makers, planners and stockholders.

As the Gumara River is one of the tributary River feeding in to Lake Tana, any change in River flow is likely to affect the Lake. Hence, continuing research should consider the impact of climate change on the Lake Tana.

Although the increase in runoff volume has positive implication for the proposed Gumara irrigation dam, inclusion of climate change impact is advantageous for future flood risks.

## 6. REFERENCES


- Abbot, M.B., Bathurst, 1986. An introduction to European hydrology system – System hydrologique European "SHE", 1: history and philosophy of a physically based, distributed modelling system.
- Ann van Griensven, 2005. Sensitivity, auto-calibration, uncertainty and model evaluation in SWAT2005 manual.
- Arnold J.G, P.M Allen, R. Muttiah, and G.Bernhardt, 1995. Automated Base Flow Separation and Recession Analysis Techniques. Ground Water vol 33(6).
- Ashenafi Tedla, 2009. Impact Assessment of Land Use / Land Cover Changes on Shaya River Flow Using Swat ,Case Study of Shaya Watershed, Bale, Ethiopia
- Betrie G, Mohamed Y, Van AG, Srinivasan R, 2011. Sediment management modeling in the Blue Nile Basin using SWAT.
- Beyene T, Lettenmaier DP, Kabat P, 2010. Hydrological impacts of climate change on the Nile River Basin: Implications of the 2007 IPCC scenarios. Clim Chang 100: 433–461. Doi:10.1007/s10584-009-9693-0
- Bates, B.C., Z.W. Kundzewicz, S. Wu and J.P. Palutikof, Eds., 2008. Climate Change and Water. Technical Paper of the Intergovernmental Panel on Climate Change, IPCC Secretariat, Geneva, 210 pp.
- Boosik Kang and Jorge A. Ramírez, 2007. Response of Stream flow to Weather Variability under Climate Change in the Colorado Rockies
- Chong-yu Xu, 1999. From GCMs to River flow: a review of downscaling methods and hydrologic modeling approaches. Department of Earth Sciences, Hydrology, Uppsala University, Villavägen 16, S-75236 Uppsala, Sweden.
- CUBASH, U., G.A. Meehl, G.J. Boer, R.J. Stouffer, M. Dix, A. Noda, C.A. Senior, S. Raper, and K.S. Yap, 2001.Projections of Future Climate Change. In: Climate Change 2001: The Scientific Basis. Contribution of Working Group I to the Third Assessment Report of the Intergovernmental Panel on Climate Change [Houghton, J.T.,Y. Ding, D.J. Griggs, M. Noguer, P.J. van der Linden, X. Dai, K. Maskell, and C.A. Johnson (eds.)]. Cambridge University Press, Cambridge, United Kingdom and New York, NY, USA, 881pp.

- CUNDERLIKM. Juraj, 2003. Hydrologic model selection fort the CFCAS project: Assessment of Water Resources Risk and Vulnerability to Changing Climatic Conditions, Project Report I
- Dagnenet Fenta, 2009. Satellite remote sensing for soil moisture estimation: catchment, Ethiopia: Master thesis.
- Dile YT, Berndtsson R, Setegn SG, 2013. Hydrological Response to Climate Change for Gilgel Abay River, in the Lake Tana Basin - Upper Blue Nile Basin of Ethiopia. PLoS ONE 8(10): e79296. Doi: 10.1371/journal.
- Dilnesaw Alamirew, 2006. Modeling of Hydrology and soil Erosion of Upper Awash River Basin. PhD Thesis, University of Bonn.
- Easton ZM, Fuka D, White E, Collick AS, Ashagre BB, 2010. A multi basin SWAT model analysis of runoff and sedimentation in the Blue Nile, Ethiopia
- Elizabeth M.Shaw, 1994. Hydrology in Practice, Third edition: PP 17-18
- Ephrem Alemu, 2011. Effects of Watershed characteristics on River Flow for the Case of Rib and Catchments, Upper Blue Nile Basin. MSc thesis.
- G. H. Fang, J. Yang, Y. N. Chen, and C. Zammit, 2014. Comparing bias correction methods in downscaling meteorological variables for hydrologic impact study in an arid area in China. Hydro. Earth Syst. Sci. Discuss., 11, 12659–12696, 2014
- Girma Yimer, Andreja Jonoski and Ann Van Griensven, 2009. Hydrological Response of a Catchment to Climate Change in the Upper Beles River Basin, Upper Blue Nile, Ethiopia. Nile Basin Water Engineering Scientific Magazine, Vol.2
- Graham Wayne, 2013. The Beginner's Guide to Representative Concentration Pathway, Version 1.0
- Habtom Mulugeta, 2009. Evaluation of Climate Change Impact on Upper Blue Nile Basin Reservoir. Case Study on Gilgel Abay Reservoir, Ethiopia. MSc thesis
- IPCC-TGCIA, 1999: Guidelines on the Use of Scenario Data for Climate Impact and Adaptation Assessment. Version 1. Prepared by Carter, T.R., M. Hulme, and M. Lal, Intergovernmental Panel on Climate Change, Task Group on Scenarios for Climate Impact Assessment, 69 pp.
- IPCC-TGICA, 2007: General Guidelines on the Use of Scenario Data for Climate Impact and Adaptation Assessment. Version 2. Prepared by T.R. Carter on behalf of the

Intergovernmental Panel on Climate Change, Task Group on Data and Scenario Support for Impact and Climate Assessment, 66 pp.

- IPCC, 2013: Climate Change 2013: The Physical Science Basis. Contribution of Working Group I to the Fifth Assessment Report of the Intergovernmental Panel on Climate Change [Stocker, T.F., D. Qin, G.-K. Plattner, M. Tignor, S.K. Allen, J. Boschung, A. Nauels, Y. Xia, V. Bex and P.M. Midgley (eds.)]. Cambridge University Press, Cambridge, United Kingdom and New York, NY, USA, 1535 pp.
- Kim, U.; Kaluarachchi, J. J.; Smakhtin, V. U., 2008. Climate change impacts on hydrology and water resources of the Upper Blue Nile River Basin, Ethiopia. Colombo, Sri Lanka: International Water Management Institute. 27p (IWMI Research Report 126)
- Kim, U. et al., 2008. Application of parameter estimation and regionalization methodologies to ungauged basins of upper Blue Nile River basin.
- LENHART, T., K. Eckhardt, N. Fohrer, H.-G. Frede, 2002. Comparison of two different approaches of sensitivity analysis, Physics and Chemistry of the Earth 27 (2002), Elsevier Science Ltd., 645–654pp.
- Lijalem Zeray, 2006. Climate Change impact on Lake Ziway Watershed Water Availability. M.sc Thesis, Cologne, Germany.
- María Del Rocío Rivas Lopez, 2012. Climate and Land Use Change Impact in Gumara catchment, Lake Tana Basin, Ethiopia. Master thesis
- Mequanint Tenaw, 2008. Swat Based Run off and Sediment Yield Modeling, A Case Study of Watershed in Lake Tana Sub Basin, Ethiopia. MSc thesis.
- M.Kigobe, 2010. Assessing hydrological response to change in climate: Statistical downscaling and hydrological modeling within the upper Nile.
- M.Winchell, R.Srininasan, M.Diluzio, J.Arnold, 2010. Soil and Water Assessment Tool (SWAT) user guide, Version 2009, Grassland Soil and Water Research Laboratory, USDA Agricultural Research Service, Black land Research Center, Texas Agrilife research.
- Neitsch S, Arnold J, Kiniry J, Williams J, 2005. Soil and Water Assessment Tool (SWAT) Theoretical Documentation, version 2005, Temple, TX: Grassland Soil and Water Research Laboratory. Agricultural Research Service, Black land Research Center, Texas Agricultural Experiment Station.

- Neitsch S.L., J.G. Arnold, J.R. Kiniry, J.R. Williams, 2009. Soil and Water Assessment Tool (SWAT) Theoretical Documentation, Version 2009, Grassland Soil and Water Research Laboratory, Agricultural Research Service, Black land Research Center, Texas Agricultural experiment Station.
- Penman, H, L., 1956. Evaporation: an introductory survey. Netherlands journal of agriculture science.
- PHILIP M. NYENJE & OKKE BATELAAN, 2009. Estimating the effects of climate change on groundwater recharge and base flow in the upper Sezibwa catchment, Uganda. Hydrological Sciences–Journal 54(4)
- R.L. Wilby and T.M.L. Wigley, 2000. Precipitation Predictors For Downscaling: Observed And General Circulation Model Relationships. International Journal of Climatology. Int. J. Climatol. 20: 641 – 661
- RALPH C. HEATH, 1987. Basic Ground-Water Hydrology. U.S. Geological Survey water-supply paper ; 2220
- Refsgaard, J.C. and Storm, B., 1996. Construction, calibration and validation of hydrological models, Distributed Hydrological Modeling (eds. M.B. Abbott and J.C. Refsgaard), Kluwer Academic Publishers, 41-54
- Rizwan Nawaz, Timothy Bellerby, Mohamed Sayed and Mohamed Elshamy, 2010. Blue Nile Runoff Sensitivity to Climate Change. Open Hydrology Journal, 2010, 4, 137-151.
- Santhi, C., J.G. Arnold, J.R. Williams, W.A Dugas, R. Srinivasan, and L.M.Hauck, 2001. Validation of the SWAT model on a large River basin with point and nonpoint sources: Journal of the American Water Resources Association.
- Satoshi Watanabe, Shinjiro Kanae, Shinta Seto, Pat J.-F. Yeh, Yukiko Hirabayashi, and Taikan Oki, 2012. Intercomparison of bias-correction methods for monthly temperature and precipitation simulated by multiple climate models. JOURNAL OF GEOPHYSICAL RESEARCH, VOL. 117, D23114,doi: 10.1029/2012JD018192, 2012.
- Setegn SG, Srinivasan R, Melesse AM, Dargahi B, 2010. SWAT model application and prediction uncertainty analysis in the Lake Tana Basin, Ethiopia
- Setegn, Shimelis G., Ragahavan Srinivasan, Bijan Dargahi, 2008. Hydrological Modeling in the Lake Tana Basin, Ethiopia using SWAT model. The Open Hydrology Journal Vol 2(2008): 49-62

- Siri Eriksen, Karen O'Brien and Lynn Rosentrater, 2008. Climate Change in Eastern and Southern Africa, Impacts, Vulnerability and Adaptation. GECHS Report 2008:2
- Stefan Hagemann, Cuichen, and Jano. Haerter, 2011. Impact of a Statistical Bias Correction on the Projected Hydrological Changes Obtained from Three GCMs and Two Hydrology Models. Journal of Hydrometeorology, Volume12
- Taye M. T., 2010. Hydrological modeling of climate change impact on selected catchment of Nile River basin. Journal of Hydrology and Earth System Sciences Discussions 7, 5441–5465. doi:10.5194/hessd-7-5441-2010
- UNFCCC, 2007. United Nations Framework Convention on Climate Change. Impacts, vulnerabilities and adaptation in developing countries. Bonn, Germany.
- Wilby RL, Dawson CW, 2007. Using SDSM version 4.1 SDSM 4.2; a decision support tool for the assessment of regional climate change impacts. User Manual. Leics, LE11 3TU, UK.
- Wilby, R., Charles, S., Zorita, E., Timbl, B., Whetton, P., and Means, L., 2004. Guidelines for use of Climate Scenarios Developed from Statistical Downscaling Methods
- Yibeltal Ayenew, 2011. Rainfall-Runoff Modeling for Sustainable Water Resources Management: The Case of Watershed, Ethiopia. MSc thesis
- Zeryehun Haile, 2009. Assessment of climate change impacts on the net basin supply of Lake Tana water balance.
- WWDSE, 2007. Catchment Development Plan, Irrigation Project. Ministry of water resources, Addis Ababa.

## 7. APPENDIXES

**Appendix A:** Calibration Parameters – SDSM

Calibration parameters generated by SDSM for the Scenario Generation

i. Maximum temperature calibration parameters

3

12

360

1/1/1986

5479

1/1/1986

3652

#FALSE#

1

1

False

D.tabor tmax (1986-1995).DAT

ncepp__zaf.dat

ncepshumaf.dat

nceptempaf.dat

| | | | | | |
|---|---|---|---|---|---|
| 21.512 | 0.197 | 0.115 | 0.069 | 1.209 | 0.011 |
| 23.324 | -0.618 | -0.087 | 0.541 | 1.215 | 0.067 |
| 22.622 | 0.691 | -0.426 | -0.139 | 1.554 | 0.191 |
| 24.190 | 0.412 | 0.041 | -0.244 | 1.451 | 0.021 |
| 23.707 | 0.372 | 0.014 | 0.228 | 2.025 | 0.046 |
| 22.088 | 0.534 | 0.779 | 0.944 | 1.904 | 0.158 |
| 20.620 | -0.783 | 0.698 | 1.625 | 1.758 | 0.216 |

17.832 -0.803 1.375 1.159 1.690 0.186

22.198 0.642 -1.411 1.944 1.405 0.110

21.316 0.674 -1.006 0.580 1.273 0.150

20.747 0.297 0.041 0.211 1.204 0.031

21.147 0.344 0.036 0.014 1.239 0.019

C:\Users\andarg\Desktop\final data\transformed data\D.tabor tmax (1986-1995).DAT

ii. Minimum temperature calibration parameters

4

12

360

1/1/1986

5479

1/1/1986

3652

#FALSE#

1

1

False

D.Tabor tmin (1986-1995).DAT

ncepp500af.dat

ncepp8_vaf.dat

ncepshumaf.dat

nceptempaf.dat

8.476 0.040 0.342 0.631 -0.022 0.958 0.213

8.644 -0.067 0.180 0.463 0.196 1.408 0.093

9.594 0.185 -0.063 0.394 0.300 1.269 0.075

9.877 -0.454 -0.131 0.231 0.074 1.632 0.073

10.537 -0.626 0.369 0.107 0.418 1.281 0.134

10.600 -0.080 0.617 0.319 0.343 1.271 0.093

10.054 0.129 -0.336 0.106 0.421 0.988 0.102

10.372 0.509 -0.395 -0.711 0.243 0.972 0.120

9.266 0.479 0.029 -0.041 -1.042 0.931 0.189

8.880 0.110 -0.157 0.131 -0.375 0.858 0.047

8.369 0.094 0.085 0.541 -0.543 1.060 0.135

8.187 0.074 0.294 0.603 -0.423 1.066 0.185

C:\Users\andarg\Desktop\final data\transformed data\D.Tabor tmin (1986-1995).DAT

iii. Precipitation calibration parameters

3

12

360

1/1/1986

5479

1/1/1986

3652

#TRUE#

2

1

False

D.Tabor prec. (1986-1995).DAT

ncepp__vaf.dat

ncepp8zhaf.dat

ncepr850af.dat

0.255 -0.237 -0.147 -0.303 0.000 0.202

0.284 -0.284 -0.129 -0.169 0.000 0.112

| | | | | | | |
|---|---|---|---|---|---|---|
| 0.208 | 0.156 | 0.092 | -0.072 | 0.000 | 0.057 | |
| 0.401 | -0.031 | 0.074 | -0.102 | 0.000 | 0.058 | |
| 0.530 | -0.214 | 0.046 | -0.071 | 0.000 | 0.065 | |
| 0.576 | 0.045 | 0.221 | -0.041 | 0.000 | 0.039 | |
| 0.565 | -0.114 | -0.098 | 0.184 | 0.000 | 0.073 | |
| 0.701 | 0.070 | 0.099 | 0.139 | 0.000 | 0.020 | |
| 0.220 | -0.156 | 0.074 | 0.357 | 0.000 | 0.117 | |
| 0.697 | -0.277 | 0.005 | -0.087 | 0.000 | 0.115 | |
| 0.756 | -0.046 | 0.343 | -0.299 | 0.000 | 0.216 | |
| 0.399 | -0.279 | -0.136 | -0.290 | 0.000 | 0.171 | |
| 0.952 | 1.000 | 0.149 | 0.154 | 0.013 | 0.327 | 0.018 |
| 0.933 | 1.000 | 0.259 | 0.141 | 0.104 | 0.344 | 0.083 |
| 1.164 | 1.000 | -0.157 | -0.239 | 0.123 | 0.371 | 0.131 |
| 1.256 | 1.000 | 0.044 | 0.014 | -0.027 | 0.290 | 0.018 |
| 1.378 | 1.000 | -0.095 | -0.097 | -0.039 | 0.326 | 0.016 |
| 1.642 | 1.000 | -0.029 | 0.004 | 0.013 | 0.398 | 0.005 |
| 1.768 | 1.000 | 0.080 | -0.083 | 0.291 | 0.504 | 0.101 |
| 2.261 | 1.000 | 0.475 | 0.463 | -0.180 | 0.509 | 0.057 |
| 1.978 | 1.000 | 0.452 | 0.542 | -0.048 | 0.446 | 0.102 |
| 1.633 | 1.000 | 0.106 | 0.191 | 0.085 | 0.440 | 0.041 |
| 1.491 | 1.000 | -0.096 | -0.165 | -0.020 | 0.343 | 0.018 |
| 1.464 | 1.000 | 0.234 | 0.255 | 0.158 | 0.296 | 0.093 |

C:\Users\andarg\Desktop\final data\transformed data\D.Tabor prec. (1986-1995).DAT

**Appendix B:** Weather Generator Parameters

Weather generator (WGEN) parameters used by the SWAT model

| Symbol | | Description |
|---|---|---|
| TMPMX | (1) | Average or mean daily maximum air temperature for month (°C). |
| TMPMN | (2) | Average or mean daily minimum air temperature for month (°C). |
| TMPSTDMX | (3) | Standard deviation for daily maximum air temperature in month (°C). |
| TMPSTDMN | (4) | Standard deviation for daily minimum air temperature in month (°C). |
| SOLARAV | (5) | Average daily solar radiation for month (MJ/m2/day). |
| DEWPT | (6) | Average daily dew point temperature in month (°C). |
| WNDAV | (7) | Average daily wind speed in month (m/s) |
| PCPMM | (8) | Average or mean total monthly precipitation (mm H2O) |
| PCPSTD | (9) | Standard deviation for daily precipitation in month (mm H2O/day). |
| PCPSKW | (10) | Skew coefficient for daily precipitation in month. |
| PR_W1 | (11) | Probability of a wet day following a dry day in the month. |
| PR_W2 | (12) | Probability of a wet day following a wet day in the month. |
| PCPD | (13) | Average number of days of precipitation in month |

| Station: D.Tabor | | | | | | | | | | | | | |
|---|---|---|---|---|---|---|---|---|---|---|---|---|---|
| month | 1 | 2 | 3 | 4 | 5 | 6 | 7 | 8 | 9 | 10 | 11 | 12 | 13 |
| jan | 22.7 | 8.23 | 0.52 | 0.43 | 5.92 | 3.48 | 1.06 | 8.56 | 1.68 | 13.3 | 0.05 | 0.7 | 4.7 |
| feb | 24.2 | 9.16 | 0.51 | 0.73 | 14.8 | 3.76 | 1.21 | 3.59 | 0.53 | 6.69 | 0.04 | 0.69 | 3.5 |
| mar | 24.6 | 10.37 | 0.45 | 0.54 | 19.5 | 5.33 | 1.25 | 38.94 | 3.84 | 6.66 | 0.12 | 0.65 | 8.4 |
| apr | 24.1 | 11.38 | 0.59 | 0.37 | 13.8 | 8.01 | 1.27 | 58.77 | 4.36 | 3.52 | 0.19 | 0.66 | 11.5 |
| may | 23.2 | 11.08 | 0.73 | 0.35 | 6.94 | 10.3 | 1.34 | 136.6 | 8.44 | 3.27 | 0.3 | 0.68 | 15.6 |
| jun | 21.9 | 10.46 | 0.84 | 0.28 | 1.27 | 12.1 | 1.19 | 200.2 | 8.7 | 1.57 | 0.47 | 0.8 | 21.9 |
| jul | 18.3 | 10.16 | 0.62 | 0.27 | 3.81 | 12.3 | 1.08 | 508.9 | 14.5 | 1.18 | 0.8 | 0.94 | 30 |
| aug | 18.6 | 10.08 | 0.37 | 0.27 | 10.6 | 11.9 | 1.19 | 501.1 | 14.3 | 1.1 | 0.83 | 0.95 | 30.4 |
| sep | 20 | 9.28 | 0.61 | 0.34 | 13.9 | 11.1 | 1.06 | 234.3 | 9.75 | 1.68 | 0.43 | 0.84 | 23.5 |
| oct | 20.6 | 8.86 | 0.36 | 0.36 | 11.7 | 8.79 | 0.87 | 131.6 | 9.62 | 5.54 | 0.22 | 0.76 | 16.3 |
| nov | 21.4 | 8.07 | 0.32 | 0.27 | 5.93 | 6.62 | 0.87 | 37.76 | 3.27 | 3.45 | 0.1 | 0.66 | 7.4 |
| dec | 21.8 | 7.84 | 0.32 | 0.26 | 1.09 | 5.34 | 0.95 | 20.19 | 3.41 | 10.9 | 0.08 | 0.63 | 5.6 |

| Station: Woreta | | | | | | | | | | | | | |
|---|---|---|---|---|---|---|---|---|---|---|---|---|---|
| month | 1 | 2 | 3 | 4 | 5 | 6 | 7 | 8 | 9 | 10 | 11 | 12 | 13 |
| jan | 21.6 | 8 | 0.62 | 0.53 | 5.17 | 3.48 | 1.16 | 8.66 | 1.78 | 13.7 | 0.05 | 0.6 | 5.7 |
| feb | 23.2 | 8.16 | 0.61 | 0.65 | 14 | 3.8 | 1.41 | 3.69 | 0.53 | 6.8 | 0.04 | 0.79 | 3.6 |
| mar | 23.6 | 11.37 | 0.47 | 0.64 | 18.5 | 5 | 1.25 | 37.94 | 3.64 | 5.66 | 0.12 | 0.75 | 7.4 |
| apr | 25.1 | 10.38 | 0.59 | 0.37 | 12.8 | 7.01 | 1.27 | 57.77 | 4.36 | 3.52 | 0.19 | 0.66 | 11.5 |
| may | 23.2 | 11.08 | 0.73 | 0.35 | 6.94 | 10.3 | 1.34 | 136.6 | 8.44 | 3.27 | 0.3 | 0.68 | 15.6 |
| jun | 21 | 10.56 | 0.81 | 0.28 | 1.26 | 12 | 1.16 | 198.2 | 8 | 1.57 | 0.47 | 0.8 | 20.9 |
| jul | 19.3 | 9.16 | 0.72 | 0.27 | 3.41 | 11.3 | 1.08 | 500.9 | 13.5 | 1.18 | 0.8 | 0.94 | 29 |
| aug | 17.6 | 10 | 0.4 | 0.27 | 10 | 11 | 1.19 | 502.1 | 13.3 | 1.1 | 0.73 | 0.85 | 30 |
| sep | 20 | 9.28 | 0.61 | 0.34 | 13.9 | 11.1 | 1.06 | 234.3 | 9.75 | 1.68 | 0.43 | 0.84 | 23.5 |
| oct | 20 | 8.6 | 0.57 | 0.36 | 10.7 | 8.9 | 0.87 | 130.6 | 8.62 | 5.54 | 0.22 | 0.66 | 15.3 |
| nov | 20.2 | 7.07 | 0.32 | 0.27 | 4.93 | 6 | 0.67 | 36.76 | 3 | 3.25 | 0.1 | 0.66 | 7.4 |
| dec | 21 | 7 | 0.32 | 0.26 | 1.09 | 5.34 | 0.95 | 20.19 | 3.41 | 11.9 | 0.08 | 0.63 | 5.6 |

Station: Bahir Dar

| Months | 1 | 2 | 3 | 4 | 5 | 6 | 7 | 8 | 9 | 10 | 11 | 12 |
|---|---|---|---|---|---|---|---|---|---|---|---|---|
| TMPMX | 26.9 | 28.5 | 29.8 | 29.7 | 29.6 | 26.9 | 24 | 24.3 | 17.4 | 26.6 | 26.5 | 21.1 |
| TMPMN | 8.7 | 10.8 | 12.7 | 15.2 | 15 | 13.8 | 11.3 | 14.7 | 5.2 | 13.9 | 11.6 | 5.3 |
| TMPSTDMX | 1.6 | 6.5 | 1.7 | 8.8 | 10.5 | 6.2 | 8.3 | 1.4 | 21.2 | 1.2 | 6 | 26.2 |
| TMPSTDMN | 5.5 | 2.6 | 5.9 | 2.6 | 7.7 | 10.8 | 18.8 | 6.2 | 29.9 | 1.4 | 5.7 | 22.2 |
| PCPMM | 1.8 | 2.4 | 12.7 | 26.8 | 78.8 | 208.9 | 411.4 | 371 | 199.3 | 100.6 | 14 | 3.2 |
| PCPSTD | 2.87 | 6.75 | 9.1 | 8.07 | 10.95 | 13.04 | 15.51 | 15.57 | 11.52 | 9.44 | 6.51 | 3.22 |
| PCPSKW | 0.74 | 2.04 | 4.8 | 2.07 | 2.5 | 2.3 | 2.13 | 2.69 | 2.65 | 1.23 | 1.53 | 1.3 |
| PR_W1 | 0.01 | 0.02 | 0.06 | 0.1 | 0.22 | 0.55 | 0.83 | 0.94 | 0.58 | 0.24 | 0.05 | 0.03 |
| PR_W2 | 0.33 | 0.13 | 0.4 | 0.38 | 0.52 | 0.7 | 0.9 | 0.9 | 0.77 | 0.57 | 0.35 | 0.18 |
| PCPD | 0.6 | 0.5 | 3 | 4.2 | 9.8 | 19.5 | 28.7 | 27.9 | 21.3 | 11.3 | 2.3 | 1.1 |
| SOLARAV | 20.52 | 22.43 | 22.73 | 22.7 | 21.41 | 19.04 | 16.14 | 15.76 | 18.75 | 20.67 | 20.7 | 20.43 |
| DEWPT | 9.64 | 9.28 | 9.39 | 10.58 | 12.86 | 15.47 | 15.47 | 15.85 | 7.4 | 14.02 | 11.7 | 5.52 |
| WNDAV | 0.45 | 0.54 | 0.66 | 0.74 | 0.71 | 0.73 | 0.61 | 0.61 | 0.61 | 0.61 | 0.53 | 0.43 |

**Appendix C:** Average monthly flows used for calibration and validation at Gumara gauge station (m3/s)

i. Calibration

| | 1993 | | 1994 | | 1995 | | 1996 | | 1997 | | 1998 | | 1999 | | 2000 | |
|---|---|---|---|---|---|---|---|---|---|---|---|---|---|---|---|---|
| Mo | Ob | Sim | Ob | Sim | Ob | Sim | Ob | Sim | Ob | Sim | Ob | Sim | Ob | Sim | Ob | Sim |
| Jan | 2.7 | 0.6 | 2.4 | 0.5 | 2.2 | 1 | 7.5 | 0.5 | 11 | 1.9 | 3.5 | 7.8 | 6.8 | 2.8 | 3.5 | 0.5 |
| Feb | 1.3 | 0.2 | 1.3 | 0.3 | 1.7 | 0.3 | 3.6 | 0.3 | 8 | 0.4 | 2.2 | 0.5 | 1.7 | 0.4 | 2.2 | 0.2 |
| Mar | 0.7 | 3.5 | 0.6 | 0.3 | 1.5 | 0.7 | 3.4 | 2.2 | 6.6 | 4.5 | 1.8 | 1.1 | 0.8 | 0.1 | 1.7 | 0 |
| Apr | 0.9 | 5.8 | 0.4 | 0.5 | 1.4 | 1.6 | 3.4 | 5.9 | 5 | 2.6 | 0.9 | 0.4 | 0.6 | 0 | 2.7 | 8.4 |
| May | 2.1 | 25 | 1 | 7.8 | 1.6 | 5.1 | 8 | 20 | 7.4 | 21 | 1.9 | 27 | 0.7 | 1.7 | 1.9 | 6.2 |
| Jun | 10 | 36 | 19 | 34 | 5 | 11 | 56 | 40 | 48 | 43 | 11 | 18 | 5 | 15 | 13 | 20 |
| Jul | 86 | 96 | 85 | 106 | 62 | 69 | 179 | 91 | 142 | 129 | 67 | 92 | 72 | 93 | 108 | 103 |
| Aug | 140 | 105 | 194 | 193 | 149 | 116 | 200 | 120 | 151 | 122 | 138 | 128 | 98 | 111 | 172 | 132 |
| Sep | 100 | 86 | 122 | 133 | 99 | 96 | 102 | 82 | 80 | 75 | 93 | 106 | 53 | 87 | 54 | 103 |
| Oct | 38 | 43 | 20 | 44 | 24 | 24 | 37 | 24 | 59 | 87 | 28 | 42 | 60 | 87 | 48 | 59 |
| Nov | 12 | 11 | 7 | 4.5 | 17 | 1.3 | 22 | 8.5 | 55 | 38 | 8.8 | 2.4 | 13 | 25 | 13 | 17 |
| Dec | 4.7 | 1.4 | 4.1 | 5.5 | 13 | 2.1 | 15 | 6 | 17 | 24 | 8.7 | 0.5 | 7.2 | 3.4 | 5.4 | 2 |

i. Validation

| | 2001 | | 2002 | | 2003 | | 2004 | | 2005 | |
|---|---|---|---|---|---|---|---|---|---|---|
| Mon | Obs | Simu | Obs | Simu | Obs | Simu | Obs | Simu | Obs | Simu |
| Jan | 3.18 | 0 | 2.84 | 0.39 | 3.88 | 0.54 | 3.81 | 0.541 | 4.02 | 1.11 |
| Feb | 1.97 | 0 | 2.05 | 0.13 | 3.16 | 0.5 | 3.24 | 1.743 | 3.3 | 0.28 |
| Mar | 1.76 | 0.333 | 2.02 | 2.2 | 3.2 | 0.84 | 2.66 | 2.255 | 3.63 | 0.98 |
| Apr | 1.34 | 0.922 | 1.74 | 4.64 | 2.42 | 0.7 | 3.09 | 5.318 | 2.63 | 0.49 |
| May | 1.83 | 6.03 | 1.21 | 2.57 | 2.29 | 0.92 | 2.49 | 2.391 | 3.45 | 2.96 |
| Jun | 14.3 | 26.96 | 23.3 | 37.8 | 14.1 | 5.09 | 9.46 | 15.29 | 13.9 | 22.5 |
| Jul | 91 | 111.6 | 89.9 | 66.2 | 88.2 | 67.5 | 77.1 | 71.34 | 75.3 | 117 |
| Aug | 196 | 160.2 | 153 | 111 | 172 | 144 | 105 | 116.3 | 119 | 172 |
| Sep | 56.7 | 120.7 | 78.7 | 97.6 | 154 | 126 | 52.7 | 78.26 | 130 | 129 |
| Oct | 13.8 | 54.23 | 12.4 | 37.8 | 45.9 | 53.7 | 20.5 | 39.05 | 40 | 54 |
| Nov | 5.98 | 4.816 | 6.88 | 1.33 | 8.07 | 6.81 | 8.19 | 5.664 | 9.04 | 6.19 |
| Dec | 3.73 | 0.899 | 5.22 | 2.16 | 5.16 | 1.87 | 5.45 | 3.12 | 5.88 | 0.58 |

Appendix D: Summary of Gumara River flows at Gauge station (1986-2005)

| | average daily flow of Gumara river at gauging station (m3/s) | | | | | | | | | | | | | | | | | | | |
|---|---|---|---|---|---|---|---|---|---|---|---|---|---|---|---|---|---|---|---|---|
| Mon | 1986 | 1987 | 1988 | 1989 | 1990 | 1991 | 1992 | 1993 | 1994 | 1995 | 1996 | 1997 | 1998 | 1999 | 2000 | 2001 | 2002 | 2003 | 2004 | 2005 |
| Jan | 4.074 | 1.59 | 0.931 | 2.133 | 2.394 | 1.008 | 3.046 | 2.705 | 2.378 | 2.165 | 7.455 | 10.78 | 3.541 | 6.79 | 3.541 | 3.175 | 2.844 | 3.879 | 3.81 | 4.022 |
| Feb | 2.285 | 0.97 | 0.563 | 1.128 | 0.911 | 0.531 | 2.074 | 1.309 | 1.311 | 1.673 | 3.633 | 7.993 | 2.164 | 1.72 | 2.164 | 1.972 | 2.053 | 3.159 | 3.24 | 3.3 |
| Mar | 1.103 | 0.65 | 0.351 | 0.612 | 0.606 | 0.379 | 2.764 | 0.697 | 0.609 | 1.481 | 3.366 | 6.631 | 1.794 | 0.75 | 1.723 | 1.759 | 2.015 | 3.201 | 2.69 | 3.633 |
| Apr | 0.829 | 0.44 | 0.249 | 0.519 | 0.404 | 0.443 | 0.851 | 0.911 | 0.348 | 1.395 | 3.114 | 4.968 | 0.859 | 0.56 | 2.654 | 1.345 | 1.743 | 2.418 | 3.08 | 2.629 |
| May | 0.425 | 3.33 | 0.413 | 0.843 | 0.539 | 0.814 | 1.901 | 2.125 | 1.013 | 1.555 | 7.759 | 7.351 | 1.908 | 0.74 | 1.861 | 1.829 | 1.207 | 2.288 | 2.51 | 3.454 |
| Jun | 18.41 | 14.6 | 1.853 | 10.57 | 1.312 | 14.22 | 1.448 | 10.37 | 19.35 | 4.987 | 55.09 | 48.03 | 10.8 | 5 | 12.8 | 14.29 | 23.28 | 14.13 | 8.32 | 13.93 |
| Jul | 100.5 | 34.2 | 150.7 | 86.3 | 52.81 | 83.22 | 40.36 | 85.92 | 84.88 | 61.61 | 171.7 | 142 | 67.38 | 71.5 | 105.8 | 90.97 | 89.93 | 88.23 | 73.4 | 75.3 |
| Aug | 115.6 | 127 | 167.1 | 144.9 | 180.4 | 168.1 | 157 | 140.2 | 194.4 | 148.6 | 203 | 150.5 | 138.1 | 97.5 | 168.5 | 196.2 | 153 | 171.7 | 108 | 119.5 |
| Sep | 83.65 | 42.7 | 89.37 | 65.42 | 109.3 | 76.81 | 74.01 | 100.4 | 122.5 | 98.55 | 106.8 | 79.62 | 92.61 | 52.8 | 59.08 | 56.72 | 78.71 | 153.6 | 53.7 | 129.8 |
| Oct | 34.19 | 10.2 | 55.93 | 22.42 | 19.82 | 23.43 | 50.47 | 37.67 | 19.99 | 24.95 | 37.79 | 58.9 | 28.14 | 59.8 | 47.83 | 13.76 | 12.41 | 45.89 | 20.9 | 40.01 |
| Nov | 12.52 | 4.78 | 10.16 | 15.54 | 4.144 | 4.757 | 15.52 | 11.71 | 7.016 | 17.02 | 22.28 | 54.58 | 8.815 | 13 | 14.04 | 5.982 | 6.88 | 8.071 | 8.3 | 9.037 |
| Dec | 7.109 | 2.04 | 4.464 | 4.924 | 1.931 | 4.788 | 6.412 | 4.738 | 4.14 | 12.74 | 15.41 | 16.69 | 8.698 | 7.23 | 5.484 | 3.731 | 5.224 | 5.158 | 5.48 | 5.879 |
| | total seasonal and annual flow of Gumara river (m3/s) | | | | | | | | | | | | | | | | | | | |
| Bega | 1846 | 600 | 2221 | 1412 | 898.3 | 1063 | 2381 | 1787 | 1069 | 1793 | 2650 | 4539 | 1577 | 2725 | 2244 | 875.2 | 898.6 | 2033 | 1275 | 1911 |
| Belg | 72.24 | 137 | 31.15 | 60.67 | 47.63 | 50.28 | 170.1 | 114.8 | 60.71 | 136 | 438.3 | 582.5 | 140.5 | 62.9 | 190.7 | 151.6 | 152.2 | 242.7 | 253 | 298.6 |
| Kiremit | 9762 | 6704 | 12586 | 9448 | 10546 | 10521 | 8383 | 10333 | 12911 | 9622 | 16470 | 12897 | 9472 | 6973 | 10659 | 11032 | 10590 | 13093 | 7483 | 10350 |
| Annual | 11680 | 7441 | 14839 | 10920 | 11492 | 11635 | 10935 | 12234 | 14040 | 11550 | 19559 | 18018 | 11189 | 9761 | 13094 | 12059 | 11641 | 15369 | 9011 | 12559 |